Hao Gao

Thermo-hydro-mechanical Simulation of Frost Heave using Extended Finite Element Method

Hao Gao

Doctoral thesis

NTNU
Norwegian University of
Science and Technology

NTNU
Norwegian University of
Science and Technology

NTNU

Hao Gao

Thermo-hydro-mechanical Simulation of Frost Heave using Extended Finite Element Method

Thesis for the degree of Philosophiae Doctor

Trondheim, "April" "2024"

Norwegian University of Science and Technology
Faculty of Engineering
Department of Civil and Environmental Engineering

◨ NTNU
Norwegian University of
Science and Technology

PRINTED IN
NORWAY
NO - 1598

NORDIC SWAN ECOLABEL

Printed matter
2041 0731

Table of Contents

List of Figures

List of Tables

Nomenclature

Symbol	Property	In SI base Units
β_1	A model parameter	
β_2	A model parameter	
δ	Dirac delta function	
ε_v	Volumetric strain of soil skeleton	
Γ	Boundary of solution domain	
Γ_d	Discontinuity interface	
γ_{iw}	The surface energy between ice and water	$m^2 \cdot kg \cdot s^{-2}$
κ	Elastic compressibility	$kg^{-1} \cdot m \cdot s^2$
λ	A model parameter	
λ_i	Thermal conductivity of ice	$m \cdot kg \cdot s^{-3} \cdot K^{-1}$
λ_s	Thermal conductivity of soil	$m \cdot kg \cdot s^{-3} \cdot K^{-1}$
λ_w	Thermal conductivity of water	$m \cdot kg \cdot s^{-3} \cdot K^{-1}$
μ_{iT}	The difference in chemical potential of ice due to changes in composition and pressure	$m \cdot kg \cdot s^{-3} \cdot K^{-1} \cdot mol^{-1}$
μ_w	Dynamic viscosity of water	$kg \cdot m^{-1} \cdot s^{-1}$
ν	Poisson's ratio	
ν_i	Specific volumes of ice	$m^3 \cdot kg^{-1}$
ν_s	Specific volumes of soil	$m^3 \cdot kg^{-1}$
ν_w	Specific volumes of water	$m^3 \cdot kg^{-1}$
ξ	Position in the natural coordinate system of the element	
ξ_{Γ_d}	The closest point projection of ξ onto the discontinuity interface Γ_d	
$(\rho C)_{eff}$	Effective heat capacity of the mixture	$m^2 \cdot kg \cdot s^{-2} \cdot K^{-1}$
ρ	Density of mixture	$kg \cdot m^{-3}$
ρ_i	Density of ice	$kg \cdot m^{-3}$
ρ_r	A model parameter	
ρ_s	Density of soil	$kg \cdot m^{-3}$
ρ_w	Density of water	$kg \cdot m^{-3}$
σ	Total stress of the system	$kg \cdot m^{-1} \cdot s^{-2}$
σ_e	Effective stress	$kg \cdot m^{-1} \cdot s^{-2}$
σ_n^*	Normal stress on the crack plane	$kg \cdot m^{-1} \cdot s^{-2}$
σ_t	Total stress	$kg \cdot m^{-1} \cdot s^{-2}$
$\boldsymbol{\sigma}^*$	Solid phase stress	$kg \cdot m^{-1} \cdot s^{-2}$
ϕ	Semi-empirical stress partition function	$kg \cdot m^{-1} \cdot s^{-2}$
Ω	Solution domain	

Symbol	Description	Units
a	Tensile stress of frozen soil as a result of ice cementation	$kg \cdot m^{-1} \cdot s^{-2}$
$\hat{\mathbf{a}}$	Enhanced nodal degree of freedom	
a_0	Maximum effect of ice cementation at the fully frozen state and zero overburden/total stress	$kg \cdot m^{-1} \cdot s^{-2}$
$\mathbf{b}$	Enhanced nodal DOFs for pressure	
$\hat{\mathbf{c}}$	Enhanced nodal DOFs for temperature	
C_i	Specific heat capacity for ice	$m^2 \cdot s^{-2} \cdot K^{-1}$
C_s	Specific heat capacity for soil grains	$m^2 \cdot s^{-2} \cdot K^{-1}$
C_w	Specific heat capacity for water	$m^2 \cdot s^{-2} \cdot K^{-1}$
$\mathbf{D}^e$	Elastic stiffness tensor	
$\mathbf{g}$	Gravitational acceleration	$m \cdot s^{-2}$
G	Shear modulus	$kg \cdot m^{-1} \cdot s^{-2}$
$\mathbf{I}$	Unit tensor	
k	Hydraulic permeability of soil	$m \cdot s^{-1}$
k_d	Relative permeability in crack for unfrozen water	
k_r	Relative permeability for unfrozen water	
K	Absolute permeability of soil	m^2
K_b	Bulk modulus	$kg \cdot m^{-1} \cdot s^{-2}$
l	Latent heat of fusion at the bulk freezing temperature T_0	$m^2 \cdot s^{-2}$
$\mathbf{L}$	Transformation matrix between the local system and the global systems	
n	Porosity of soil	
$\mathbf{n}_\Gamma$	Unit outward normal vector to the boundary	
$\mathbf{n}_{\Gamma_d}$	Unit normal vector to the discontinuity Γ_d pointing to Ω^+	
p_c	Clapeyron pressure	$kg \cdot m^{-1} \cdot s^{-2}$
p_i	Ice pressure	$kg \cdot m^{-1} \cdot s^{-2}$
p_{ob}	Overburden pressure	$kg \cdot m^{-1} \cdot s^{-2}$
p_r	Pressure of water reservoir	$kg \cdot m^{-1} \cdot s^{-2}$
p_w	Water pressure	$kg \cdot m^{-1} \cdot s^{-2}$
$\mathbf{p}_w$	Nodal water pressure	$kg \cdot m^{-1} \cdot s^{-2}$
q_h	Velocity of heat flux	$m \cdot s^{-1}$
q_w	Velocity of water flux	$m \cdot s^{-1}$
r	The radius of ice adjacent to a pore	$m \cdot m^{-1}$
s_i	Ice saturation	
s_{i_d}	Ice saturation in crack	
s_w	Unfrozen water saturation	
s_{w_d}	Unfrozen water saturation in crack	
$s_{w_{res}}$	Residual unfrozen water saturation at temperatures below T_i	

S_{cry}	Cryogenic suction	$kg \cdot m^{-1} \cdot s^{-2}$
T	Temperature	K
$\hat{\boldsymbol{T}}$	Nodal temperature	K
T_0	Bulk freezing temperature	K
T_i	Temperature (below T_0) from which unfrozen water saturation in the crack starts changing	K
T_{ff}	Temperature for fully frozen condition	K
u	Displacement	m
$\mathbf{u}$	Nodal displacement	m
$\mathbf{w}_w$	Relative velocity of the water phase with respect to solid skeleton	$m \cdot s^{-1}$
$\mathbf{v}_i$	Absolute velocity of ice phase	$m \cdot s^{-1}$
$\mathbf{v}_s$	Absolute velocity of solid skeleton	$m \cdot s^{-1}$
$\mathbf{v}_w$	Absolute velocity of water phase	$m \cdot s^{-1}$
$\Im$	Deferential operator linking deformations and strains	
N	The set of enriched nodes	
M	The set of all nodes	
$\mathbf{J}$	Jacobian matrix	
$\mathbf{R}$	Residual vector	
Δt	Time step increment	s
$\| \ \|$	Euclidean norm	

Preface

This dissertation is submitted to the Norwegian University of Science and Technology (NTNU) in partial fulfillment of the requirements for the degree of philosophiae doctor. The work was carried out at the Geotechnical Division of the Department of Civil and Environmental Engineering at the Faculty of Engineering. The PhD Research Fellowship was a part of the PoreLab Center of Excellence, Thermodynamic Driving Forces, Work Package 5. This is a joint research project between the Geotechnical research group, the Road, Transport and Geomatics research group and the PoreLab Center of Excellence. It was supported by the Research council of Norway through its Centers of Excellence funding scheme, Project Number 262644 Porelab, and through Frost Protection of Roads and Railways project (FROST) under Grant Number 246826.

The main supervisor of this dissertation was Professor Gustav Grimstad at the Department of Civil and Environmental Engineering at the Faculty of Engineering at the Norwegian University of Science and Technology (NTNU). Dr. Seyed Ali Ghoreishian Amiri and Dr. Elena Scibilia, senior researchers in the same NTNU department, were co-supervisors. The initial idea and fundamental theory of this dissertation came from Professor Signe Kjelstrup, Principal Investigator of PoreLab Center of Excellence and professor at the Department of Chemistry at the Norwegian University of Science and Technology (NTNU).

The governing equations with solutions employing extended finite element method for the simulation were developed and inferred by the author based on the initial idea and fundamental theory. The simulation is implemented in Fortran 90, which is verified and then validated by comparing with the existing test results from Devon silt, which were reported by Konrad and Morgenstern (Konrad, 1980). The model had been improved and completed all through the coding process by the author, with the valuable inputs from all three supervisors and Professor Signe Kjelstrup.

Enjoy!

The committee for the appraisal of this thesis comprises the following members:

Professor Jelke Dijkstra (first opponent)
Chalmers University of Technology, Sweden

Associate Professor Claire Chassagne (second opponent)
Delft University of Technology, Netherlands

Professor Gudmund Eiksund
Norwegian University of Science and Technology, Norway

The supervisors of this study were:

Dr. Seyed Ali Ghoreishian Amiri
Norwegian University of Science and Technology, Norway

Professor Gustav Grimstad
Norwegian University of Science and Technology, Norway

Dr. Elena Scibilia
Norwegian University of Science and Technology, Norway

Abstract

The starting point of this work is a conceptual model for frost heave based on non-equilibrium thermodynamics. According to the theory, the temperature gradient in the soil under frozen condition is the main driving force for transport of water from the warmer (unfrozen or less frozen) soil towards the colder, partly frozen, soil volume. The tendency of water flow results in increase of pore water pressure close to the freezing front, which means a reduction in the effective stress. An ice lens can start to form after a crack appears. However, freezing front may continue moving forward, and the formation of active ice lens will stop when soil permeability behind freezing front dramatically decreases.

According to the conceptual model, a new fully coupled THM model is developed. The mass balance equation, energy balance equation and momentum balance equation are presented herein. In order to consider ice lenses, Extended Finite Element Method (X-FEM) is employed to solve the governing equations. The primary variables of the governing equations, i.e., displacement, water pressure and temperature are approximated according to the properties of discontinuities with shifted Heaviside function and modified level-set function.

The calculated results are compared with the available results of three lab scale one-dimensional freezing tests on Devon silt. These tests include one freezing test without overburden pressure and two freezing tests with different overburden pressure of 100 kPa and 45 kPa, and reasonable agreement is achieved.

Shut-off pressures is also estimated, and the results are as expected from the coupled transport equations.

Publication List

I   H. Gao, S. A. Ghoreishian Amiri, S. Kjelstrup, G. Grimstad, B. Loranger, E. Scibilia.
Formation and growth of multiple, distinct ice lenses in frost heave
International Journal for Numerical and Analytical Methods in Geomechanics, 2023, 47(1): 82-105.

II   S. Kjelstrup, S. A. Ghoreishian Amiri, and B. Loranger,H. Gao,G. Grimstad.
Transport coefficients and pressure conditions for growth of ice lens in frozen soil.
Acta Geotechnica, Volume:4/350 (2021).

III   S.A. Ghoreishian Amiri, G. Grimstad, H. Gao, and S. Kjelstrup.
Numerical modelling of distinct ice lenses in frost heave
IOP Conference Series: Earth and Environmental Science. IOP Publishing, 2021, 710(1): 012039.

IV   Lyu. C, S. A. Ghoreishian Amiri, H. Gao.
Joint Acoustic and Electrical Measurements for Unfrozen Water Saturation Estimate—A Review.
Cold Regions Engineering 2019, 2019: 26-34.

Contributions from the dissertation author to the listed publications above:

I   Author Hao Gao inferred the governing equations with solutions based on the initial idea and fundamental theory and then implemented with coding in Fortran 90; Performed simulation results interpretation and the comparison with the exist experience results; Drafted the manuscript.

II   Co-author Hao Gao contributed to the literature review and provided comments and feedback during manuscript refinement.

III   Co-author Hao Gao contributed to the inferred governing equations and solutions with preliminary results, which were in the middle stage of the current thesis work and provided comments and feedback during manuscript refinement.

IV   Co-author Hao Gao contributed to the literature review and provided some inputs to the section of comparison between electrical and acoustic models, provided comments during manuscript refinement.

Acknowledgement

From the very beginning of this work, many people were involved by providing support, guidance, and inspiration. Their continuous encouragement was of paramount importance in completing this research.

First of all, I would like to express my sincere thanks to my main supervisor, Professor Gustav Grimstad, for giving me the opportunity to take part in this project and thank to his inspiration and critical discussions on the research of the physical process based on non-equilibrium thermodynamic theory. His expertise was critical on shaping the boundaries and core of this project. Furthermore, his supervision style, always engaging, honest and with in-depth involvement, was a real asset to my cause. I am also grateful for our discussions and fun we had in both workplace and pubs, restaurants, barbeque events, conferences, and other places.

I would also like to thank my co-supervisor, Seyed Ali Ghoreishian Amiri, for his continuous guidance throughout this work. This research would not have been possible without him. Ali has always addressed my concerns about the fundamental theory, the establishment of governing equations, the advanced numerical method and the programming part with patience and offered significant guidance throughout this work. Throughout the Ph.D. period, I also encountered a lot of confusion, whether in research work or life, as well as depression, Ali will always come to me to encourage me, and use his own experience to help me see the challenges that I will face and let me be prepared. Ali has set an example to me both as a person and as an academic, and his guidance on various aspects was invaluable.

I would also like to thank another co-supervisor, Elena Scibilia, for her patient guidance on my work. I am also grateful for her support with various matters while I studied in NTNU, and suggestions for my Ph.D and future development. I still remember our first meeting, which is at Cafe-Sito Stripa in NTNU campus. During that conversation, her caring and considerate dispelled my worries of the unknown in my PhD career and helped me have an overall plan for my future development, which has made a great start for my three years of work and life in Norway.

I would also like to thank Professor Steinar Nordal for his essential discussions during the initial theoretical framework construction, as well as his super-high level of teaching ability to explain profound theories in simple language, which has helped me a lot in the process of entering this new field. I would also like to thank Professor Gudmund Reidar Eiksund for all his support and meticulous help to my project and life here, and all the information he provided in the lunchroom and offices, which is always interesting, funny, and useful.

Special thanks go to Professor Signe Kjelstrup for her guidance and encouragement on my work, and her proposed non-equilibrium thermodynamic theory which makes this model can be achieved. I am also grateful for accommodating me with an office at PoreLab. I would also like to thank Marie-Laure Olivier for all the help with various matters while I was at PoreLab.

Further, I would like to thank my Ph.D. colleagues in Geotechnical Engineering group and PoreLab for all the time we had together. For all the discussions we have had, whether academic or not, I would like to thank Chuangxin Lyu and Davood Dadrasajirlou especially. I would also like to give a special appreciation to Marit skjåk-Bræk for helping me at the beginning of my Ph.D. with administrative issues.

I would also like to thank my parents and my brother for their belief in this adventure.

My daughter, my heart sweety Xiaoran, for your accompaniment over the years, I am deeply grateful.

Finally, thanks to Ying, my dear partner, with whom I have lived this adventure. Thanks for all the things you have done as a wife, a mother, and a daughter, and for encouraging me at the most difficult moments. Thank you for all the support you have given me over all these years, for believing in me.

<div align="right">

Hao Gao
Oslo, 2024.03

</div>

Chapter 1   Introduction

1.1 Background and Motivation

Frost heave is one of the major concerns in earthwork engineering in areas that experience seasonal frost. Its occurrence is often accompanied by severe damage to infrastructure influencing the construction cost, safety, serviceability, durability, and maintenance costs. Figure 1 shows two roads in Norway damaged by frost heave.

Figure 1 The damage to the road by frost heave. The left photo was taken at Vikevegen, from http://vikebygd.org. The right photo was taken at road FV26 in Norway, by Lars Andreas Solås.

According to Zhang et al. (Zhang et al., 1999), nearly 60% of the land area in the northern hemisphere is coved by permafrost and seasonal frozen soil. Figure 2 shows the distribution of permafrost and seasonally and intermittently frozen ground in the Northern Hemisphere. Each year, a large part of the fiscal expenditures of the governments in these areas are used to mitigate the impact from soil freezing. In the United States, the cost of repairing road damage caused by frost heave alone requires more than two billion dollars per year (DiMillio, 1999). From another perspective, from 2011 to 2016, 16 million drivers in the United States suffered damage from potholes which is largely due to frost heave, and this also cost three billion each year. The British government estimates that it will cost £12 billion to fix all roads with potholes in the country (Jeekel, 2012). Thus worldwide, the cost is tremendous. Generally, cold climate countries must deal with the impact of road deterioration which is mainly a result of frost heave. In Scandinavia countries such as Norway, this accounts for about 30% of the maintenance budget (Committee, 2010).

With the shift of the strategies of countries around the world, the north frigid zone, which stores amazing resource (Spohr et al., 2021) but is very sensitive to climate and environmental changes, is getting more and more attention. In other words, the situation that a large area of permafrost is transformed into seasonal frozen soil caused by global climate change will become a huge obstacle to our development. According to the report of Snow, Water, Ice and Permafrost in the Arctic (SWIPA) (Monitoring, 2017), In the past 50 years, the Arctic has been warming at more than twice the rate of the entire world. Monitoring of

permafrost in Svalbard has been going on since 1998 (Norway, 2018), and the results show that the temperature on average has increased 0.8 °C per decade in the upper part of the permafrost. The active layer has become 25-30 cm thicker since 1998, which makes the ground more unstable and become an ineligible threat to buildings and other infrastructure. Research on frost heave is necessary and meaningful.
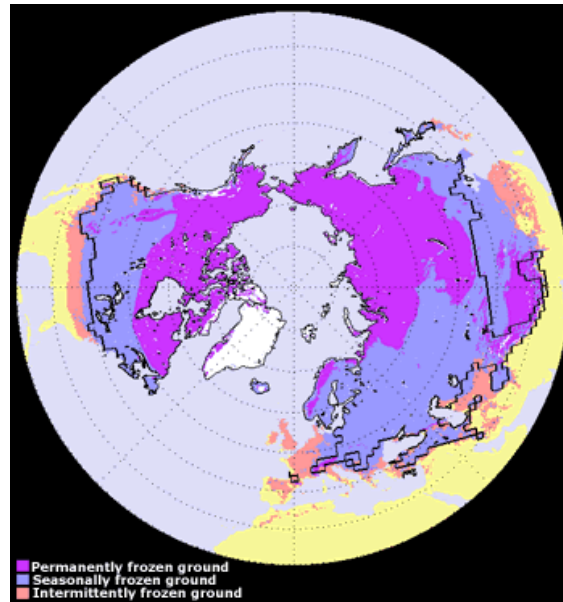
Figure 2 Distribution of permafrost and seasonally and intermittently frozen ground in the Northern Hemisphere(Brown et al., 1997).

Frost heave refers to the upwards movement of the ground surface due to formation of ice lens within fine-grained soils. According to Taber (Taber, 1930), frost heave mainly due to water migration from the unfrozen volume to the frozen volume of the ground. The research on frost heave has lasted more than a hundred years since the phenomenon was observed in 1914 by arctic explorer Nansen (Nansen, 1914). Afterwards, Taber (Taber, 1929) and Beskow (Beskow, 1930), as the first to study the process of frost heave and did some experiments, have a profound influence on later researchers in this area. Up until now, a number of experimental investigations have been conducted, which varies from small-scale one-dimensional tests (Konrad, 1980; Penner, 1986) to large-scale three-dimensional (Williams et al., 1993) cases.

While more and more researchers have been attracted to the field, various models for frozen soil have been proposed to predict the growth of ice lenses with their own strength and limitations. The process of soil freezing, especially accompanied with the formation of ice lenses, involves complex thermal, hydraulic, and mechanical processes which are strongly coupled to each other. The main thermo-hydraulic-mechanical (THM) interactions considered are illustrated in Figure 3. In addition to the complexity of the fully coupled processes, the discontinuity caused by ice lens formation must be taken into account for modelling the freezing process, without mentioning the inherit nonlinearity. Furthermore, due to the difficulty

of probing directly the pore-scale effects for model validation (Xu et al., 2008), there is no conclusive model to simulate the phenomena.

Thermal conduction considering latent heat

Thermal

Heat transfer due to water convection considering latent

Thermal expansion: volumetric expansion due to phase change

Water transfers due to thermal gradient (yielded by non-equilibrium thermodynamic theory) considering latent heat

Heat content change due to volumetric strain

Hydraulic

Effective stress changes due to pore pressure change due to volumetric strain

Mechanical

Hydraulic conduction

Pore pressures change due to volumetric strain

Force equilibrium

Figure 3 Thermo-hydro-mechanical interaction mechanism in soil freezing [After Thomas et al., 2009].

There is common believe among some geotechnical engineers that there is a tremendous suction in the frozen area which contributes to transport of water and frost heave phenomena (Ghoreishian Amiri et al., 2016; Nishimura et al., 2009). However, previous studies at NTNU measured only a few kPa of suction, which is much smaller than the suction predicted by capillary models (Holten, 2017). This large discrepancy prompts us to re-examine these existing frozen soil theories. At this time, the accuracy of the prediction results obtained based on non-equilibrium thermodynamic theory (Kjelstrup & Bedeaux, 2008) fully reflects the superiority, which explains not only the phenomenon in the terms of physical processes. An improvement on the description of soil freezing process and more accurate prediction of frost heave can be expected using the discrete theory of non-equilibrium thermodynamics. At present, since there is no practical model that fully considers the coupled thermo-hydro-mechanical process based on this theory, it is necessary to establish a systematic model. Therefore, the motivation to investigate and assess the new THM model for ice lens formation is clear.

Based on the above, the project started as a joint research project between the PoreLab Center of Excellence and the Geotechnical research group, NTNU.

1.2 Research objectives

The main objectives of the PhD project are:

- Provide a better understanding of the physical processes behind the frost heave phenomenon.

- Develop a coupled THM model for the phenomenon

- Defining a mechanical criterion introducing the onset of ice lens formation.

- Developing a discontinuous solution of the governing equations that takes into account the growth of distinct ice lenses inside the system.

1.3 Research methodology

Firstly, a comprehensive literature review has been conducted to get the big picture of the topic, and the following points are focused on:

- Coupled mass and heat transport equations using non-equilibrium thermodynamics.

- Governing equations of the system at global level.

- Constitutive modelling of frozen soils.

- Numerical modelling of frost heave phenomenon.

Based on the literature review, the main shortcomings of the current theories are highlighted: the physical mechanism behind the frost heave phenomenon, and the continuum-based solution of the governing equations.

After that, the governing equations of the system are modified based on the non-equilibrium thermodynamics. Non-equilibrium thermodynamics helps us to find the actual driving forces of the transports in our system of concern. These transport equations are then coupled with the mechanical equations through global force balance equations, and local constitutive equations for soil behaviour and crack propagation.

The governing equations are discretized and solved in a discontinuous domain. The extended finite element method is used for this purpose.

The developed model is then implemented in a computer program to provide a scientific computer simulator. The model is verified using the existing laboratory measurements.

1.4 Scope of the work

1.4.1 Scope of the work

To achieve the objectives stated above, the scope of work is defined as follows:

- Literature review of the existing models on frozen soil including the driving force for frost heave, constitutive modelling, and numerical solution of the governing equations.

- Deriving the governing equations of the system including mass, energy, and force balance equations by considering thermodynamic driving force for mass and heat fluxes.

- Describing the mechanical behavior of frozen soil including crack (segregation) criterion.

- Numerical discretization of the governing equations using the extended finite element method.

- Implementation of the numerical solution in a computer program.

- Verification of the proposed model with experiments measurements.

1.4.2 Issues outside the scope of work

The following issues are outside the scope of the work:

- Unsaturated conditions will not be considered in this study.

- The hysteretic nature of soil freezing curve will be not considered in this study.

1.5 Outline of the dissertation

This dissertation has seven chapters including this introductory chapter, which covers the background and motivation of the research. In addition, the objectives, methodology, and scope of this dissertation are also given here. An outline of the other seven chapters is given below.

Chapter 2 contains two parts which are the history of frozen soil theory development and the literature review regarding the models for prediction of frost heave. The first part

introduces different theoretical hypotheses dominated in different periods, including the capillary theory, revised capillary theory and frozen-fringe models. In the second section, only the relevant topics to this work are selected and presented, although a wide range of literature in relation to frost heave is available.

Chapter 3 presents the non-equilibrium thermodynamic theory as a theoretical support of our model and describes the concept of the model using schematic diagrams. It gives a macroscopical description of the coupled mass and heat flux and the required parameters to model the coupled transport process.

Chapter 4 presents the three governing equations: mass balance equation, energy balance equation and force balance equation. In addition, a literature review regarding mechanics criterions of initiation of ice lens is given. At the end, the one-dimensional stress (crack) criteria employed in the model is presented.

Chapter 5 gives a discussion about the necessity of employing Extended Finite Element Method (X-FEM) instead of classical FEM, and presents a review of X-FEM. After that, the weak forms of the three governing equations obtained in previous chapter is discretized by X-FEM and fully implicit first order accurate finite difference scheme. Consequently, the system of fully coupled non-linear equations are solved by the Newton-Raphson procedure.

Chapter 6 gives three simulation cases based on Konrad's tests on Devon silt(Konrad, 1980), and compares the calculated and test's results, which shows a reasonable agreement. After that, the shut-off pressure is estimated based on the three tests data. Some conclusions are obtained.

Chapter 7 summarizes and concludes the work conducted during this Ph.D. period.

Chapter 8 gives recommendations for future work.

Chapter 2   State of the art

2.1 Introduction

2.1.1 Description

As the first to carry out experimental research on frost heave associated with ice lens formation, Stephen Taber demonstrated basic characteristics of frost heave in soils (Taber, 1916, 1929, 1930). As Figure 4 shows, excessive heaving is the result of water transport which pulls through the soil to build up layers of segregated ice. The conclusion of Taber's tests indicated that ice lenses, which deposits as bands of pure ice, led to almost unlimited heave of the soil surface as they grow, as long as the temperature is lower than the normal freezing point of bulk water and there is enough water supply (Beskow, 1930; Taber, 1930). Subsequent researchers are still actively working on exploring and simulating the frost heave, aiming to explain the physical processes behind and propose theoretical models to accurately predict the height of frost heave.
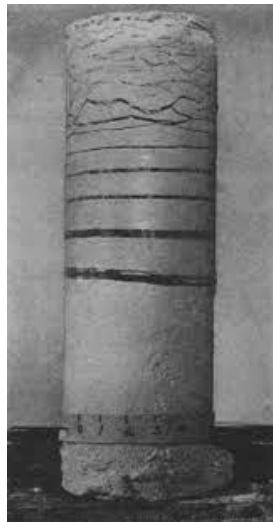
Figure 4 Distinct ice lenses from Taber's test(Taber, 1930).

Therefore, any quantitative models must inevitably explain the formation and growth of ice lens, which should include the movement of water and the mechanism of soil grains segregation. For nearly a century, there have been several different widely accepted theories on this issue. Among these theories, there are mainly two categories, one is based on capillary theory and another one relies on frozen-fringe theory.

2.1.2 History of frozen soil theory development

Taber proposed an explanation for frost heave in 1930 (Taber, 1930), which was quantitatively supported by Beskow (Beskow, 1930), Gold (Gold, 1957) and Jackson et al. (Jackson et al., 1966). They believed that water transport is due to the suction on the interface of ice and water, that caused by the decrease of Clapeyron pressure required to keep the system at thermodynamic equilibrium during freezing.

According to the Clapeyron equation which describes the thermodynamic equilibrium in a system at temperature T containing ice at pressure p_i and water at p_w (Prigogine & Defay, 1954):

$$p_i - p_w = \frac{\rho_w l}{T_0}(T_0 - T)$$
(2.1)

where l is latent heat of fusion at the bulk freezing temperature T_0, and p_w is the density of water, and ρ_i is the density of ice. The term $\Delta p(\frac{\rho_w}{\rho_i} - 1)$ has been neglected as it is minor comparing to the other terms.
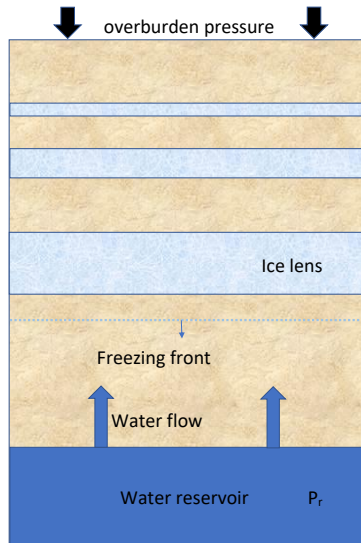
Figure 5 A column of frozen soil with ice lenses and water reservoir [After Peppin 2013](Peppin & Style, 2013).

Figure 5 illustrates a column of frozen soil connected to a water reservoir with pressure p_r (Jackson & Chalmers, 1958). The whole system is isothermal with temperature $T < T_0$. We can obtain the water pressure for keeping the system at thermodynamic equilibrium from equation (2.1):

$$p_c = p_i - \frac{\rho_w l}{T_0}(T_0 - T) \tag{2.2}$$

which we call the Clapeyron pressure, p_c. Normally the pressure of ice p_i depends on the overburden pressure, which is assumed to be a constant here. Before freezing starts, we set $p_r = p_c$, which makes the system equilibrium with no water flow.

When the soil is subject to freezing, p_c will decrease due to reduced temperature as equation (2.2) shows. As a result, water will transport from water reservoir, which has relatively higher pressure, towards the ice lens. Laboratory tests (Biermans et al., 1978; Ozawa & Kinosita, 1989; Radd & Oertle, 1973) also demonstrated that the frost heave can be stopped by either decreasing the reservoir pressure or increasing the overburden pressure to satisfy the equilibrium condition $p_r = p_c$.

To apply the capillary theory properly, an essential assumption has been made that ice does not immediately invade into the pores. The hypothesis is reasonable based on the Young–Laplace equation that relates the pressure difference to the shape of the contact surface between two static fluids (Defay et al., 1966; Everett, 1961):

$$p_i - p_w = \frac{2\gamma_{iw}}{r} \tag{2.3}$$

Where γ_{iw} represents the ice–water surface energy and r is the radius of ice adjacent to a pore, as is shown in Figure 6. The Young–Laplace equation indicates that a maximum pressure difference exists, which allows ice penetrates into soil pores and stops frost heave:

$$\Delta p_{max} = \frac{2\gamma_{iw}}{r} \tag{2.4}$$

by which we can get a maximum overburden pressure $p_{max} = p_r + \frac{2\gamma_{iw}}{r}$, because of the water pressure in the soil satisfying $p_w < p_r$.
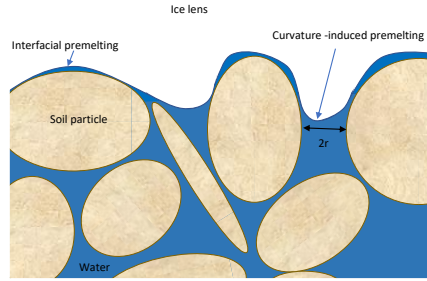
Figure 6 Microscopic view of the ice-water interface, r is half the distance between two adjacent particles.

The experimental results have also confirmed the existence of a maximum pressure, which seems to validate the capillary theory (Gaskin & Sutherland, 1973; Loch & Miller, 1975; Penner, 1959). However, a minimum temperature can also be obtain by substituting equation (2.1) to equation (2.4):

$$T_{\min} = T_0(1 - \frac{2\gamma_{iw}}{\rho_w lr}) \tag{2.5}$$

which indicates that frost heave stops once $T \leq T_{\min}$ since the pore ice clogging the water flow tending to feed the ice lens. However, Miller (Miller, 1972) and Harlan (Harlan, 1973) proposed that ice lenses would also be formed at temperature $T \leq T_{\min}$, and the experiments of Cahn et al. (Cahn et al., 1992) showed that a low-speed flow existed in the partially frozen region of the soil at this temperatures. Apart from this contradiction, the mechanism for the initiation of new lenses cannot be explained by capillary theory (Miller, 1977). Although these deficiencies of this theory were substantially solved later, some researchers put forward another hypothesis at that time, frozen-fringe theory.

Based on frozen-fringe theory, the slow water transport in fringe is owing to thermomolecular pressure gradients in the premelted films (Dash, 1989; Rempel et al., 2004). Wilen et al. carried out a test which simulated the frozen fringe and measured the flow in the premelted films to verify this theory (Wilen & Dash, 1995). Herlan derived a system coupled equations for heat and mass transport (Harlan, 1973). Afterwards, some quantitative models have been proposed, which had good agreements with the experimental results (Wettlaufer & Worster, 1995; J. Wettlaufer & M. G. Worster, 2006).

The frozen-fringe theory provided a potential resolution to the limitations of capillary theory. For instance, it allows lager values of maximum overburden pressure $p_{\max}$, which can explain the significantly larger heaving pressures e.g. reported by Penner (Penner, 1967) and Loch (Loch & Kay, 1978). It also provides a mechanism for initiation of new lenses which can happened in the fringe zone ahead of the growing lens (R. R. Gilpin, 1980; Miller, 1972, 1977;

O'Neill & Miller, 1985). The frozen-fringe concept laid the foundation for a lot of theoretical development in later works (Bronfenbrener & Korin, 1997; Fowler, 1989; Fremond et al., 1985; Ghoreishian Amiri et al., 2016; R. R. Gilpin, 1980; Hopke, 1980; Horiguchi, 1987; Hromadka II et al., 1981; Konrad & Morgenstern, 1980; Konrad & Duquennoi, 1993; Li et al., 2002; Michalowski, 1993; Nakano, 1990; Nishimura et al., 2009; Nixon, 1991; Rempel et al., 2004; Sheshukov & Egorov, 2002; Takagi, 1980; Talamucci, 2003; Thomas et al., 2009; Walder & Hallet, 1985).

2.2 Literature review

Harlan (Harlan, 1973) might be mentioned among the first that proposed a set of combined equations to express the coupling between mass transport and heat flow in partially frozen soils. His model showed a decrease in water flow rate with increasing depth to the water table and increasing proportion of finer particles in the soil. However, Harlan's model did not permit the formation of discrete ice lenses.

In a series of papers, Konrad and Morgenstern (Konrad, 1980; Konrad & Morgenstern, 1982; Konrad & Morgenstern, 1980, 1981), defined the concept of segregation potential (SP) as the ratio of water intake-flux to temperature gradient. However, this model indicates that the heave rate is not sensitive to cooling rate, which is inconsistent with the experimental and field observation (Konrad, 1989; Zhao et al., 2014). And that model didn't take into account the effect from the overburden pressure and suction. In addition, the SP model has a semi-empirical nature and does not explicitly formulate the SP coefficient in terms of more fundamental soil characteristics like soil freezing characteristic curve. Konrad (Konrad & Duquennoi, 1993) improved the SP model in 1993 with considering the overburden pressure effect, based on the thermodynamic equilibrium of open system freezing. Moreover, this model also takes into account the initiation of new ice lens by introducing a criterion which is the failure strain of the frozen soil. However, this model is not easy to establish because of the difficulty of obtaining appropriate input values. Other shortcomings of Konrad's model were summarized by Nixon (Nixon, 1991).

Miller (Miller, 1972, 1977; Miller & RD, 1978) and O'neil (O'Neill & Miller, 1985) put forward a concept of secondary heaving, which occurs when the freezing extends below the nominal base of the distinct ice lens. In Miller's theory, mass transport in frozen fringe is owing to the presence of liquid water films between bulk ice and soil grains. Water flow is enhanced and dominated by the movement of solid ice in this zone, and the direction is determined by the temperature gradient. The ice existed in both ice lens and connected soil pores is seen as a continuous rigid solid, moving as a whole in the thermal field, which is driven by regelation process. Miller et al. (Miller et al., 1975) also derived the detailed formulations of what they called series-parallel transport of liquid water and solid ice in the frozen fringe between the growing lens and the unfrozen soil. Moreover, Miller (Miller, 1972, 1977; Miller & RD, 1978) presented an effective stress-based criterion to find the position and onset of ice lens formation using a semi-empirical stress partition function ϕ, as equation (2.6) shows blow:

$$\sigma_e = \sigma_t - (1-\phi)p_i - \phi p_w \tag{2.6}$$

in which σ_e is the effective stress and σ_t is the total stress, p_i and p_w are ice pressure and water pressure respectively.

Based on the regelation theory, Gilpin (R. Gilpin, 1980; R. R. Gilpin, 1980) proposed a frost heave model as a function of basic soil properties, heat conductivity, grains size, external boundary conditions, freezing temperature and overburden pressure. Furthermore, from the aspect of free energy principle, the driving force of water flux in fringe was expressed in term of both pressure gradient and temperature gradient, which also has been verified by Gilpin's test (R. R. Gilpin, 1980), and the equation for calculation of water flux is showed below:

$$q = -k \frac{\upsilon_i}{\upsilon_w} \frac{d}{dz}[p_i + \frac{lT}{\upsilon_s T_0}] \tag{2.7}$$

where q is flow rate, and k presents hydraulic conductivity of the soil. υ_i and υ_w are the specific volumes of ice and water, p_i is the bulk ice pressure. And l is latent heat of fusion at the bulk freezing temperature T_0. Apart from this, a criterion based on the ice pressure required to separate the soil particles was presented for initiation of ice lens.

Nixon (Nixon, 1991) proposed a model on the base of Gilpin's studies (R. R. Gilpin, 1980), taking into account the distributed phase change in frozen fringe, which made the interaction between mass and heat transfer more sensible. However, in this model there is an assumption that the phase change of in-situ pore water only takes place at the bulk water freezing temperature, and the temperature profile is linear in the frozen fringe zone. Moreover, it had another assumption that there is no phase expansion for pore water changing to ice, and the rate of water flow in pores is a constant in the frozen fringe.

In addition to Miller (Miller & RD, 1978), irreversible thermodynamics was also applied by Derjaguin and Churaev (Derjaguin & Churaev, 1978, 1986, 1993; Derjaguin et al., 1981, 1993), and Førland and Kjelstrup Ratkje (Førland & Ratkje, 1982; Ratkje et al., 1982). Their approach is macroscopic, so it only correlated macroscopic measurable parameters. They proposed a set of equations which coupled mass and heat flux yielded by irreversible thermodynamics, which has the following form:

$$q_w = -\bar{L}_{21}\Delta \ln T - \bar{L}_{22}\Delta\mu_{iT} \tag{2.8}$$

$$q_h = -\bar{L}_{11}\Delta \ln T - \bar{L}_{12}\Delta\mu_{iT} \tag{2.9}$$

where q_w and q_h are water flux and heat flux, and μ_{iT} is the difference in chemical potential of the ice due to changes in composition and pressure through the frozen fringe. This approach doesn't need to assume local equilibrium in the fringe. The temperature gradient over the region led to a water flux, which in turn causes a build-up of pressure gradients, see Figure 7.

Rempel et al. (Rempel, 2007; Rempel et al., 2001; Rempel et al., 2004) emphasized more on the microscopic physics that drives the frost-heave process, as the disjoining pressure

between ice and soil grains leading to premelted fluid to migrate and feed ice growth. Figure 8 shows the thermal regelation of a single particle: A thin water film is formed because the total energy of ice-water interface and water-grain interface is less than the surface energy of ice-grain interface. The thinner premelted film with larger disjoining pressure in the colder side will push the substrate towards the warmer side, resisted by the water flow in the premelted film from the front of the particle towards its rear (Rempel et al., 2004; You et al., 2021). The model applied a force balance on grains in the fringe to distinguish parameter regimes for single ice layer, multiple ice layers and pore ice without ice lens. An effective stress-based criterion was employed for the start of soil particles segregation. They obtained a similar formulation to Førland and Kjelstrup Ratkje (Førland & Ratkje, 1982; Ratkje et al., 1982) from a very different approach.
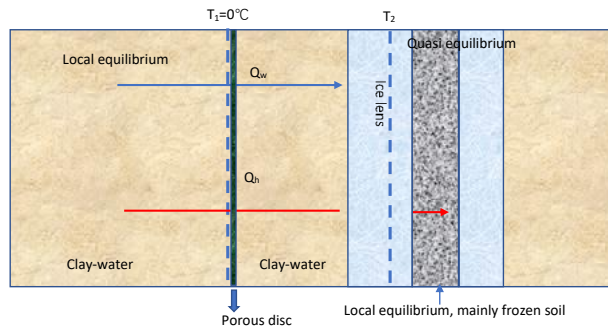
Figure 7 The frost heave situation. Bulk ice is allowed to form at T_2, The pressure gradient is developed across the region of transport. A porous disc is inserted to resist the pressure. [After Kjelstrup 1981].

Nishimura et al. (Nishimura et al., 2009) proposed a fully coupled THM model for freezing and thawing process of frozen soil, by applying net stress, which is defined as the excess of total stress over ice pressure, and the cryogenic suction as the two main stress variables. His model is at constitutive level and simulates the heave as a result of plastic dilation. According to this model, the initiation of ice lens starts once net stress becomes zero as ice pressure increasing. And it can also simulate the soil behavior in unfrozen state by replacing ice pressure with water pressure, which is also available for thawing process modelling. Zhou(Zhou, 2014) proposed another two stress-variable based model for frozen soil, adopting the temperature in the freezing process and net pressure. In addition, by raising the strength of the microstructure of a mixture, the dependency of the failure criterion on temperature and ice content of frozen soil was obtained in this model. Zhang and Michalowski (Michalowski, 1993; Michalowski & Zhu, 2006; Zhang & Michalowski, 2015) also presented another THM model for frost heave simulation, by introducing a porosity rate function which can simulate the growth of ice lenses as an average growth in porosity. The effective stress (total stress minus water pressure) and pore ice ratio (the ratio of the volume of ice on the volume of solid particles) were employed as two main variables for the constitutive model. However, when the unfrozen

water content tends to zero, this kind of effective stress would lead to a higher effective confining pressure than the reality. Ghoreishian Amiri et al. (Ghoreishian Amiri et al., 2016) proposed another constitutive model for frozen soil with two independent stress variables, by dividing the total stress into fluid pressure and solid phase stress, accompanied with cryogenic suction. These approach from Nishimura (Nishimura et al., 2009), Ghoreishian Amiri (Ghoreishian Amiri et al., 2016), Zhang (Zhang & Michalowski, 2015) and Michalowski et al. (Michalowski, 1993) are popular among geotechnical engineers, since it is relatively easy to be implemented in the existing computational codes, and at the same time, is able to produce reasonable results. However, samples that have experienced a tensile failure will always have a tendency of volume expansion under shearing, so these models do not follow the actual physic of the problem.
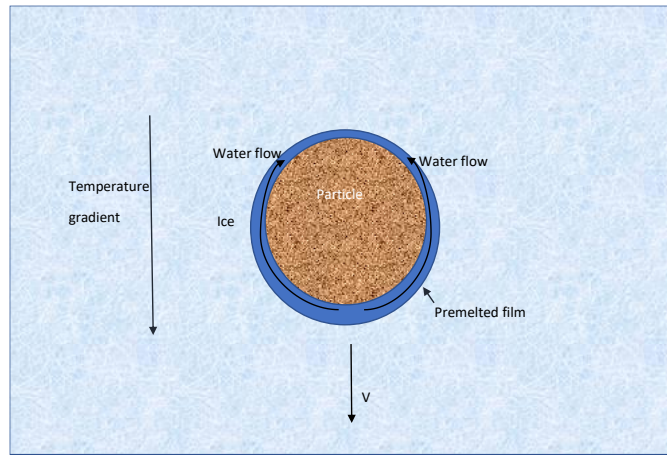
Figure 8 A schematic diagram of a particle that is separated from ice by a premelted film and held within a temperature gradient ∇T. The thickness of the premelted film is thinner on the colder side, which makes it possible to push the particle towards warmer zone.

Thomas et al.(Thomas et al., 2009) investigated the THM behavior of soils under freezing and thawing, and proposed a coupled THM model for soil freezing and ice segregation processes based on traditional theory of frozen soil mechanics, considering both one-sided freezing (freezing is from the surface downwards) and two-sided freezing (freezing from the permafrost table upwards and from the ground surface downwards).

Lu et al. (Lu et al., 2011) proposed a phase field model on the basis of the mixture theory and phase field theory. In this model, an assumption that both the solid skeleton and pore fluid will undergo phase transition was made. Moreover, the memory effect associated with phase change was considered by assuming Stieltjes integral for the strain energy of the porous medium. Zhou and Li (Zhou & Li, 2012) presented a concept of "separating void ratio" to distinguish the initiation of ice lens, and proposed a coupled THM model for saturated frozen soils. Liu (Liu et al., 2018) presented an elastoplastic theory for saturated freezing soils based on thermoporomechanics. The frozen soils are described as an open thermodynamics continuum.

Li et al. (Li et al., 2000) proposed a heat-moisture-deformation (HMD) coupled model, considering the force interaction between the soil skeleton and ice particle, and the energy jump behaviors during the phase change. Lai et al. (Lai et al., 2014) proposed a coupled THM model based on a series of experiments they carried out. Furthermore, a comprehensive criterion for determining where and when new ice lenses can form has been presented, which is related to initial porosity, soil compression, temperature gradient and overburden pressure etc.

Chen et al. (Chen et al., 2020) presented a coupled THM model for the dynamic process of soil freezing with a criterion in terms of flux rate. In this work, the long duration for forming a water-resisting layer, which consist of soil grains and ice crystals, is considered as an essential requirement for the formation of ice lenses before the final ice lens. The unfrozen area closed to active ice layer will be compressed, which leads to a decrease of void ratio in unfrozen zone. As a result, the growth of ice lens stops when the void ratio is less than the critical value. In his model, the role of temperature gradient in the freezing process is also highly valued.

Chapter 3   The conceptual model for frost heave

3.1 Non-equilibrium thermodynamic

In this chapter, the model for frost heave from Konrad and Morgenstern (Konrad, 1980; Konrad & Morgenstern, 1982), is used to describe the frost heave process. As Figure 9 shows, the frozen soil can be divided into three layers: (1) the frozen zone behind the active ice lens, (2) a partially frozen layer in front of the active ice lens, which is called frozen fringe, (3) the unfrozen zone at the bottom.
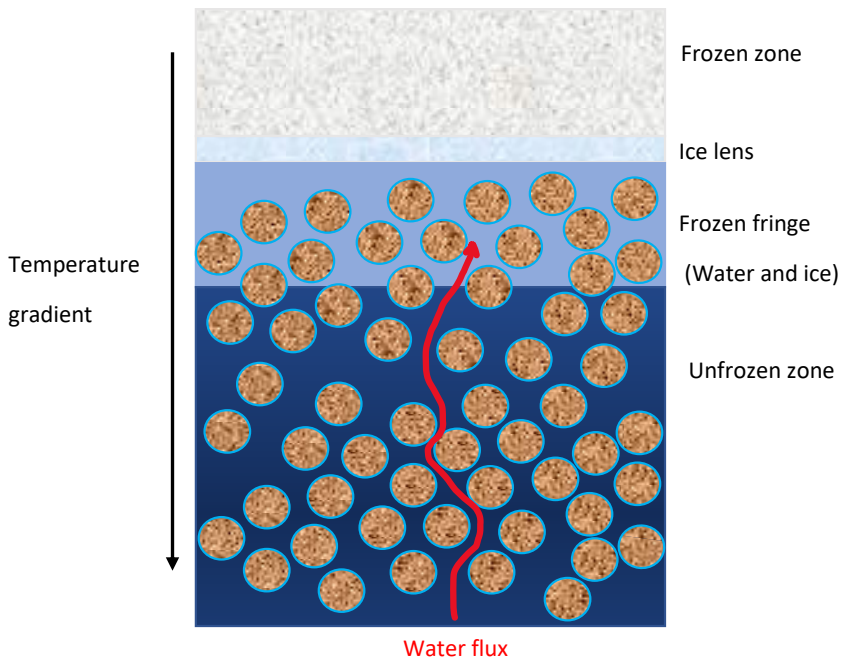
Figure 9 Schematic illustration of three layers in freezing soil.

In the frozen zone and unfrozen zone, the simple laws of Darcy's and Fourier's are adopted. In the frozen fringe that includes includes water–ice phase transitions at both boundaries, according to Førland and Kjelstrup Ratkje et al. (Kjelstrup et al., 2021; Kjelstrup & Bedeaux, 2008), the coupled water and heat flux can be described using non-equilibrium thermodynamics for a water-saturated sample in the absence of solutes, as given by equations (3.1) and (3.2).

$$q_w = \upsilon_w L_{wH} \frac{\Delta(T^{-1})}{\Delta z} - L_{ww} \frac{\upsilon_w}{T_0} \frac{\Delta\mu_{w,T_0}}{\Delta z} \tag{3.1}$$

$$q_H = L_{HH} \frac{\Delta(T^{-1})}{\Delta z} - L_{Hw} \frac{1}{T_0} \frac{\Delta\mu_{w,T_0}}{\Delta z} \tag{3.2}$$

where the thermal driving force $\Delta(T^{-1})/\Delta z$ is the main driving force for heat transport, while $\frac{1}{T_0} \frac{\Delta\mu_{w,T_0}}{\Delta z}$ is the main driving force for the mass transport, $\Delta\mu_{w,T_0}$ is the difference in chemical potential of the water from the pressure change in T_0, which can be described as:

$$\Delta\mu_{w,T_0} = \upsilon_w \Delta(p_w - \frac{1}{\upsilon_w} gz) \tag{3.3}$$

where υ_w is the specific volume of water, while Δp_w is the difference between the pressure below the ice lens and the pressure at the water table. Derjaguin and Churaev (Derjaguin & Churaev, 1978, 1986, 1993; Derjaguin et al., 1981, 1993) has indicated that equations (3.1) and (3.2) describes the mass and heat transportation macroscopically, without taking into account the disjoining pressure. According to the Onsager reciprocal relations (Onsager, 1931), the coefficient matrix of the coupled equation of heat and mass is symmetric, which means $L_{Hw} = L_{wH}$, when they are written in the special form dictated by the entropy production (Kjelstrup & Bedeaux, 2008). In addition, $L_{HH}L_{ww} - L_{Hw}L_{wH} \geq 0$ should be satisfied according to the second law of thermodynamics (Kjelstrup & Bedeaux, 2008). The transport coefficients can be determined as described in details in Kjelstrup et al. (Kjelstrup et al., 2021), and the equations can be rewritten accordingly:

$$\mathbf{q}_w = -\frac{k_r K}{\mu_w} (\frac{\Delta p_w}{\Delta z} - \rho_w \mathbf{g}) - \alpha \frac{k_r K}{\mu_w} \frac{\rho_i l}{T} \frac{\Delta T}{\Delta z} \tag{3.4}$$

$$\mathbf{q}_H = -\alpha \frac{k_r K}{\mu_w} \rho_i l \, (\frac{\Delta p_w}{\Delta z} - \rho_w \mathbf{g}) - \left(\lambda_s^{1-n} . \lambda_w^{ns_w} . \lambda_i^{ns_i} \right) \frac{\Delta T}{\Delta z} \tag{3.5}$$

where $\mathbf{q}_w$ is the relative velocity of the water phase, $\mathbf{q}_H$ is conductive heat flux, n is the porosity, ρ_i denotes ice density, s_w and s_i refer to the unfrozen water saturation and ice saturation, $\mathbf{g}$ denotes the gravitational acceleration, K is the absolute permeability, μ_w is the dynamic viscosity of water, k_r denotes relative permeability for unfrozen water, λ_α is the thermal conductivity of each phase, and α is a parameter.

3.2 Model concept

The frost heave model can be conceptually illustrated by Figure 10. Here one can consider a one-dimensional saturated, solute-free soil column with a free access to water from the bottom boundary. When the soil column is subjected to freezing from the top boundary (Figure 10 (a)). An upward water flux is expected, according to the second term in equation (3.4). However, it will be limited by the deformability of the soil body. Accordingly a downward pressure gradient will appear in the system to cancel the temperature-gradient-induced water flux, according to the first term in equation (3.4). As a result, pore water pressure in the frozen fringe will increase, and consequently the effective stress will decrease. At some point, the effective stress will be small enough to introduce a crack in the fringe (Figure 10 (b)). From this point, the temperature-gradient-induced water flow is able to migrate freely to this crack and introduce a growing ice lens to the system (Figure 10 (c)). More penetration of the freezing front will lead to a dramatic decrease of the relative permeability in front of the ice lens. Consequently, the growth of the ice lens stops (Figure 10), while the freezing front moves forward. This mechanism will become operational again, and another crack/ice lens might be introduced (Figure 10 (e) and Figure 10 (f)).

(a)   (b)
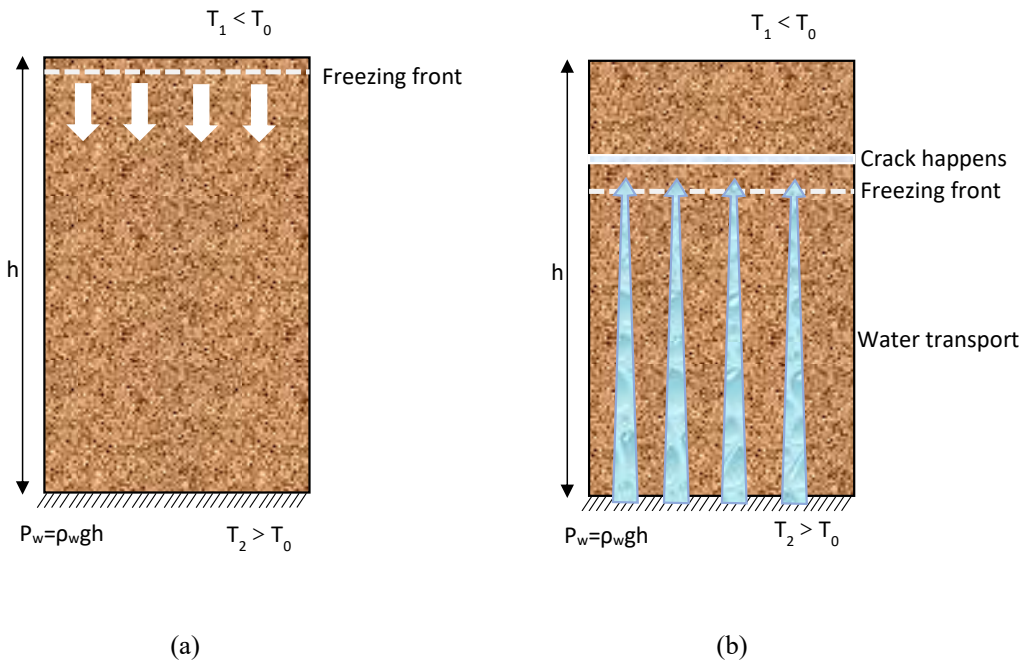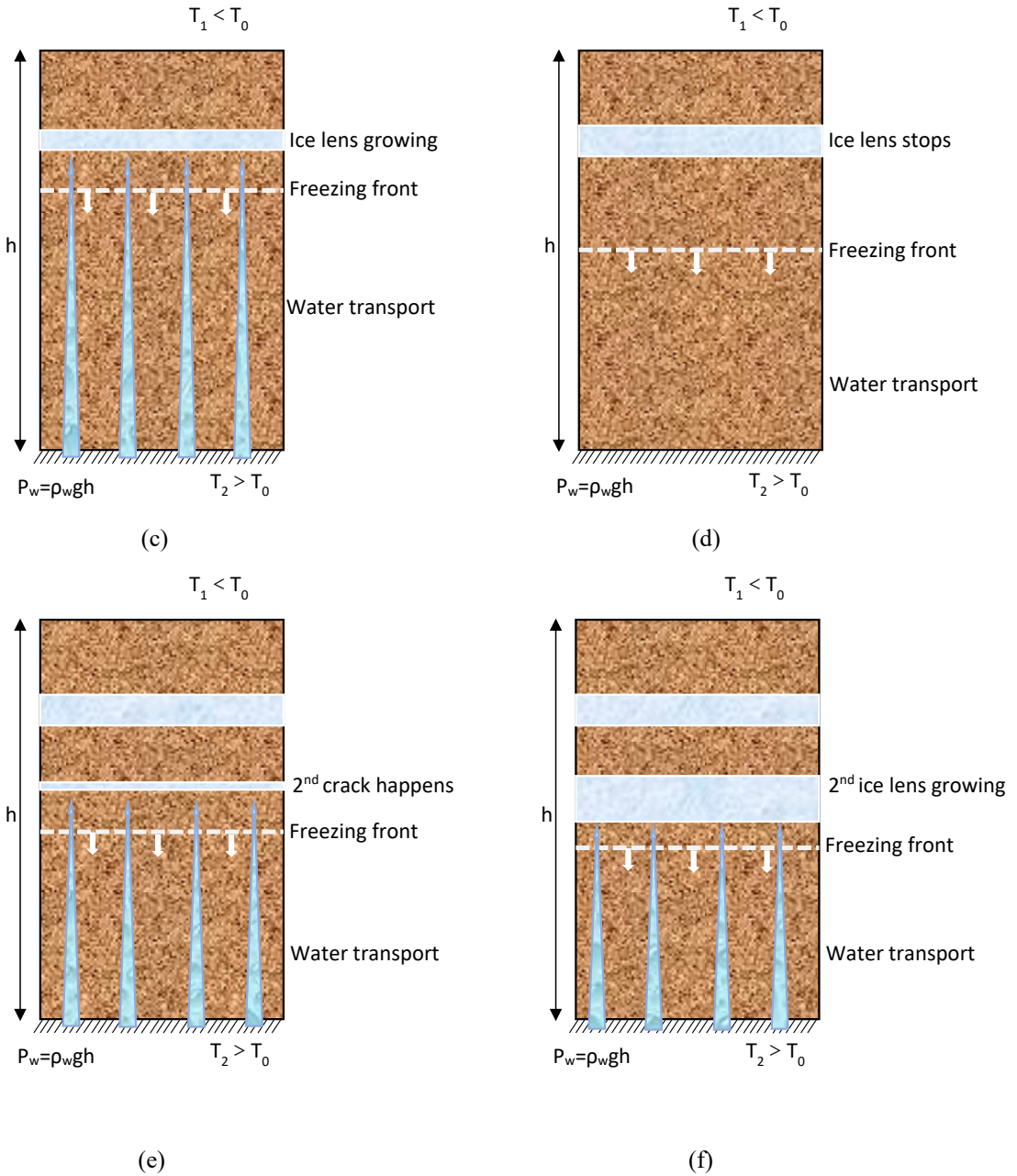
Figure 10 Formation of multiple ice lenses in soil column.

Chapter 4   Governing equations

The system of concern is a mixture of a deformable porous medium saturated with ice and unfrozen water. The system is described as the superposition of all phases, i.e. in the actual configuration, any spatial point ($\mathbf{x}$) in the domain spanned by the solid skeleton is simultaneously occupied by material points ($\mathbf{X}$) of all phases, while, the motion state of each phase is described independently.

4.1 Kinematics

In deriving the balance equations, it is assumed that the ice phase has a similar motion of the solid skeleton. Thus, the Lagrangian form is used for the ice phase and solid skeleton, while motion of the unfrozen water phase is described relative to the motion of the solid skeleton (or ice phase), i.e. the Eulerian form of the balance equations with respect to the motion of the solid skeleton are used for the unfrozen water phase. Therefore, relative velocities of the fluids should be described referring to the motion of the solid skeleton:

$$\mathbf{w}_w = \mathbf{v}_w - \mathbf{v}_s \tag{4.1}$$

$$\mathbf{v}_s = \mathbf{v}_i \tag{4.2}$$

where $\mathbf{w}_w$ is the relative velocity of the water phase with respect to the solid skeleton, $\mathbf{v}_w$ is the absolute velocity of water phase, $\mathbf{v}_s$ is the absolute velocity of the solid skeleton, and $\mathbf{v}_i$ is the absolute velocity of the ice phase. Moreover, the material time derivative of any differentiable function ($f_\alpha(\mathbf{x},t)$), given in its spatial description, should be referred to the solid skeleton:

$$\dot{f}_\alpha = \frac{D^s f_\alpha}{Dt} = \frac{\partial f_\alpha}{\partial t} + \left(\nabla f_\alpha \right) \cdot \mathbf{v}_s \tag{4.3}$$

where $\dot{f}_\alpha = \dfrac{D^s f_\alpha}{Dt}$ indicates the material time derivative of function f (in phase α) with respect the solid skeleton.

In the following, quasi static condition with irrotational velocity field in addition to small displacements and displacement gradients are assumed. So, the following expressions are considered:

$$\frac{\partial f}{\partial \mathbf{x}} \approx \frac{\partial f}{\partial \mathbf{X}} \tag{4.4}$$

$$\nabla \cdot \mathbf{v}_s = -\dot{\varepsilon}_v \tag{4.5}$$

$$\boldsymbol{\varepsilon} = -\frac{1}{2}\left(\nabla\mathbf{u} + \left(\nabla\mathbf{u}\right)^T\right) = -\Im\mathbf{u} \tag{4.6}$$

where $\boldsymbol{\varepsilon}$ is the strain of the soil skeleton, ε_v is the volumetric strain of the soil skeleton, and $\Im$ is a differential operator linking deformations and strains. Note that throughout the thesis, compressive stress and strain are assumed to be positive.

4.2 Governing equations
4.2.1 Mass balance equation

The mass balance equations for the solid phase can be written as:

$$\frac{D^s\left[(1-n)\rho_s\right]}{Dt} + (1-n)\rho_s\nabla\cdot\mathbf{v}_s = 0 \tag{4.7}$$

where n is the porosity, and ρ_s denotes the solid phase density. Assuming that solid grains is incompressible with a volumetric thermal expansion coefficient, β_s, one can write:

$$\dot{\rho}_s = -\rho_s\beta_s\dot{T} \tag{4.8}$$

where T is temperature. Substituting Equation (4.5) into Equation (4.7), variation of the porosity can be expressed by:

$$\dot{n} = -(1-n)(\dot{\varepsilon}_v + \beta_s\dot{T}) \tag{4.9}$$

The mass balance equation for water and ice phases can be written as:

$$n\left(\rho_w - \rho_i\right)\dot{s}_w + \nabla\cdot\left(ns_w\rho_w\mathbf{w}_w\right) + \left(s_w\rho_w + s_i\rho_i\right)\nabla\cdot\mathbf{v}_s + \chi\dot{T} = 0 \tag{4.10}$$

where $\chi = ns_w\rho'_{wT} + ns_i\rho'_{iT} + (n-1)\beta_s\left(s_w\rho_w + s_i\rho_i\right)$, and ρ_w is water density, ρ_i denotes ice density, $\rho'_{wT} = \dfrac{\partial\rho_w}{\partial T}$ and $\rho'_{iT} = \dfrac{\partial\rho_i}{\partial T}$, s_w is the unfrozen water saturation, and s_i is ice saturation.

The relative velocity of the water phase can be described with the generalized Darcy's law proposed by Ratkje et al. (Førland & Ratkje, 1982) and Derjaguin and Churaev (Derjaguin et al., 1993):

$$\mathbf{q}_w = n s_w \mathbf{w}_w = -\frac{k_r K}{\mu_w}(\nabla p_w - \rho_w \mathbf{g}) - \alpha \frac{k_r K}{\mu_w}\frac{\rho_i l}{T}\nabla T \qquad (4.11)$$

where p_w is the measurable water pressure, $\mathbf{g}$ denotes the gravity, T is temperature, K is the absolute permeability, μ_w is the dynamic viscosity of water, k_r denotes relative permeability for unfrozen water, l is the latent heat of fusion, and α is a parameter defined as:

$$\begin{cases} \alpha = 1 - \left(\dfrac{T_0 - T}{T_0 - T_{ff}}\right) & T_{ff} < T < T_0 \\ \alpha = 0 & T \geq T_0 \ \text{or}\ T \leq T_{ff} \end{cases} \qquad (4.12)$$

where T_0 is the freezing temperature, and T_{ff} is the temperature for fully frozen condition.

According to Watanabe and Osada (Watanabe & Osada, 2016), the relative permeability for unfrozen water should be estimated from that of unsaturated soil based on the liquid (unfrozen) water saturation. Thus, the model proposed by van Genuchten (van Genuchten, 1980) for estimating the relative permeability in unsaturated soil might be used here for frozen soil:

$$k_r = \sqrt{s_w}\left[1 - \left(1 - s_w^{1/\lambda}\right)^{\lambda}\right]^2 \qquad (4.13)$$

where λ is a model parameter.

The other required relation is to introduce the unfrozen water saturation as a function of pressure and temperature (soil freezing curve). Referring to Kurylyk and Watanabe (Kurylyk & Watanabe, 2013), the soil freezing curve might be formulated based on the pressure difference between ice and water phase. Considering the Clapeyron equation as the basis for the pressure difference between ice and water phases, the following mathematical relation can be used here(van Genuchten, 1980):

$$s_w = \left[1 + \left(\frac{S_{cry}}{\rho_r}\right)^{1/(1-\lambda)}\right]^{-\lambda} \qquad (4.14)$$

where S_{cry} is the cryogenic suction, ρ_r and λ are model parameters. Note that the model parameter λ in Equation (4.14) is the same as Equation (4.13). The cryogenic suction is calculated based on Clapeyron equation (J. S. Wettlaufer & M. G. Worster, 2006):

$$S_{cry} = p_i - p_w \simeq -\rho_i l\, ln\frac{T}{T_0} \qquad (4.15)$$

Note that the hysteretic nature of soil freezing curve is not considered in this study.

4.2.2 Energy balance equation

Assuming the local thermal equilibrium condition for any spatial point of the mixture, a single energy balance equation can be used to describe the heat transfer process. Neglecting the kinetic energy as well as the viscous and intrinsic dissipation, the energy balance equation on an infinitesimal multiphase element can be written as:

$$\left(\rho C\right)_{\text{eff}} \dot{T} + \left(\rho_w C_w \mathbf{q}_w\right) \cdot \nabla T + \nabla \cdot \mathbf{q}_H - l \cdot \dot{m}_{w \to i} = 0 \tag{4.16}$$

where $m_{w \to i}$ denotes the mass rate of phase change from water to ice, $\mathbf{q}_H$ is the conductive heat flux and $\left(\rho C\right)_{\text{eff}}$ is the effective heat capacity of the mixture that can be calculated as:

$$\left(\rho C\right)_{\text{eff}} = (1-n)\rho_s C_s + n s_w \rho_w C_w + n s_i \rho_i C_i \tag{4.17}$$

where C_s, C_w and C_i are the specific heat capacity for soil grains, unfrozen water and ice phase respectively. To find $\dot{m}_{w \to i}$ in Equation (4.16), the mass balance equation of the ice phase needs to be established as following:

$$\frac{D^S[n s_i \rho_i]}{Dt} + n s_i \rho_i \nabla \cdot \boldsymbol{v}_S - \dot{m}_{w \to i} = 0 \tag{4.18}$$

which can give:

$$\dot{m}_{w \to i} = -n \rho_i \dot{s}_w + s_i \rho_i \nabla \cdot \mathbf{v}_s + [(n-1)s_i \rho_i \beta_s + n s_i \rho'_{iT}]\dot{T} \tag{4.19}$$

Finally the conductive heat flux term, $\mathbf{q}_H$, can be written based on Equation (3.5):

$$\mathbf{q}_H = -\alpha \frac{k_r K}{\mu_w} \rho_i l \ (\nabla p_w - \rho_w \mathbf{g}) - \left(\lambda_s^{1-n} \cdot \lambda_w^{n s_w} \cdot \lambda_i^{n s_i}\right) \nabla T \tag{4.20}$$

As a result, the final form of the heat transfer equation can be obtained as:

$$\left(\rho C\right)_{\text{eff}} \dot{T} + \left(\rho_w C_w \mathbf{q}_w\right) \cdot \nabla T - \nabla \cdot [\alpha \frac{k_r K}{\mu_w} \rho_i l \ (\nabla p_w - \rho_w \mathbf{g})] - \nabla \cdot [\left(\lambda_s^{1-n} \cdot \lambda_w^{n s_w} \cdot \lambda_i^{n s_i}\right) \nabla T]$$
$$- l \cdot [-n \rho_i \dot{s}_w + s_i \rho_i \nabla \cdot \mathbf{v}_s + [(n-1)s_i \rho_i \beta_s + n s_i \rho'_{iT}]\dot{T}] = 0 \tag{4.21}$$

4.2.3 Momentum balance equation

The momentum balance equation of the system can be expressed as following:

$$\nabla \cdot \boldsymbol{\sigma} - \rho \boldsymbol{g} = 0 \tag{4.22}$$

where σ is the total stress of the system, and ρ is the density of the mixture:

$$\rho = (1-n)\rho_s + ns_w\rho_w + ns_i\rho_i \tag{4.23}$$

The total stress can be divided to the normalized water pressure and solid phase stress:

$$\boldsymbol{\sigma} = \boldsymbol{\sigma} * + s_w p_w \mathbf{I} \tag{4.24}$$

where $\boldsymbol{\sigma}*$ is the solid phase stress defined as the combined stress of soil grains and ice, and $\mathbf{I}$ is the unit tensor. The solid phase stress is considered as the part of the total stress responsible for the mechanical deformation of the system. In this model, an elastic constitutive mode is employed to connect the mechanical deformation/strain to the solid phase stress:

$$\dot{\boldsymbol{\sigma}}^* = \mathbf{D}^e (\dot{\boldsymbol{\varepsilon}} - \dot{\boldsymbol{\varepsilon}}_T) \tag{4.25}$$

in which $\mathbf{D}^e$ is the elastic stiffness tensor, $\boldsymbol{\varepsilon}_T$ is the thermal strain of the skeleton. According to the observations of Campanella and Mitchell(Campanella & Mitchell, 1968), the thermal strain of the soil skeleton can be assumed equal to that of the soil particles. Thus:

$$\dot{\boldsymbol{\varepsilon}}_T = -\frac{\mathbf{m}}{3}\beta_s \dot{T} \tag{4.26}$$

where $\mathbf{m}^T$ is defined as:

$$\mathbf{m}^T = \begin{bmatrix} 1 & 1 & 0 \end{bmatrix} \tag{4.27}$$

The elastic parameters of the system can be computed as:

$$\begin{cases} G = (1-s_i)G_s + s_i G_i \\ K_b = (1-s_i)\dfrac{(1+e)}{\kappa}p* + s_i K_i \end{cases} \tag{4.28}$$

where G and K_b are shear modulus and bulk modulus, respectively. $p*$ is the mean solid phase stress, and κ is compressibility of soil.

Here we need to introduce a crack criterion in order to complete the mathematical description based on the conceptual model described in chapter 3. From the physics of the problem, the crack direction can be assumed normal to the temperature gradient, $\mathbf{n}$ .Then, a simple crack criterion can be defined as:

$$F = -\sigma^*_n - a \geq 0 \tag{4.29}$$

where σ^*_n is the normal stress on the crack plane, and a is the tensile stress of the frozen soil as a result of ice cementation, which can be expressed as:

$$a = a_0 - \beta_1 s_i \sigma_n \qquad (4.30)$$

where a_0 is the maximum effect of ice cementation at the fully frozen state and zero overburden/total stress, and β_1 is a parameter to reflect the effect of ice pressure which acts as a disjoining pressure on the grains.

Chapter 5   Numerical solutions using XFEM

5.1 Introduction

Numerical methods were firstly employed by John von Neumann (Ulam et al., 2013) to solve partial differential equations (PDEs), which can provide quantitative descriptions for models in physical sciences, as well as biological and social sciences etc. Continuum, discontinuum and hybrid continuum/discontinuum numerical methods (Jing & Hudson, 2002; Jing et al., 2001; Nikolić et al., 2016) are employed according to different types of engineering problems. In the continuum approach, the domain concerned should not be separated and the continuity between nodes are imposed which guarantees the existence of derivatives. Therefore, the continuity between the elements is imposed as well. However, discontinuities in the medium can exist explicitly or implicitly. While in discontinuum approach, the discrete elements are calculated individually with interaction between each other. Another difference of these two approaches is that the main case is of interest is the rigid body motion with large movements in discontinuum approach, while the deformation of the system is mainly treated by continuum method. The hybrid continuum/discontinuum approach has the advantages of both continuum and discontinuum approaches which can deal with the problem with both large movements and deformation.

The Finite Element Method (FEM), as the most applied numerical method in many research fields (Bettess, 1977; Cheng, 1996; Van Staden et al., 2006; Wilson & Nickell, 1966; Zienkiewicz et al., 1983) after it emerges from 1960s (Argyris & Kelsey, 1960; Clough, 1960), is capable of considering material heterogeneities, non-linearities, irregular geometries and boundary conditions. By using FEM, the domain of interest is divided into finite elements with nodes, within which the local approximations will be adopted using appropriate interpolation functions (Abed & Sołowski, 2017; Amiri et al., 2021; Potts et al., 2021). Subsequently, numerical integration is performed in each element. After assembling the integrations of each element, a global algebraic system of equations will be obtained, which is solvable. However, as a continuum-based approach, FEM is not efficient to simulate the problems with failure, cracking, singularities or damage induced discontinuities (Ibrahimbegovic, 2009; Wriggers, 2008).

The solution domain of concern, containing discontinuities, is showed in Figure 11. There are two different types of representative elementary volume (REV) in the solution domain. For REV1, which is continuous without ice lens, classical FEM is sufficient. While the standard FEM is too cumbersome to simulate REV2 containing discontinuities (ice lenses), due to the complicatedness of remeshing in each step based on the properties of discontinuities, singularities and boundary layers. So, a more advanced numerical method is required.

Extended Finite Element Method (X-FEM) is employed in this work. The name of X-FEM was firstly used by Belytschko and Moes in 1999 (Belytschko & Black, 1999; Moës et al., 1999). A research of X-FEM was conducted by Karihaloo in 2003 (Karihaloo & Xiao, 2003) and Abdelaziz (Abdelaziz & Hamouine, 2008) in 2008. A mathematical report of X-FEM was written by Babuvska on simulating fracture using X-FEM (Mohammadi, 2008). After years of

development, the X-FEM has matured and widely applied. Examples: By using X-FEM, the fluid flow in fractured saturated media was modeled by Réthoré (Réthoré et al., 2007); A hydro-mechanical model with discontinuities in multiphase porous media employing X-FEM was proposed by Mohammadnejad and Khoei (Mohammadnejad & Khoei, 2013b); The hydraulic fracturing phenomenon in deformable porous media was simulated using X-FEM by Mohammadnejad and Huang (Huang, 2021; Mohammadnejad & Khoei, 2013a) and an overview of predicting failure of pipelines using X-FEM was conducted by Shahzamanian recently (Shahzamanian et al., 2021).
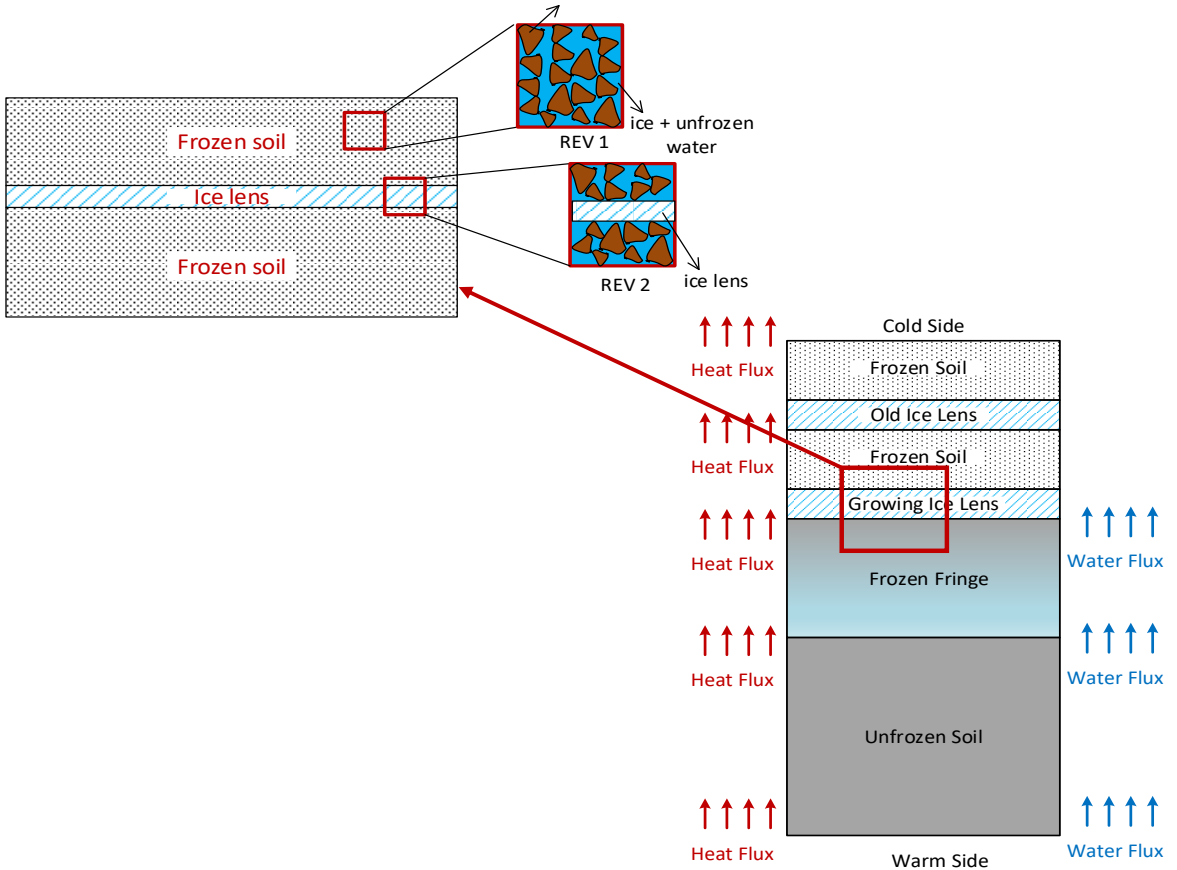
Figure 11 The solution domain.

In X-FEM, the partition of unity method (PUM) is considered a high-priority concept where some specific enrichment functions are added to the standard approximation field of FEM according to the type of discontinuity. By enriching specific nodes of elements with additional degrees of freedom (DOF), the local property in the solution can be captured (Daux et al., 2000; Sukumar et al., 2001) independently of the original finite element mesh, without remeshing as the growth of the crack (Dolbow et al., 2001; Remmers et al., 2008; Stolarska & Chopp, 2003). As Figure 12 (a) shows, a crack appears in a plate with a hole. Figure 12 (b)

shows a remeshing strategy using standard FEM, and a continuous remeshing can be expect as the crack grows. Figure 12 (c) demonstrates a uniform mesh can be used without remeshing by X-FEM.

(a)   (b)   (c)
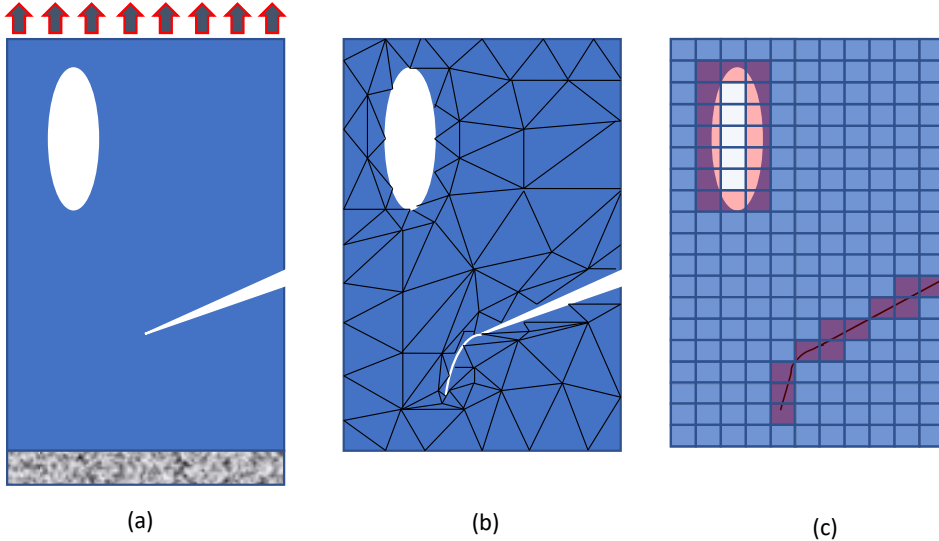
Figure 12 Comparison of the mesh from standard FEM and X-FEM simulation for weak and strong discontinuities [adapted from Khoei(Khoei, 2015)].

The governing equations have been derived in the previous chapter. In order to complete the system of equations, the initial and boundary conditions associated with the primary variables, i.e., displacement, water pressure and temperature, should be defined for the solution domain. As shown in Figure 13, the solution domain Ω is bounded by Γ, and contains a discontinuity interface Γ_d. The initial conditions should specify the full field of fluid phase pressures, temperature, and skeleton deformations at $t = 0$:

$$\begin{cases} \mathbf{u} = \mathbf{u}^0 \\ p_w = p_w^0 \qquad \text{at } t = 0 \text{ and on } \Omega \text{ \& } \Gamma \\ T = T^0 \end{cases} \qquad (5.1)$$

Dirichlet boundary conditions are imposed as prescribed values of the primary variables on the boundaries:

$$\mathbf{u} = \tilde{\mathbf{u}} \qquad \text{on } \Gamma_u$$
$$p_w = \tilde{p}_w \quad \text{on } \Gamma_{p_w} \tag{5.2}$$
$$T = \tilde{T} \qquad \text{on } \Gamma_T$$

and Neumann boundary conditions are imposed as prescribed fluxes and tractions:

$$\boldsymbol{\sigma} \cdot \mathbf{n}_\Gamma = -\bar{\mathbf{t}} \qquad \text{on } \Gamma_t$$
$$\mathbf{q}_w \cdot \mathbf{n}_\Gamma = \bar{q}_w \qquad \text{on } \Gamma_{q_w} \tag{5.3}$$
$$\mathbf{q}_H \cdot \mathbf{n}_\Gamma = \bar{q}_H \qquad \text{on } \Gamma_{q_H}$$

where $\bar{q}_w$ and $\bar{q}_H$ are the imposed mass and heat fluxes, respectively, $\bar{\mathbf{t}}$ is the imposed traction, and $\mathbf{n}_\Gamma$ denotes the unit outward normal vector to the boundary. The conditions $\Gamma_u \bigcup \Gamma_t = \Gamma$, $\Gamma_{p_w} \bigcup \Gamma_{q_w} = \Gamma$ and $\Gamma_T \bigcup \Gamma_{q_H} = \Gamma$ should hold on complementary parts of the boundary.
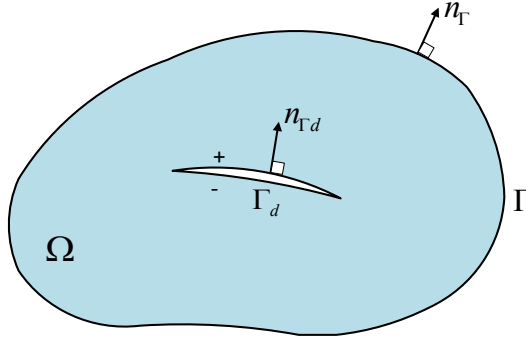
Figure 13 Illustration of the solution domain Ω, bounded by Γ, and with an open discontinuity interface Γ_d.

From the physic of the problem, the existence of ice lens in the solution domain leads to the mechanical, mass and heat transfer coupling between the ice lens and the surrounding porous medium. The mechanical coupling emanates from water pressure and ice-soil contact stress exerted on the crack surface. The mass and heat transfer coupling originate from the flux of mass and heat flowing through the crack borders. Thus, the following conditions should be fulfilled on the discontinuity Γ_d:

$$\boldsymbol{\sigma} . \boldsymbol{n}_{\Gamma_d} = \left(p_{w_d} \boldsymbol{I} + \boldsymbol{\sigma}_d^* \right) \cdot \boldsymbol{n}_{\Gamma_d} \qquad \text{on } \Gamma_d$$
$$-[\![\boldsymbol{q}_w]\!] \cdot \boldsymbol{n}_{\Gamma_d} = \bar{q}_{w_d} \qquad\qquad \text{on } \Gamma_d$$
$$-[\![\boldsymbol{q}_H]\!] \cdot \boldsymbol{n}_{\Gamma_d} = \bar{q}_{H_d} \qquad\qquad \text{on } \Gamma_d \tag{5.4}$$

where p_{w_d} is the water pressure in the crack, $\boldsymbol{\sigma}_d^*$ is the solid phase stress in the crack, $\bar{q}_{w_d}$ is the net water flow from the porous medium to the crack, $\bar{q}_{H_d}$ is the net heat flow from the porous

system to the crack, $\mathbf{n}_{\Gamma_d}$ is the unit normal vector to the discontinuity Γ_d pointing to Ω^+, and the notation $[\![F]\!] = F^+ - F^-$ represents the jump of F between the two faces of the discontinuity (i.e. ice lens).

The total stress on the crack face will be distributed among water (P_{w_d}) and ice-soil contact ($\boldsymbol{\sigma}_d^*$) based on their surface area at crack interface. This can be simply formulated as:

$$\frac{\boldsymbol{\sigma}_d^*}{p_{w_d}} = \beta_2 s_{i_d} \tag{5.5}$$

where s_{i_d} is the ice saturation in the crack, and β_2 is a parameter.

5.2 Weak form of the governing equations in a discontinuous domain

5.2.1 Mass balance equation

The weak form of the mass balance Equation (4.10) can be obtained by integrating the product of the mass balance equation multiplied by admissible test function δp_w over the domain Ω:

$$\int_\Omega \delta p_w(\mathbf{x},t) \left[n(\rho_w - \rho_i)\dot{s}_w + \nabla \cdot (n s_w \rho_w \mathbf{w}_w) + (s_w \rho_w + s_i \rho_i)\nabla \cdot \mathbf{v}_s + \chi \dot{T} \right] d\Omega = 0 \tag{5.6}$$

which must hold for any kinematically admissible test function for water pressure δp_w, satisfying the homogenized essential boundary condition. Applying the Divergence theorem:

$$\int_\Omega \delta p_w [n(\rho_w - \rho_i)\dot{s}_w] d\Omega - \int_\Omega \nabla(\delta p_w) \cdot (\rho_w \boldsymbol{q}_w) d\Omega - \int_{\Gamma_d} [\![\delta p_w \cdot \boldsymbol{q}_w]\!] \cdot (\rho_w \cdot \boldsymbol{n}_{\Gamma_d}) d\Gamma$$
$$+ \int_{\Gamma_{qw}} \delta p_w \cdot \rho_w \boldsymbol{q}_w \cdot \boldsymbol{n}_\Gamma \ d\Gamma + \int_\Omega \delta p_w [(s_w \rho_w + s_i \rho_i)\nabla \cdot \boldsymbol{v}_s] d\Omega + \int_\Omega \delta p_w \chi \dot{T} d\Omega = 0 \tag{5.7}$$

Introducing Equation (4.5) and the second part of equations (5.3) and (5.4) into Equation (5.7), and assuming pressure continuity at the discontinuity interface:

$$\int_\Omega \delta p_w \left[n(\rho_w - \rho_i)\dot{s}_w \right] d\Omega - \int_\Omega \nabla(\delta p_w) \cdot (\rho_w \mathbf{q}_w) d\Omega + \int_{\Gamma_d} \delta p_w \cdot \rho_w \bar{q}_{w_d} d\Gamma$$
$$+ \int_{\Gamma_{qw}} \delta p_w \cdot \rho_w \bar{q}_w d\Gamma - \int_\Omega \delta p_w \left[(s_w \rho_w + s_i \rho_i)\dot{\varepsilon}_v \right] d\Omega + \int_\Omega \delta p_w \chi \dot{T} d\Omega = 0 \tag{5.8}$$

where the third integral in Equation (5.8) stands for the mass transfer coupling between the crack and the porous system. In order to derive a relation for this coupling term, the mass balance equation inside the crack should be taken into account. The weak form of the mass balance equation within the crack is obtained by integrating the product of the continuity equation, i.e. Equation (4.10) with $n = 1$, multiplied by admissible test function δp_w over the domain of discontinuity Ω', as shown in Figure 14. Applying the Divergence theorem and

implementing the boundary conditions, the weak form of the continuity equation inside the discontinuity domain is written as:

$$\int_{\Omega'} \delta p_w \left[(\rho_w - \rho_i) \dot{s}_{w_d} \right] d\Omega - \int_{\Omega'} \nabla(\delta p_w) \cdot (\rho_w \mathbf{q}_w) d\Omega - \int_{\Gamma_d} \delta p_w \cdot \rho_w \bar{q}_{w_d} d\Gamma$$
$$+ \int_{\Omega'} \delta p_w \left[(s_{w_d} \rho_w + s_{i_d} \rho_i) \nabla \cdot \mathbf{v}_s \right] d\Omega + \int_{\Omega'} \delta p_w [s_{w_d} \rho'_{wT} + s_{i_d} \rho'_{iT}] \dot{T} d\Omega = 0 \tag{5.9}$$
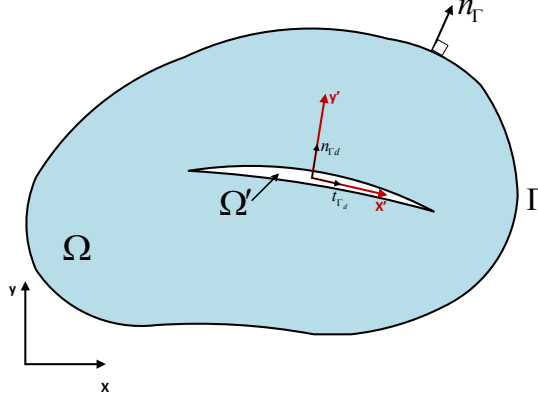
Figure 14 The domain of discontinuity and the local coordinate system.

Rearranging Equation (5.9), one can find the mass transfer coupling term by calculating the following integrals:

$$\int_{\Gamma_d} \delta p_w \cdot \rho_w \bar{q}_{w_d} d\Gamma = \underbrace{\int_{\Omega'} \delta p_w \left[(\rho_w - \rho_i) \dot{s}_{w_d} \right] d\Omega}_{\text{Integral I}} - \underbrace{\int_{\Omega'} \nabla(\delta p_w) \cdot (\rho_w \mathbf{q}_w) d\Omega}_{\text{Integral II}}$$
$$+ \underbrace{\int_{\Omega'} \delta p_w \left[(s_{w_d} \rho_w + s_{i_d} \rho_i) \nabla \cdot \mathbf{v}_s \right] d\Omega}_{\text{Integral III}} + \underbrace{\int_{\Omega'} \delta p_w [s_{w_d} \rho'_{wT} + s_{i_d} \rho'_{iT}] \dot{T} d\Omega}_{\text{Integral IV}} \tag{5.10}$$

The integral terms (I)-(IV) over the domain of discontinuity can be evaluated in the local coordinate system $(x' - y')$ constructed from the tangential and normal unit vectors to the discontinuity interface, as shown in Figure 14. from the physic of the problem, crack direction (i.e., x') is assumed normal to the temperature gradient.

Note that in what follows, the variation of the water pressure, its corresponding test function and unfrozen water content over the discontinuity width is ignored. Having this in mind, the first integral in the Equation (5.10) is evaluated as:

$$\underbrace{\int_{\Omega'} \delta p_w \left[(\rho_w - \rho_i) \dot{s}_{w_d} \right] d\Omega}_{\text{Integral I}} = \int_{\Gamma_d} \int_{-1/2 \llbracket u_{y'} \rrbracket}^{1/2 \llbracket u_{y'} \rrbracket} \delta p_w \left[(\rho_w - \rho_i) \dot{s}_{w_d} \right] dy' \, d\Gamma =$$
$$\int_{\Gamma_d} \delta p_w \cdot \llbracket u_{y'} \rrbracket \cdot \left[(\rho_w - \rho_i) \dot{s}_{w_d} \right] d\Gamma \tag{5.11}$$

The constitutive relation, to link the unfrozen water saturation in the crack s_{w_d} in Equation (5.11) to temperature, is a simple linear relation within a certain range of temperature.

$$s_{w_d} = \begin{cases} 1 & \text{if } T>T_0 \\ s_{w_{res}} + \dfrac{1-s_{w_{res}}}{T_0-T_i} \times (T-T_i) & \text{if } T_i \leq T \leq T_0 \\ s_{w_{res}} & \text{if } T<T_i \end{cases} \qquad (5.12)$$

where T_i is the temperature (below T_0) from which unfrozen water saturation in the crack starts changing, and $s_{w_{res}}$ is the residual unfrozen water saturation at temperatures below T_i.

Similar to integral I, for the second integral:

$$\underbrace{\int_{\Omega'} \nabla(\delta p_w) \cdot (\rho_w \boldsymbol{q}_w) d\Omega}_{\text{Integral II}} = \int_{\Gamma_d} \int_{-1/2[\![u_{y'}]\!]}^{1/2[\![u_{y'}]\!]} \left(\frac{\partial(\delta p_w)}{\partial x'} \cdot q_{w_{x'}} + \frac{\partial(\delta p_w)}{\partial y'} \cdot q_{w_{y'}} \right) \rho_w dy' \, d\Gamma =$$
$$\int_{\Gamma_d} \left(\frac{\partial(\delta p_w)}{\partial x'} \cdot q_{w_{x'}} \right) \cdot \rho_w [\![u_{y'}]\!] d\Gamma \qquad (5.13)$$

where $q_{w_{x'}}$ is defined as:

$$q_{w_{x'}} = -k_d \left(\frac{\partial p_w}{\partial x'} - \rho_w g_{x'} \right) \qquad (5.14)$$

Note that the longitudinal component of the thermal coupling term in the transport equation in the local coordinate system, Equation (5.14) is zero, since x' is defined normal to the temperature gradient. k_d in Equation (5.14) is the crack permeability with respect to the water phase, which is estimated as:

$$k_d = s_{w_d} \frac{[\![u]\!]^2}{12\mu_w} \qquad (5.15)$$

To calculate the third integral, from the physic of the problem, it is assumed that the displacement discontinuity only exists in the normal direction to the crack. Thus, the velocity component of the solid phase in the longitudinal direction $v_{s_{x'}}$ is constant over the width of the discontinuity $[\![u_{y'}]\!]$, so its derivative with respect to x' is also constant in y'. Having this in mind, the third integral in Equation (5.10) can be written as:

$$\underbrace{\int_{\Omega'} \delta p_w [(s_{w_d}\rho_w + s_{i_d}\rho_i)\nabla \cdot \boldsymbol{v}_s] d\Omega}_{\text{Integral III}} = \int_{\Gamma_d} \int_{-1/2[\![u_{y'}]\!]}^{1/2[\![u_{y'}]\!]} \delta p_w (s_{w_d}\rho_w + s_{i_d}\rho_i) \left(\frac{\partial v_{s_{x'}}}{\partial x'} + \frac{\partial v_{s_{y'}}}{\partial y'} \right) dy' \, d\Gamma =$$
$$\int_{\Gamma_d} \delta p_w (s_{w_d}\rho_w + s_{i_d}\rho_i)[\![u_{y'}]\!] \left(\frac{\partial v_{s_{x'}}}{\partial x'} \right) d\Gamma + \int_{\Gamma_d} \delta p_w (s_{w_d}\rho_w + s_{i_d}\rho_i) [\![v_{s_{y'}}]\!] d\Gamma =$$
$$-\int_{\Gamma_d} \delta p_w (s_{w_d}\rho_w + s_{i_d}\rho_i)[\![u_{y'}]\!] \dot{\varepsilon}_{x'x'} d\Gamma + \int_{\Gamma_d} \delta p_w (s_{w_d}\rho_w + s_{i_d}\rho_i)[\![\dot{u}_{y'}]\!] d\Gamma \qquad (5.16)$$

Ignoring the variation of temperature over the discontinuity width, the fourth integral can be written as:

$$
\underbrace{\int_{\Omega'} \delta p_w [s_{w_d}\rho'_{wT} + s_{i_d}\rho'_{iT}]\dot{T}d\Omega}_{\text{Integral IV}} = \int_{\Gamma_d} \int_{-1/2[\![u_{y'}]\!]}^{1/2[\![u_{y'}]\!]} \delta p_w [s_{w_d}\rho'_{wT} + s_{i_d}\rho'_{iT}]\dot{T}dy'\,d\Gamma
$$

$$
= \int_{\Gamma_d} \delta p_w [s_{w_d}\rho'_{wT} + s_{i_d}\rho'_{iT}]\dot{T}[\![u_{y'}]\!]d\Gamma \tag{5.17}
$$

5.2.2 Energy balance equation

The weak form of the energy balance Equation (4.16) can be obtained by integrating the product of the continuity equation multiplied by admissible test function δT over the domain Ω:

$$
\int_{\Omega} \delta T(\mathbf{x},t)\Big[(\rho C)_{\text{eff}}\,\dot{T} + (\rho_w C_w \mathbf{q}_w)\cdot\nabla T + \nabla\cdot\mathbf{q}_H - l\cdot\dot{m}_{w\to i}\Big]\,d\Omega = 0 \tag{5.18}
$$

which must hold for any kinematically admissible test function for temperature δT, satisfying the homogenized essential boundary condition. Applying the Divergence theorem:

$$
\int_{\Omega} \delta T(\rho C)_{\text{eff}}\dot{T} \quad d\Omega + \int_{\Omega} \delta T(\rho_w C_w \mathbf{q}_w)\cdot\nabla T \quad d\Omega - \int_{\Omega} \nabla(\delta T)\cdot\mathbf{q}_H \quad d\Omega -
$$
$$
\int_{\Gamma_d}[\![\delta T\cdot\mathbf{q}_H]\!] \quad \cdot\mathbf{n}_{\Gamma_d}d\Gamma + \int_{\Gamma_{q_H}} \delta T\mathbf{q}_H\cdot\mathbf{n}_\Gamma d\Gamma - \int_{\Omega}\delta T\cdot l\cdot\dot{m}_{w\to i} \quad d\Omega = 0 \tag{5.19}
$$

Introducing the third part of equations (5.3) and (5.4) into Equation (5.19), and assuming temperature continuity at the discontinuity interface:

$$
\int_{\Omega} \delta T(\rho C)_{\text{eff}}\,\dot{T}\,d\Omega + \int_{\Omega}\delta T(\rho_w C_w \mathbf{q}_w)\cdot\nabla T\,d\Omega - \int_{\Omega}\nabla(\delta T)\cdot\mathbf{q}_H\,d\Omega +
$$
$$
\int_{\Gamma_d}\delta T\,\bar{q}_{H_d}d\Gamma + \int_{\Gamma_{q_H}}\delta T\,\bar{q}_H d\Gamma - \int_{\Omega}\delta T\cdot l\cdot\dot{m}_{w\to i}\,d\Omega = 0 \tag{5.20}
$$

where the fourth integral in Equation (5.20) stands for the heat transfer between the crack and the porous system. In order to derive a relation for this term, the heat transfer equation inside the crack should be taken into account. The weak form of the heat transfer equation within the crack is obtained by integrating the product of the heat transfer equation, i.e. Equation (4.16), multiplied by admissible test function δT over the domain of discontinuity Ω', as shown in Figure 14. Applying the Divergence theorem and implementing the boundary conditions, the weak form of the heat transfer equation inside the discontinuity domain is written as:

$$
\int_{\Omega'} \delta T(\rho C)_{\text{eff}_d}\,\dot{T}\,d\Omega + \int_{\Omega'}\delta T(\rho_w C_w \mathbf{q}_w)\cdot\nabla T\,d\Omega - \int_{\Omega'}\nabla(\delta T)\cdot\mathbf{q}_H\,d\Omega -
$$
$$
\int_{\Gamma_d}\delta T\,\bar{q}_{H_d}d\Gamma - \int_{\Omega'}\delta T\cdot l\cdot(\dot{m}_{w\to i})_d\,d\Omega = 0 \tag{5.21}
$$

Rearranging Equation (5.21), one can find the heat transfer coupling term by calculating the following integrals:

$$\int_{\Gamma_d} \delta T \, \bar{q}_{H_d} d\Gamma = \underbrace{\int_{\Omega'} \delta T \left(\rho C\right)_{\text{eff}_d} \dot{T} \, d\Omega}_{\text{Integral I}} + \underbrace{\int_{\Omega'} \delta T \left(\rho_w C_w \mathbf{q}_w\right) \cdot \nabla T \, d\Omega}_{\text{Integral II}} -$$

$$\underbrace{\int_{\Omega'} \nabla(\delta T) \cdot \mathbf{q}_H \, d\Omega}_{\text{Integral III}} - \underbrace{\int_{\Omega'} \delta T \cdot l\left(\dot{m}_{w \to i}\right)_d d\Omega}_{\text{Integral IV}}$$

(5.22)

The integral terms (I)-(IV) over the domain of discontinuity can be evaluated in the local coordinate system $(x' - y')$, as shown in Figure 14, in which the variation of the temperature and its corresponding test function over the discontinuity width is ignored. Thus, the first integral in the Equation (5.22) is evaluated as:

$$\underbrace{\int_{\Omega'} \delta T (\rho C)_{\text{eff}_d} \frac{D^s T}{Dt} \, d\Omega}_{\text{Integral I}} = \int_{\Gamma_d} \int_{-1/2 \llbracket u_{y'} \rrbracket}^{1/2 \llbracket u_{y'} \rrbracket} \delta T (\rho C)_{\text{eff}_d} \dot{T} dy' \, d\Gamma =$$

$$\int_{\Gamma_d} \delta T \cdot \llbracket u_{y'} \rrbracket \cdot (\rho C)_{\text{eff}_d} \dot{T} d\Gamma \qquad (5.23)$$

where $(\rho C)_{\text{eff}_d}$ is the effective heat capacity within the discontinuity:

$$\left(\rho C\right)_{\text{eff}_d} = s_{w_d} \rho_w C_w + s_{i_d} \rho_i C_i$$

(5.24)

As mentioned earlier, the local coordinate axis x' is assumed normal to the temperature gradient, thus variation of temperature in the longitudinal direction will also vanish. Thus, the second and third integrals in Equation (5.22) are evaluated as:

$$\underbrace{\int_{\Omega'} \delta T (\rho_w C_w \mathbf{q}_w) \cdot \nabla T \, d\Omega}_{\text{Integral II}} = \int_{\Gamma_d} \int_{-1/2 \llbracket u_{y'} \rrbracket}^{1/2 \llbracket u_{y'} \rrbracket} \delta T (\rho_w C_w) \left(\frac{\partial T}{\partial x'} \cdot q_{w_{x'}} + \frac{\partial T}{\partial y'} \cdot q_{w_{y'}}\right) dy' \, d\Gamma = 0 \qquad (5.25)$$

$$\underbrace{\int_{\Omega'} \nabla(\delta T) \cdot \mathbf{q}_H \, d\Omega}_{\text{Integral III}} = \int_{\Gamma_d} \int_{-1/2 \llbracket u_{y'} \rrbracket}^{1/2 \llbracket u_{y'} \rrbracket} \left(\frac{\partial(\delta T)}{\partial x'} \cdot q_{H_{x'}} + \frac{\partial(\delta T)}{\partial y'} \cdot q_{H_{y'}}\right) dy' \, d\Gamma = 0 \qquad (5.26)$$

To calculate the fourth integral in Equation (5.22), one first needs to evaluate the phase change term within the crack (i.e. $(\dot{m}_{w \to i})_d$) using the mass balance equation of ice within the discontinuity zone (i.e. Equation (4.19) with $n = 1$):

$$(\dot{m}_{w \to i})_d = -\rho_i \dot{s}_{w_d} + s_{i_d} \rho_i \nabla \cdot \mathbf{v}_s + s_{i_d} \rho'_{iT} \dot{T}$$

(5.27)

Introducing Equation (5.27) into the fourth integral of Equation (5.22), ignoring the variation of unfrozen water content over the discontinuity width, and assuming constant $v_{s_{x'}}$ over the width of the discontinuity, one can write:

$$\underbrace{\int_{\Omega'} \delta T \cdot l(\dot{m}_{w\rightarrow i})}_{\text{Integral IV}} \, d\Omega = \int_{\Omega'} \delta T \cdot l\left(-\rho_i \dot{s}_{w_d} + s_{i_d}\rho_i \nabla \cdot \boldsymbol{v}_s + s_{i_d}\rho'_{iT}\dot{T}\right) \, d\Omega =$$

$$-\int_{\Gamma_d} \delta T \cdot l \cdot \rho_i \cdot [\![u_{y'}]\!]\dot{s}_{w_d}d\Gamma - \int_{\Gamma_d} \delta T \cdot l \cdot s_{i_d}\rho_i \cdot [\![u_{y'}]\!]\dot{\varepsilon}_{x'x'}d\Gamma +$$

$$\int_{\Gamma_d} \delta T \cdot l \cdot s_{i_d}\rho_i \cdot [\![\dot{u}_{y'}]\!]d\Gamma + \int_{\Gamma_d} \delta T \cdot s_{i_d}\rho'_{iT}\dot{T} \cdot [\![u_{y'}]\!]d\Gamma \tag{5.28}$$

5.2.3 Momentum balance equation

The weak form of the momentum balance equation (4.22) can be obtained by integrating the product of the balance equation multiplied by admissible test function $\delta\mathbf{u}$ over the domain Ω :

$$\int_{\Omega} \delta\mathbf{u}(\mathbf{x},t) \cdot (\nabla \cdot \boldsymbol{\sigma} - \rho\mathbf{g})d\Omega = 0 \tag{5.29}$$

which must hold for any kinematically admissible test function for displacement $\delta\mathbf{u}$, satisfying the homogenized essential boundary condition. Applying the Divergence theorem:

$$-\int_{\Omega} \nabla(\delta\mathbf{u}):\boldsymbol{\sigma}d\Omega - \int_{\Gamma_d}[\![\delta\mathbf{u} \quad \boldsymbol{\sigma}]\!] \cdot \boldsymbol{n}_{\Gamma_d}d\Gamma + \int_{\Gamma_t}(\delta\mathbf{u} \quad \boldsymbol{\sigma}) \cdot \boldsymbol{n}_{\Gamma} \, d\Gamma - \int_{\Omega} \delta\mathbf{u} \cdot \rho\mathbf{g}d\Omega = 0 \tag{5.30}$$

Introducing Equation (4.24) and the first part of equations (5.3) and (5.4) into Equation (5.30), and assuming traction continuity at the discontinuity interface:

$$-\int_{\Omega} \nabla(\delta\boldsymbol{u}):\boldsymbol{\sigma}^*d\Omega - \int_{\Omega} \nabla(\delta\boldsymbol{u}):(s_w p_w \boldsymbol{I})d\Omega -$$

$$\int_{\Gamma_d}[\![\delta\boldsymbol{u}]\!] \cdot (\beta_2 s_{i_d} + 1)(p_w \boldsymbol{I})_d \boldsymbol{n}_{\Gamma_d}d\Gamma - \int_{\Gamma_t} \delta\boldsymbol{u} \cdot \bar{\boldsymbol{t}} \, d\Gamma - \int_{\Omega} \delta\boldsymbol{u} \cdot \rho\mathbf{g}d\Omega = 0 \tag{5.31}$$

5.3 Discretization of the governing equation

In this section, the weak form of the governing equations obtained in the preceding section is discretized in the spatial and time domains. The X-FEM is employed for spatial discretization of the equations, while the temporal discretization of the equations is performed by the fully implicit first order accurate finite difference scheme. The resulting system of fully coupled non-linear equations is finally solved using the Newton-Raphson procedure.

5.3.1 Approximation of the primary variables

In order to discretize the weak form of the three governing equations (5.9), (5.21) and (5.31), the primary unknown variables (i.e. $\mathbf{u}(\mathbf{x},t)$, $p_w(\mathbf{x},t)$ and $T(\mathbf{x},t)$) should be approximated using appropriate shape functions.

The displacement field $\mathbf{u}(\mathbf{x},t)$, which is normal to the crack direction (i.e., in y' direction), should be discontinuous on the interface Γ_d considering the growth of ice lenses, referred as the strong discontinuity. The pressure field $p_w(\mathbf{x},t)$ and temperature field $T(\mathbf{x},t)$ should be continuous, while the fluid and heat flux which are the gradients of $p_w(\mathbf{x},t)$ and $T(\mathbf{x},t)$, in the normal direction to the crack, should be also discontinuous on the interface Γ_d, referred as the weak discontinuity. By applying X-FEM, a discontinuous enrichment function should be added to the corresponding standard approximated domain for strong discontinuities, and a continuous enrichment function with discontinuous gradient is adopted for weak discontinuities.
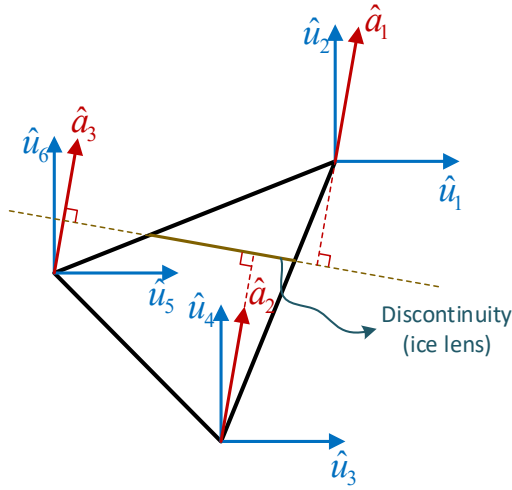
Figure 15 Illustrating the standard and enhanced degrees of freedom for a simple first-order element.

The displacement discontinuity over the crack interface is modelled using the shifted Heaviside function, and the field can be approximated as:

$$\mathbf{u}(\mathbf{x},t) = \sum_{i=1}^{N} N_{u_i}(\xi)\hat{\mathbf{u}}_i(t) + \sum_{j=1}^{M}\left[\bar{N}_{u_j}(\xi)\left(H(\varphi(\xi)) - H(\varphi(\xi_j))\right)\mathbf{n}_{\Gamma_d}\right]\hat{a}_j(t) = \mathbf{N}_u^{std}\hat{\mathbf{u}} + \mathbf{N}_u^{enr}\mathbf{L}\hat{\mathbf{a}} \qquad (5.32)$$

where ξ is the position in the natural coordinate system of the element, N is the set of all nodes, M is the set of enriched nodes. $N_u(\xi)$ and $\bar{N}_u(\xi)$ are the standard FEM shape functions for the displacement field in their standard and enriched parts, respectively, $\mathbf{u}$ is the nodal displacement, $\mathbf{L}$ is the transformation matrix between the local direction y' and the global systems (x,y), $\hat{a}$ is the enhanced nodal degree of freedom (DOF) parallel to temperature gradient (i.e. normal to the crack interface, as Figure 15 shows), $H(\varphi(\xi))$ is the Heaviside jump function defined as:

$$H(\varphi(\xi)) = \begin{cases} +1 & \varphi(\xi) \geq 0 \\ 0 & \varphi(\xi) < 0 \end{cases} \qquad (5.33)$$

and $\varphi(\xi)$ is the signed distance function defined based on the absolute value of the level set function as:

$$\varphi(\xi) = \left\| \xi - \xi_{\Gamma_d} \right\| \operatorname{sign}\left((\xi - \xi_{\Gamma_d}) \cdot \mathbf{n}_{\Gamma_d} \right) \tag{5.34}$$

where ξ_{Γ_d} is the closest point projection of ξ onto the discontinuity interface Γ_d, and $\| \; \|$ denotes the Euclidean norm; accordingly $\left\| \xi - \xi_{\Gamma_d} \right\|$ specifies the distance of point ξ to the discontinuity.

(a)   Shape and enrichment functions for approximation of the displacement field in a simple first-order 1D element

(b)   Shape and enrichment functions for approximation of the pressure and temperature fields in a simple first-order 1D element

Figure 16

It is worth noting that using the shifted Heaviside function, the enriched shape functions vanish in all elements not containing the discontinuity. Figure 16 (a) shows the elements of the approximated displacement field for a simple 1D element with a discontinuity (c) inside the element. As it is depicted in the figure, the jump in the displacement field can be approximated using a shifted Heaviside function.

Accordingly, the gradient of the displacement field with respect to the global coordinate system can be obtained:

$$\nabla \mathbf{u}(\mathbf{x},t) = \sum_{i=1}^{N} \nabla N_{u_i}(\xi)\hat{\mathbf{u}}_i(t) + \sum_{j=1}^{M}\Big[\nabla \bar{N}_{u_j}(\xi)\big(H(\varphi(\xi)) - H(\varphi(\xi_j))\big)\mathbf{n}_{\Gamma_d} +$$
$$\bar{N}_{u_j}(\xi)\nabla\big(H(\varphi(\xi)) - H(\varphi(\xi_j))\big)\mathbf{n}_{\Gamma_d} \Big]\hat{a}_j(t) \tag{5.35}$$

where the derivative of the Heaviside function is the Dirac delta function as Equation (5.36) showed, and the Dirac delta function δ can be defined as Equation (5.37):

$$\frac{dH(x)}{dx} = \delta \tag{5.36}$$

$$\delta(x) = \begin{cases} \dfrac{1}{2\varpi}(1 + \cos\dfrac{\pi\xi}{\varpi}) & -\varpi < \xi(x) < \varpi \\ \qquad 0 & \text{elsewhere} \end{cases} \tag{5.37}$$

where ϖ is a small value with respect to element size. Thus, Equation (5.35) can be rewritten as:

$$\nabla \mathbf{u}(\mathbf{x}) = \sum_{i=1}^{N} \nabla N_{u_i}(\xi)\hat{\mathbf{u}}_i(t) + \sum_{j=1}^{M}\Big[\nabla \bar{N}_{u_j}(\xi)\big(H(\varphi(\mathbf{x})) - H(\varphi(\mathbf{x}_j))\big)\mathbf{n}_{\Gamma_d} \Big]\hat{a}_j(t) = \mathbf{B}_u^{std}\hat{\mathbf{u}} + \mathbf{B}_u^{enr}\mathbf{L}\hat{\mathbf{a}} \tag{5.38}$$

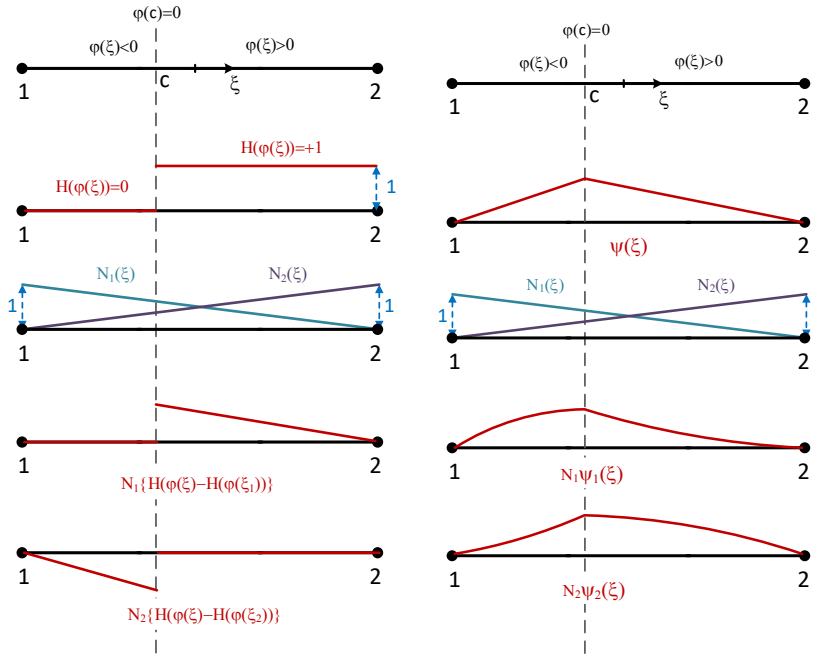The jump in the displacement field can be obtained at the discontinuity interface as:

$$[\![\boldsymbol{u}(\boldsymbol{x},t)]\!] = \boldsymbol{u}(\boldsymbol{x}^+,t) - \boldsymbol{u}(\boldsymbol{x}^-,t)$$
$$= \sum_{j=1}^{M}\Big[\bar{N}_{u_j}(\boldsymbol{\xi})(H(\varphi(\boldsymbol{\xi}^+)) - H(\varphi(\boldsymbol{\xi}^-)))\mathbf{n}_{\Gamma_d}\Big]\hat{a}_j(t) = \sum_{j=1}^{M}\bar{N}_{u_j}(\boldsymbol{\xi})\mathbf{n}_{\Gamma_d}\hat{a}_j(t) = \bar{\boldsymbol{N}}_u\boldsymbol{L}\hat{\boldsymbol{a}} \tag{5.39}$$

or the jump normal to the crack interface can be computed as:

$$[\![u_{y'}(\boldsymbol{x},t)]\!] = \sum_{j=1}^{M}\bar{N}_{u_j}(\boldsymbol{\xi})\hat{a}_j(t) = \bar{\boldsymbol{N}}_u\hat{\boldsymbol{a}} \tag{5.40}$$

Similarly, the displacement test function $\delta\mathbf{u}(\mathbf{x},t)$ can be defined in the same approximation space as the displacement field $\mathbf{u}(\mathbf{x},t)$ as:

$$\delta\mathbf{u}(\mathbf{x},t) = \sum_{i=1}^{N} N_{u_i}(\xi)\delta\hat{\mathbf{u}}_i(t) + \sum_{j=1}^{M}\Big[\bar{N}_{u_j}(\xi)\big(H(\varphi(\xi)) - H(\varphi(\xi_j))\big)\mathbf{n}_{\Gamma_d} \Big]\delta\hat{a}_j(t) = \mathbf{N}_u^{std}\delta\hat{\mathbf{u}} + \mathbf{N}_u^{enr}\mathbf{L}\delta\hat{\mathbf{a}} \tag{5.41}$$

$$\nabla\delta\mathbf{u}(\mathbf{x}) = \sum_{i=1}^{N} \nabla N_{u_i}(\xi)\delta\hat{\mathbf{u}}_i(t) + \sum_{j=1}^{M}\Big[\nabla \bar{N}_{u_j}(\xi)\big(H(\varphi(\xi)) - H(\varphi(\xi_j))\big)\mathbf{n}_{\Gamma_d} \Big]\delta\hat{a}_j(t) = \mathbf{B}_u^{std}\delta\hat{\mathbf{u}} + \mathbf{B}_u^{enr}\mathbf{L}\delta\hat{\mathbf{a}} \tag{5.42}$$

The water and heat flux which are discontinuous over the ice lens interface is approximated with the modified level-set function proposed by Moës et al. (Moës et al., 2003). Thus, pressure and temperature fields can be described as:

$$p_w(\mathbf{x},t) = \sum_{i=1}^{N} N_{p_i}(\xi)\hat{p}_{w_i}(t) + \sum_{j=1}^{M} \bar{N}_{p_j}(\xi)\psi_p(\xi)\hat{b}_j(t) = \mathbf{N}_p^{std}\hat{\mathbf{p}}_w + \mathbf{N}_p^{enr}\hat{\mathbf{b}} \qquad (5.43)$$

$$T(\mathbf{x},t) = \sum_{i=1}^{N} N_{T_i}(\xi)\hat{T}_i(t) + \sum_{j=1}^{M} \bar{N}_{T_j}(\xi)\psi_T(\xi)\hat{c}_j(t) = \mathbf{N}_T^{std}\hat{\mathbf{T}} + \mathbf{N}_T^{enr}\hat{\mathbf{c}} \qquad (5.44)$$

where $N_{p_i}(\xi)$ and $N_{T_i}(\xi)$ are the standard FEM shape functions for pressure and temperature fields in the added enrichment functions, respectively, $\bar{N}_{p_j}(\xi)$ and $\bar{N}_{T_j}(\xi)$ are the standard FEM shape functions for pressure and temperature fields in the added enrichment functions, respectively. $\mathbf{p}_w$ and $\mathbf{T}$ are the nodal water pressure and temperature, $\mathbf{b}$ and $\hat{\mathbf{c}}$ are the enhanced nodal DOFs for pressure and temperature, respectively, and $\psi(\xi)$ is the modified level-set function given by:

$$\psi_\alpha(\xi) = \sum_{k=1}^{M}\left[\bar{N}_{\alpha_k}(\xi)|\varphi(\xi_k)|\right] - |\varphi(\xi)| \approx \sum_{k=1}^{M} \bar{N}_{\alpha_k}(\xi)|\varphi(\xi_k)| - \left|\sum_{k=1}^{M} \bar{N}_{\alpha_k}(\xi)\varphi(\xi_k)\right| \quad ; \quad \alpha = p,T \qquad (5.45)$$

The above added enriched function is a ridge centered on the discontinuity interface and will vanish in elements which do not have a crack. Figure 16 (b) shows the enriched elements of the approximated pressure and temperature fields for a one-dimensional element with a crack (*c*) inside the element. As it is depicted in the figure, the modified level-set function provides a continuous field for the main variables (i.e., pressure and temperature), while their gradient (i.e., mass and heat fluxes) are considered to be discontinuous.

Accordingly, the gradient of the pressure and temperature fields with respect to the global coordinate system can be obtained:

$$\nabla p_w(\mathbf{x},t) = \sum_{i=1}^{N} \nabla N_{p_i}(\xi)\hat{p}_{w_i}(t) + \sum_{j=1}^{M}\left[\nabla\bar{N}_{p_j}(\xi)\psi_p(\xi) + \bar{N}_{p_j}(\xi)\nabla\psi_p(\xi)\right]\hat{b}_j(t) = \mathbf{B}_p^{std}\hat{\mathbf{p}}_w + \mathbf{B}_p^{enr}\hat{\mathbf{b}} \qquad (5.46)$$

$$\nabla T(\mathbf{x},t) = \sum_{i=1}^{N} \nabla N_{T_i}(\xi)\hat{T}_i(t) + \sum_{j=1}^{M}\left[\nabla\bar{N}_{T_j}(\xi)\psi_T(\xi) + \bar{N}_{T_j}(\xi)\nabla\psi_T(\xi)\right]\hat{c}_j(t) = \mathbf{B}_T^{std}\hat{\mathbf{T}} + \mathbf{B}_T^{enr}\hat{\mathbf{c}} \qquad (5.47)$$

where the gradient of the modified level-set function can be calculated as:

$$\nabla\psi_\alpha(\xi) = \sum_{k=1}^{M} \nabla\bar{N}_{\alpha_k}(\xi)|\varphi(\xi_k)| - \text{sign}\left(\varphi(\xi)\right)\mathbf{n}_{\Gamma_d} \quad ; \quad \alpha = p,T \qquad (5.48)$$

The jump in the pressure gradient can be obtained at the discontinuity interface as:

$$[\![\nabla p_w(\boldsymbol{x},t)]\!] = \nabla p_w(\boldsymbol{x}^+,t) - \nabla p_w(\boldsymbol{x}^-,t)$$
$$= \sum_{i=1}^{N} \nabla N_{p_i}(\xi^+)\hat{p}_{w_i}(t) - \sum_{i=1}^{N} \nabla N_{p_i}(\xi^-)\hat{p}_{w_i}(t) +$$

$$\sum_{j=1}^{M}\left[\nabla\bar{N}_{p_j}(\boldsymbol{\xi}^+)\psi_p(\boldsymbol{\xi}^+) + \bar{N}_{p_j}(\boldsymbol{\xi}^+)\left(\sum_{k=1}^{M}\nabla\bar{N}_{p_k}(\boldsymbol{\xi}^+)\left|\varphi(\boldsymbol{\xi}^+{}_k)\right|\text{-sign}(\varphi(\boldsymbol{\xi}^+))\boldsymbol{n}_{\Gamma_d}\right)\right]\hat{b}_j(t)-$$

$$\sum_{j=1}^{M}\left[\nabla\bar{N}_{p_j}(\boldsymbol{\xi}^-)\psi_p(\boldsymbol{\xi}^-) + \bar{N}_{p_j}(\boldsymbol{\xi}^-)\left(\sum_{k=1}^{M}\nabla\bar{N}_{p_k}(\boldsymbol{\xi}^-)\left|\varphi(\boldsymbol{\xi}^-{}_k)\right|\text{-sign}(\varphi(\boldsymbol{\xi}^-))\boldsymbol{n}_{\Gamma_d}\right)\right]\hat{b}_j(t)$$

$$= -2\sum_{j=1}^{M}\bar{N}_{p_j}(\boldsymbol{\xi})\boldsymbol{n}_{\Gamma_d}\hat{b}_j(t)$$

$$(5.49)$$

or the jump normal to the crack interface can be computed as:

$$\left[\!\left[\nabla p_w(\boldsymbol{x},t)\boldsymbol{n}_{\Gamma_d}\right]\!\right] = -2\sum_{j=1}^{M}\bar{N}_{p_j}(\boldsymbol{\xi})\hat{b}_j(t) \tag{5.50}$$

and for the temperature gradient:

$$\left[\!\left[\nabla T(\boldsymbol{x},t)\boldsymbol{n}_{\Gamma_d}\right]\!\right] = -2\sum_{j=1}^{M}\bar{N}_{T_j}(\boldsymbol{\xi})\hat{c}_j(t) \tag{5.51}$$

Thus, the pressure and temperature test functions $\delta p_w(\mathbf{x},t)$ and $\delta T(\mathbf{x},t)$ can be described in the same approximation space as:

$$\delta p_w(\mathbf{x},t) = \sum_{i=1}^{N}N_{p_i}(\xi)\delta\hat{p}_{w_i}(t) + \sum_{j=1}^{M}\bar{N}_{p_j}(\xi)\psi_p(\xi)\delta\hat{b}_j(t) = \mathbf{N}_p^{std}\,\delta\hat{\mathbf{p}}_w + \mathbf{N}_p^{enr}\,\delta\hat{\mathbf{b}} \tag{5.52}$$

$$\delta T(\mathbf{x},t) = \sum_{i=1}^{N}N_{T_i}(\xi)\delta\hat{T}_i(t) + \sum_{j=1}^{M}\bar{N}_{T_j}(\xi)\psi_T(\xi)\delta\hat{c}_j(t) = \mathbf{N}_T^{std}\,\delta\hat{\mathbf{T}} + \mathbf{N}_T^{enr}\,\delta\hat{\mathbf{c}} \tag{5.53}$$

$$\nabla\delta p_w(\mathbf{x},t) = \sum_{i=1}^{N}\nabla N_{p_i}(\xi)\delta\hat{p}_{w_i}(t) +$$

$$\sum_{j=1}^{M}\left[\nabla\bar{N}_{p_j}(\xi)\psi_p(\xi) + \bar{N}_{p_j}(\xi)\nabla\psi_p(\xi)\right]\delta\hat{b}_j(t) = \mathbf{B}_p^{std}\,\delta\hat{\mathbf{p}}_w + \mathbf{B}_p^{enr}\,\delta\hat{\mathbf{b}} \tag{5.54}$$

$$\nabla\delta T(\mathbf{x},t) = \sum_{i=1}^{N}\nabla N_{T_i}(\xi)\delta\hat{T}_i(t) +$$

$$\sum_{j=1}^{M}\left[\nabla\bar{N}_{T_j}(\xi)\psi_T(\xi) + \bar{N}_{T_j}(\xi)\nabla\psi_T(\xi)\right]\delta\hat{c}_j(t) = \mathbf{B}_T^{std}\,\delta\hat{\mathbf{T}} + \mathbf{B}_T^{enr}\,\delta\hat{\mathbf{c}} \tag{5.55}$$

5.3.2 Approximation of the primary variables

5.3.2.1 Mass balance equation

Substituting Equation (4.11) into Equation (5.9) gives the final form of the mass balance equation:

$$\int_{\Omega} \delta p_w \left[n(\rho_w - \rho_i)\frac{\partial s_w}{\partial T} + \chi \right]\dot{T}d\Omega + \int_{\Omega}\nabla(\delta p_w)\cdot\frac{k_r K}{\mu_w}\rho_w(\nabla p_w - \rho_w\mathbf{g})d\Omega +$$

$$\int_{\Omega}\nabla(\delta p_w)\cdot\alpha\frac{k_r K}{\mu_w}\frac{\rho_i l}{T}\rho_w(\nabla T)d\Omega + \int_{\Gamma_d}\delta p_w\cdot\rho_w\bar{q}_{w_d}d\Gamma + \tag{5.56}$$

$$\int_{\Gamma_{q_w}}\delta p_w\cdot\rho_w\bar{q}_w d\Gamma - \int_{\Omega}\delta p_w\left[(s_w\rho_w + s_i\rho_i)\dot{\varepsilon}_v\right]d\Omega = 0$$

The discretized form of the continuity equation can now be obtained by substituting equations (5.38), (5.43), (5.44), (5.46), (5.47), (5.52) and (5.54) into Equation (5.56).

$$\int_{\Omega}\left(\mathbf{N}_p^{std}\delta\hat{\mathbf{p}}_w + \mathbf{N}_p^{enr}\delta\hat{\mathbf{b}}\right)^T\left[n(\rho_w - \rho_i)\frac{\partial s_w}{\partial T}\right]\left(\mathbf{N}_T^{std}\dot{\hat{\mathbf{T}}} + \mathbf{N}_T^{enr}\dot{\hat{\mathbf{c}}}\right)d\Omega +$$

$$\int_{\Omega}\left(\mathbf{B}_p^{std}\delta\hat{\mathbf{p}}_w + \mathbf{B}_p^{enr}\delta\hat{\mathbf{b}}\right)^T\cdot\frac{k_r K}{\mu_w}\rho_w\left(\mathbf{B}_p^{std}\hat{\mathbf{p}}_w + \mathbf{B}_p^{enr}\hat{\mathbf{b}}\right)d\Omega - \int_{\Omega}\left(\mathbf{B}_p^{std}\delta\hat{\mathbf{p}}_w + \mathbf{B}_p^{enr}\delta\hat{\mathbf{b}}\right)^T\cdot\frac{k_r K}{\mu_w}\rho_w\left(\rho_w\mathbf{g}\right)d\Omega +$$

$$\int_{\Omega}\left(\mathbf{B}_p^{std}\delta\hat{\mathbf{p}}_w + \mathbf{B}_p^{enr}\delta\hat{\mathbf{b}}\right)^T\cdot\alpha\frac{k_r K}{\mu_w}\frac{\rho_i l}{T}\rho_w\left(\mathbf{B}_T^{std}\hat{\mathbf{T}} + \mathbf{B}_T^{enr}\hat{\mathbf{c}}\right)d\Omega + \int_{\Gamma_d}\left(\mathbf{N}_p^{std}\delta\hat{\mathbf{p}}_w + \mathbf{N}_p^{enr}\delta\hat{\mathbf{b}}\right)^T\cdot\rho_w\bar{q}_{w_d}d\Gamma + \tag{5.57}$$

$$\int_{\Gamma_{q_w}}\left(\mathbf{N}_p^{std}\delta\hat{\mathbf{p}}_w + \mathbf{N}_p^{enr}\delta\hat{\mathbf{b}}\right)^T\cdot\rho_w\bar{q}_w d\Gamma +$$

$$\int_{\Omega}\left(\mathbf{N}_p^{std}\delta\hat{\mathbf{p}}_w + \mathbf{N}_p^{enr}\delta\hat{\mathbf{b}}\right)^T\left(s_w\rho_w + s_i\rho_i\right)\mathbf{m}^T\left(\mathbf{B}_u^{std}\dot{\hat{\mathbf{u}}} + \mathbf{B}_u^{enr}\mathbf{L}\dot{\hat{\mathbf{a}}}\right)d\Omega$$

$$+\int_{\Omega}\left(\mathbf{N}_p^{std}\delta\hat{\mathbf{p}}_w + \mathbf{N}_p^{enr}\delta\hat{\mathbf{b}}\right)^T\chi\left(\mathbf{N}_T^{std}\dot{\hat{\mathbf{T}}} + \mathbf{N}_T^{enr}\dot{\hat{\mathbf{c}}}\right)d\Omega = 0$$

Equation (5.57) can be rewritten as:

$$\delta\hat{\mathbf{p}}_w^T\left\{\int_\Omega\left(\mathbf{N}_p^{std}\right)^T\left[n\left(\rho_w-\rho_i\right)\frac{\partial s_w}{\partial T}+\chi\right]\left(\mathbf{N}_T^{std}\dot{\hat{\mathbf{T}}}+\mathbf{N}_T^{enr}\dot{\hat{\mathbf{c}}}\right)d\Omega+\right.$$

$$\int_\Omega\left(\mathbf{B}_p^{std}\right)^T\cdot\frac{k_rK}{\mu_w}\rho_w\left(\mathbf{B}_p^{std}\hat{\mathbf{p}}_w+\mathbf{B}_p^{enr}\hat{\mathbf{b}}\right)d\Omega-\int_\Omega\left(\mathbf{B}_p^{std}\right)^T\cdot\frac{k_rK}{\mu_w}\rho_w\left(\rho_w\mathbf{g}\right)d\Omega+$$

$$\int_\Omega\left(\mathbf{B}_p^{std}\right)^T\cdot\alpha\frac{k_rK}{\mu_w}\frac{\rho_i l}{T}\rho_w\left(\mathbf{B}_T^{std}\hat{\mathbf{T}}+\mathbf{B}_T^{enr}\hat{\mathbf{c}}\right)d\Omega+\int_{\Gamma_d}\left(\mathbf{N}_p^{std}\right)^T\cdot\rho_w\overline{q}_{w_d}d\Gamma+$$

$$+\int_{\Gamma_{q_w}}\left(\mathbf{N}_p^{std}\right)^T\cdot\rho_w\overline{q}_w d\Gamma+\int_\Omega\left(\mathbf{N}_p^{std}\right)^T\left(s_w\rho_w+s_i\rho_i\right)\mathbf{m}^T\left(\mathbf{B}_u^{std}\dot{\hat{\mathbf{u}}}+\mathbf{B}_u^{enr}\mathbf{L}\dot{\hat{\mathbf{a}}}\right)d\Omega\right\}$$

$$\delta\hat{\mathbf{b}}^T\left\{\int_\Omega\left(\mathbf{N}_p^{enr}\right)^T\left[n\left(\rho_w-\rho_i\right)\frac{\partial s_w}{\partial T}+\chi\right]\left(\mathbf{N}_T^{std}\dot{\hat{\mathbf{T}}}+\mathbf{N}_T^{enr}\dot{\hat{\mathbf{c}}}\right)d\Omega+\right.$$

$$\int_\Omega\left(\mathbf{B}_p^{enr}\right)^T\cdot\frac{k_rK}{\mu_w}\rho_w\left(\mathbf{B}_p^{std}\hat{\mathbf{p}}_w+\mathbf{B}_p^{enr}\hat{\mathbf{b}}\right)d\Omega-\int_\Omega\left(\mathbf{B}_p^{enr}\right)^T\cdot\frac{k_rK}{\mu_w}\rho_w\left(\rho_w\mathbf{g}\right)d\Omega+$$

$$\int_\Omega\left(\mathbf{B}_p^{enr}\right)^T\cdot\alpha\frac{k_rK}{\mu_w}\frac{\rho_i l}{T}\rho_w\left(\mathbf{B}_T^{std}\hat{\mathbf{T}}+\mathbf{B}_T^{enr}\hat{\mathbf{c}}\right)d\Omega+\int_{\Gamma_d}\left(\mathbf{N}_p^{enr}\right)^T\cdot\rho_w\overline{q}_{w_d}d\Gamma+$$

$$\int_{\Gamma_{q_w}}\left(\mathbf{N}_p^{enr}\right)^T\cdot\rho_w\overline{q}_w d\Gamma+\int_\Omega\left(\mathbf{N}_p^{enr}\right)^T\left(s_w\rho_w+s_i\rho_i\right)\mathbf{m}^T\left(\mathbf{B}_u^{std}\dot{\hat{\mathbf{u}}}+\mathbf{B}_u^{enr}\mathbf{L}\dot{\hat{\mathbf{a}}}\right)d\Omega\right\}=0$$

$$(5.58)$$

which can be split into the following equations:

$$\mathbf{Q}_{pp}\hat{\mathbf{p}}_w+\mathbf{Q}_{pb}\hat{\mathbf{b}}+\overline{\mathbf{C}}_{pT}\dot{\hat{\mathbf{T}}}+\overline{\mathbf{C}}_{pc}\dot{\hat{\mathbf{c}}}+\mathbf{C}_{pT}\hat{\mathbf{T}}+\mathbf{C}_{pc}\hat{\mathbf{c}}+\overline{\mathbf{C}}_{pu}\dot{\hat{\mathbf{u}}}+\overline{\mathbf{C}}_{pa}\dot{\hat{\mathbf{a}}}=\mathbf{F}_p^{int}+\mathbf{F}_p^{ext} \tag{5.59}$$

$$\mathbf{Q}_{bp}\hat{\mathbf{p}}_w+\mathbf{Q}_{bb}\hat{\mathbf{b}}+\overline{\mathbf{C}}_{bT}\dot{\hat{\mathbf{T}}}+\overline{\mathbf{C}}_{bc}\dot{\hat{\mathbf{c}}}+\mathbf{C}_{bT}\hat{\mathbf{T}}+\mathbf{C}_{bc}\hat{\mathbf{c}}+\overline{\mathbf{C}}_{bu}\dot{\hat{\mathbf{u}}}+\overline{\mathbf{C}}_{ba}\dot{\hat{\mathbf{a}}}=\mathbf{F}_b^{int}+\mathbf{F}_b^{ext} \tag{5.60}$$

where the coefficients are defined as:

$$\mathbf{Q}_{pp}=\int_\Omega\left(\mathbf{B}_p^{std}\right)^T\cdot\frac{k_rK}{\mu_w}\rho_w\cdot\mathbf{B}_p^{std}d\Omega \tag{5.61}$$

$$\mathbf{Q}_{pb}=\int_\Omega\left(\mathbf{B}_p^{std}\right)^T\cdot\frac{k_rK}{\mu_w}\rho_w\cdot\mathbf{B}_p^{enr}d\Omega \tag{5.62}$$

$$\overline{\mathbf{C}}_{pT}=\int_\Omega\left(\mathbf{N}_p^{std}\right)^T\left[n\left(\rho_w-\rho_i\right)\frac{\partial s_w}{\partial T}+\chi\right]\mathbf{N}_T^{std}d\Omega \tag{5.63}$$

$$\overline{\mathbf{C}}_{pc}=\int_\Omega\left(\mathbf{N}_p^{std}\right)^T\left[n\left(\rho_w-\rho_i\right)\frac{\partial s_w}{\partial T}+\chi\right]\mathbf{N}_T^{enr}d\Omega \tag{5.64}$$

$$\mathbf{C}_{pT}=\int_\Omega\left(\mathbf{B}_p^{std}\right)^T\cdot\alpha\frac{k_rK}{\mu_w}\frac{\rho_i l}{T}\rho_w\cdot\mathbf{B}_T^{std}d\Omega \tag{5.65}$$

$$\mathbf{C}_{pc}=\int_\Omega\left(\mathbf{B}_p^{std}\right)^T\cdot\alpha\frac{k_rK}{\mu_w}\frac{\rho_i l}{T}\rho_w\cdot\mathbf{B}_T^{enr}d\Omega \tag{5.66}$$

$$\bar{\mathbf{C}}_{pu} = \int_{\Omega} \left(\mathbf{N}_p^{std} \right)^T \left(s_w \rho_w + s_i \rho_i \right) \mathbf{m}^T \mathbf{B}_u^{std} d\Omega \tag{5.67}$$

$$\bar{\mathbf{C}}_{pa} = \int_{\Omega} \left(\mathbf{N}_p^{std} \right)^T \left(s_w \rho_w + s_i \rho_i \right) \mathbf{m}^T \mathbf{B}_u^{enr} \mathbf{L} d\Omega \tag{5.68}$$

$$\mathbf{Q}_{bp} = \int_{\Omega} \left(\mathbf{B}_p^{enr} \right)^T \cdot \frac{k_r K}{\mu_w} \rho_w \cdot \mathbf{B}_p^{std} d\Omega \tag{5.69}$$

$$\mathbf{Q}_{bb} = \int_{\Omega} \left(\mathbf{B}_p^{enr} \right)^T \cdot \frac{k_r K}{\mu_w} \rho_w \cdot \mathbf{B}_p^{enr} d\Omega \tag{5.70}$$

$$\bar{\mathbf{C}}_{bT} = \int_{\Omega} \left(\mathbf{N}_p^{enr} \right)^T \left[n(\rho_w - \rho_i) \frac{\partial s_w}{\partial T} + \chi \right] \mathbf{N}_T^{std} d\Omega \tag{5.71}$$

$$\bar{\mathbf{C}}_{bc} = \int_{\Omega} \left(\mathbf{N}_p^{enr} \right)^T \left[n(\rho_w - \rho_i) \frac{\partial s_w}{\partial T} + \chi \right] \mathbf{N}_T^{enr} d\Omega \tag{5.72}$$

$$\mathbf{C}_{bT} = \int_{\Omega} \left(\mathbf{B}_p^{enr} \right)^T \cdot \alpha \frac{k_r K}{\mu_w} \frac{\rho_i l}{T} \rho_w \cdot \mathbf{B}_T^{std} d\Omega \tag{5.73}$$

$$\mathbf{C}_{bc} = \int_{\Omega} \left(\mathbf{B}_p^{enr} \right)^T \cdot \alpha \frac{k_r K}{\mu_w} \frac{\rho_i l}{T} \rho_w \cdot \mathbf{B}_T^{enr} d\Omega \tag{5.74}$$

$$\bar{\mathbf{C}}_{bu} = \int_{\Omega} \left(\mathbf{N}_p^{enr} \right)^T \left(s_w \rho_w + s_i \rho_i \right) \mathbf{m}^T \mathbf{B}_u^{std} d\Omega \tag{5.75}$$

$$\bar{\mathbf{C}}_{ba} = \int_{\Omega} \left(\mathbf{N}_p^{enr} \right)^T \left(s_w \rho_w + s_i \rho_i \right) \mathbf{m}^T \mathbf{B}_u^{enr} \mathbf{L} d\Omega \tag{5.76}$$

$$\mathbf{F}_p^{ext} = \int_{\Omega} \left(\mathbf{B}_p^{std} \right)^T \cdot \frac{k_r K}{\mu_w} \rho_w \left(\rho_w \mathbf{g} \right) d\Omega - \int_{\Gamma_{q_w}} \left(\mathbf{N}_p^{std} \right)^T \cdot \rho_w \bar{q}_w d\Gamma \tag{5.77}$$

$$\mathbf{F}_b^{ext} = \int_{\Omega} \left(\mathbf{B}_p^{enr} \right)^T \cdot \frac{k_r K}{\mu_w} \rho_w \left(\rho_w \mathbf{g} \right) d\Omega - \int_{\Gamma_{q_w}} \left(\mathbf{N}_p^{enr} \right)^T \cdot \rho_w \bar{q}_w d\Gamma \tag{5.78}$$

The terms related to discontinuity are calculated using Equation (5.10)

$$\mathbf{F}_p^{int} = \int_{\Gamma_d} \left(\mathbf{N}_p^{std} \right)^T \cdot \rho_w \bar{q}_{w_d} d\Gamma \tag{5.79}$$

$$\mathbf{F}_b^{int} = \int_{\Gamma_d} \left(\mathbf{N}_p^{enr} \right)^T \cdot \rho_w \bar{q}_{w_d} d\Gamma \tag{5.80}$$

5.3.2.2 Energy balance equation

Substituting Equation (3.5) into Equation (5.20) gives the final form of the heat transfer equation:

$$\int_{\Omega} \delta T (\rho C)_{\text{eff}} \dot{T} \, d\Omega + \int_{\Omega} \delta T (\rho_w C_w \mathbf{q}_w) \cdot \nabla T \, d\Omega +$$

$$\int_{\Omega} \nabla(\delta T) \cdot \alpha \frac{k_r K}{\mu_w} \rho_i l \ \cdot (\nabla p_w - \rho_w \mathbf{g}) d\Omega + \int_{\Omega} \nabla(\delta T) \cdot \left(\lambda_s^{1-n} \cdot \lambda_w^{ns_w} \cdot \lambda_i^{ns_i} \right) \nabla T d\Omega +$$

$$\int_{\Gamma_d} \delta T \, \bar{q}_{H_d} d\Gamma + \int_{\Gamma_{q_H}} \delta T \, \bar{q}_H d\Gamma - \int_{\Omega} \delta T \cdot l \cdot \dot{m}_{w \to i} \ d\Omega = 0 \tag{5.81}$$

The discretized form of the heat transfer equation can now be obtained by substituting equations (5.44), (5.46), (5.47), (5.53) and (5.55) into Equation (5.81):

$$\delta \hat{\mathbf{T}}^T \left\{ \int_{\Omega} \left(\mathbf{N}_T^{std} \right)^T (\rho C)_{\text{eff}} \left(\mathbf{N}_T^{std} \dot{\hat{\mathbf{T}}} + \mathbf{N}_T^{enr} \dot{\hat{\mathbf{c}}} \right) d\Omega + \int_{\Omega} \left(\mathbf{N}_T^{std} \right)^T (\rho_w C_w \mathbf{q}_w) \cdot \left(\mathbf{B}_T^{std} \hat{\mathbf{T}} + \mathbf{B}_T^{enr} \hat{\mathbf{c}} \right) d\Omega + \right.$$

$$\int_{\Omega} \left(\mathbf{B}_T^{std} \right)^T \cdot \alpha \frac{k_r K}{\mu_w} \rho_i l \ \cdot \left(\mathbf{B}_p^{std} \hat{\mathbf{p}}_w + \mathbf{B}_p^{enr} \hat{\mathbf{b}} \right) d\Omega - \int_{\Omega} \left(\mathbf{B}_T^{std} \right)^T \cdot \alpha \frac{k_r K}{\mu_w} \rho_i l \ \cdot (\rho_w \mathbf{g}) \, d\Omega +$$

$$\int_{\Omega} \left(\mathbf{B}_T^{std} \right)^T \cdot \left(\lambda_s^{1-n} \cdot \lambda_w^{ns_w} \cdot \lambda_i^{ns_i} \right) \left(\mathbf{B}_T^{std} \hat{\mathbf{T}} + \mathbf{B}_T^{enr} \hat{\mathbf{c}} \right) \, d\Omega + \int_{\Gamma_d} \left(\mathbf{N}_T^{std} \right)^T \bar{q}_{H_d} d\Gamma +$$

$$\left. \int_{\Gamma_{q_H}} \left(\mathbf{N}_T^{std} \right)^T \bar{q}_H d\Gamma - \int_{\Omega} \left(\mathbf{N}_T^{std} \right)^T \cdot l \cdot \dot{m}_{w \to i} \ d\Omega = 0 \right\} +$$

$$\delta \hat{\mathbf{c}}^T \left\{ \int_{\Omega} \left(\mathbf{N}_T^{enr} \right)^T (\rho C)_{\text{eff}} \left(\mathbf{N}_T^{std} \dot{\hat{\mathbf{T}}} + \mathbf{N}_T^{enr} \dot{\hat{\mathbf{c}}} \right) d\Omega + \int_{\Omega} \left(\mathbf{N}_T^{enr} \right)^T (\rho_w C_w \mathbf{q}_w) \cdot \left(\mathbf{B}_T^{std} \hat{\mathbf{T}} + \mathbf{B}_T^{enr} \hat{\mathbf{c}} \right) d\Omega + \right.$$

$$\int_{\Omega} \left(\mathbf{B}_T^{enr} \right)^T \cdot \alpha \frac{k_r K}{\mu_w} \rho_i l \ \cdot \left(\mathbf{B}_p^{std} \hat{\mathbf{p}}_w + \mathbf{B}_p^{enr} \hat{\mathbf{b}} \right) d\Omega - \int_{\Omega} \left(\mathbf{B}_T^{enr} \right)^T \cdot \alpha \frac{k_r K}{\mu_w} \rho_i l \ \cdot (\rho_w \mathbf{g}) \, d\Omega +$$

$$\int_{\Omega} \left(\mathbf{B}_T^{enr} \right)^T \cdot \left(\lambda_s^{1-n} \cdot \lambda_w^{ns_w} \cdot \lambda_i^{ns_i} \right) \left(\mathbf{B}_T^{std} \hat{\mathbf{T}} + \mathbf{B}_T^{enr} \hat{\mathbf{c}} \right) \, d\Omega + \int_{\Gamma_d} \left(\mathbf{N}_T^{enr} \right)^T \bar{q}_{H_d} d\Gamma +$$

$$\left. \int_{\Gamma_{q_H}} \left(\mathbf{N}_T^{enr} \right)^T \bar{q}_H d\Gamma - \int_{\Omega} \left(\mathbf{N}_T^{enr} \right)^T \cdot l \cdot \dot{m}_{w \to i} \ d\Omega \right\} = 0 \tag{5.82}$$

which can be split into the following equations:

$$\mathbf{C}_{Tp} \hat{\mathbf{p}}_w + \mathbf{C}_{Tb} \hat{\mathbf{b}} + \bar{\mathbf{H}}_{TT} \dot{\hat{\mathbf{T}}} + \bar{\mathbf{H}}_{Tc} \dot{\hat{\mathbf{c}}} + \mathbf{H}_{TT} \hat{\mathbf{T}} + \mathbf{H}_{Tc} \hat{\mathbf{c}} = \mathbf{F}_T^{\text{int}} + \mathbf{F}_T^{\text{ext}} \tag{5.83}$$

$$\mathbf{C}_{cp} \hat{\mathbf{p}}_w + \mathbf{C}_{cb} \hat{\mathbf{b}} + \bar{\mathbf{H}}_{cT} \dot{\hat{\mathbf{T}}} + \bar{\mathbf{H}}_{cc} \dot{\hat{\mathbf{c}}} + \mathbf{H}_{cT} \hat{\mathbf{T}} + \mathbf{H}_{cc} \hat{\mathbf{c}} = \mathbf{F}_c^{\text{int}} + \mathbf{F}_c^{\text{ext}} \tag{5.84}$$

where the coefficients are defined as:

$$\mathbf{C}_{Tp} = \int_{\Omega} \left(\mathbf{B}_T^{std} \right)^T \cdot \alpha \frac{k_r K}{\mu_w} \rho_i l \ \cdot \mathbf{B}_p^{std} d\Omega \tag{5.85}$$

$$\mathbf{C}_{Tb} = \int_{\Omega} \left(\mathbf{B}_T^{std} \right)^T \cdot \alpha \frac{k_r K}{\mu_w} \rho_i l \ \cdot \mathbf{B}_p^{enr} d\Omega \tag{5.86}$$

$$\bar{\mathbf{H}}_{TT} = \int_{\Omega} \left(\mathbf{N}_T^{std}\right)^T (\rho C)_{\text{eff}} \, \mathbf{N}_T^{std} \, d\Omega \tag{5.87}$$

$$\bar{\mathbf{H}}_{Tc} = \int_{\Omega} \left(\mathbf{N}_T^{std}\right)^T (\rho C)_{\text{eff}} \, \mathbf{N}_T^{enr} \, d\Omega \tag{5.88}$$

$$\mathbf{H}_{TT} = \int_{\Omega} \left(\mathbf{N}_T^{std}\right)^T \left(\rho_w C_w \mathbf{q}_w\right) \cdot \mathbf{B}_T^{std} \, d\Omega + \int_{\Omega} \left(\mathbf{B}_T^{std}\right)^T \cdot \left(\lambda_s^{1-n} \cdot \lambda_w^{ns_w} \cdot \lambda_i^{ns_i}\right) \cdot \mathbf{B}_T^{std} \, d\Omega \tag{5.89}$$

$$\mathbf{H}_{Tc} = \int_{\Omega} \left(\mathbf{N}_T^{std}\right)^T \left(\rho_w C_w \mathbf{q}_w\right) \cdot \mathbf{B}_T^{enr} \, d\Omega + \int_{\Omega} \left(\mathbf{B}_T^{std}\right)^T \cdot \left(\lambda_s^{1-n} \cdot \lambda_w^{ns_w} \cdot \lambda_i^{ns_i}\right) \cdot \mathbf{B}_T^{enr} \, d\Omega \tag{5.90}$$

$$\mathbf{C}_{cp} = \int_{\Omega} \left(\mathbf{B}_T^{enr}\right)^T \cdot \alpha \frac{k_r K}{\mu_w} \rho_i l \; \cdot \mathbf{B}_p^{str} \, d\Omega \tag{5.91}$$

$$\mathbf{C}_{cb} = \int_{\Omega} \left(\mathbf{B}_T^{enr}\right)^T \cdot \alpha \frac{k_r K}{\mu_w} \rho_i l \; \cdot \mathbf{B}_p^{enr} \, d\Omega \tag{5.92}$$

$$\bar{\mathbf{H}}_{cT} = \int_{\Omega} \left(\mathbf{N}_T^{enr}\right)^T (\rho C)_{\text{eff}} \, \mathbf{N}_T^{std} \, d\Omega \tag{5.93}$$

$$\bar{\mathbf{H}}_{cc} = \int_{\Omega} \left(\mathbf{N}_T^{enr}\right)^T (\rho C)_{\text{eff}} \, \mathbf{N}_T^{enr} \, d\Omega \tag{5.94}$$

$$\mathbf{H}_{cT} = \int_{\Omega} \left(\mathbf{N}_T^{enr}\right)^T \left(\rho_w C_w \mathbf{q}_w\right) \cdot \mathbf{B}_T^{std} \, d\Omega + \int_{\Omega} \left(\mathbf{B}_T^{enr}\right)^T \cdot \left(\lambda_s^{1-n} \cdot \lambda_w^{ns_w} \cdot \lambda_i^{ns_i}\right) \mathbf{B}_T^{std} \, d\Omega \tag{5.95}$$

$$\mathbf{H}_{cc} = \int_{\Omega} \left(\mathbf{N}_T^{enr}\right)^T \left(\rho_w C_w \mathbf{q}_w\right) \cdot \mathbf{B}_T^{enr} \, d\Omega + \int_{\Omega} \left(\mathbf{B}_T^{enr}\right)^T \cdot \left(\lambda_s^{1-n} \cdot \lambda_w^{ns_w} \cdot \lambda_i^{ns_i}\right) \mathbf{B}_T^{enr} \, d\Omega \tag{5.96}$$

$$\mathbf{F}_T^{\text{ext}} = \int_{\Omega} \left(\mathbf{B}_T^{std}\right)^T \cdot \alpha \frac{k_r K}{\mu_w} \rho_i l \; \cdot \left(\rho_w \mathbf{g}\right) d\Omega - \int_{\Gamma_{q_H}} \left(\mathbf{N}_T^{std}\right)^T \bar{q}_H \, d\Gamma \tag{5.97}$$

$$\mathbf{F}_c^{\text{ext}} = \int_{\Omega} \left(\mathbf{B}_T^{enr}\right)^T \cdot \alpha \frac{k_r K}{\mu_w} \rho_i l \; \cdot \left(\rho_w \mathbf{g}\right) d\Omega - \int_{\Gamma_{q_H}} \left(\mathbf{N}_T^{enr}\right)^T \bar{q}_H \, d\Gamma \tag{5.98}$$

$$\mathbf{F}_T^{\text{int}} = \int_{\Omega} \left(\mathbf{N}_T^{std}\right)^T \cdot l \cdot \dot{m}_{w \to i} \; d\Omega + \int_{\Gamma_d} \left(\mathbf{N}_T^{std}\right)^T \bar{q}_{H_d} \, d\Gamma \tag{5.99}$$

$$\mathbf{F}_c^{\text{int}} = \int_{\Omega} \left(\mathbf{N}_T^{enr}\right)^T \cdot l \cdot \dot{m}_{w \to i} \; d\Omega + \int_{\Gamma_d} \left(\mathbf{N}_T^{enr}\right)^T \bar{q}_{H_d} \, d\Gamma \tag{5.100}$$

5.3.2.3 Momentum balance equation

Substituting (4.6) and (4.25) into (5.31) gives the final form of the momentum balance equation:

$$-\int_{\Omega}\nabla(\delta\boldsymbol{u}):\boldsymbol{\sigma}^*d\Omega-\int_{\Omega}\nabla(\delta\boldsymbol{u}):(s_w p_w \boldsymbol{I})d\Omega-$$
$$\int_{\Gamma_d}[\![\delta\boldsymbol{u}]\!]\cdot(\beta_2 s_{i_d}+1)(p_w\boldsymbol{I})_d\boldsymbol{n}_{\Gamma_d}d\Gamma-\int_{\Gamma_t}\delta\boldsymbol{u}\cdot\bar{\boldsymbol{t}}\;\;d\Gamma-\int_{\Omega}\delta\boldsymbol{u}\cdot\rho\boldsymbol{g}d\Omega=0 \tag{5.101}$$

The discretized form of the force balance equation can be obtained by substituting equations (5.32), (5.38), (5.41), (5.42) and (5.43) into Equation (5.101):

$$\delta\hat{\boldsymbol{u}}^T\left\{-\int_{\Omega}\left(\mathbf{B}_u^{std}\right)^T:\boldsymbol{\sigma}^*d\Omega-\int_{\Omega}\left(\mathbf{B}_u^{std}\right)^T:s_w\left(\mathbf{N}_p^{std}\hat{\mathbf{p}}_w+\mathbf{N}_p^{enr}\hat{\mathbf{b}}\right)\mathbf{I}d\Omega-\right.$$
$$\left.\int_{\Gamma_t}\left(\mathbf{N}_u^{std}\right)^T\cdot\bar{\mathbf{t}}\,d\Gamma-\int_{\Omega}\left(\mathbf{N}_u^{std}\right)^T\cdot\rho\mathbf{g}d\Omega\right\}+$$
$$\delta\hat{\mathbf{a}}^T\left\{-\int_{\Omega}\left(\mathbf{B}_u^{enr}\mathbf{L}\right)^T:\boldsymbol{\sigma}^*d\Omega-\int_{\Omega}\left(\mathbf{B}_u^{enr}\mathbf{L}\right)^T:s_w\left(\mathbf{N}_p^{std}\hat{\mathbf{p}}_w+\mathbf{N}_p^{enr}\hat{\mathbf{b}}\right)\mathbf{I}d\Omega-\right.$$
$$\left.\int_{\Gamma_d}\left(\bar{\mathbf{N}}_u\mathbf{L}\right)^T\cdot\left(\beta_2 s_{i_d}+1\right)\left(p_w\mathbf{I}\right)\mathbf{n}_{\Gamma_d}d\Gamma-\int_{\Gamma_t}\left(\mathbf{N}_u^{enr}\mathbf{L}\right)^T\cdot\bar{\mathbf{t}}\,d\Gamma-\int_{\Omega}\left(\mathbf{N}_u^{enr}\mathbf{L}\right)^T\cdot\rho\mathbf{g}d\Omega=0\right. \tag{5.102}$$

which can be split into the following equations:

$$\mathbf{C}_{up}\hat{\mathbf{p}}_w+\mathbf{C}_{ub}\hat{\mathbf{b}}=\mathbf{F}_u^{intS}+\mathbf{F}_u^{ext} \tag{5.103}$$

$$\mathbf{C}_{ap}\hat{\mathbf{p}}_w+\mathbf{C}_{ab}\hat{\mathbf{b}}=\mathbf{F}_a^{intS}+\mathbf{F}_a^{int}+\mathbf{F}_a^{ext} \tag{5.104}$$

where the coefficients are defined as:

$$\mathbf{C}_{up}=-\int_{\Omega}s_w\left(\mathbf{B}_u^{std}\right)^T\cdot\mathbf{N}_p^{std}\mathbf{I}d\Omega \tag{5.105}$$

$$\mathbf{C}_{ub}=-\int_{\Omega}s_w\left(\mathbf{B}_u^{std}\right)^T\cdot\mathbf{N}_p^{enr}\mathbf{I}d\Omega \tag{5.106}$$

$$\mathbf{C}_{ap}=-\int_{\Omega}s_w\left(\mathbf{B}_u^{enr}\mathbf{L}\right)^T\cdot\mathbf{N}_p^{std}\mathbf{I}d\Omega \tag{5.107}$$

$$\mathbf{C}_{ab}=-\int_{\Omega}s_w\left(\mathbf{B}_u^{enr}\mathbf{L}\right)^T\cdot\mathbf{N}_p^{enr}\mathbf{I}d\Omega \tag{5.108}$$

$$\mathbf{F}_u^{ext}=\int_{\Gamma_t}\left(\mathbf{N}_u^{std}\right)^T\cdot\bar{\mathbf{t}}\,d\Gamma+\int_{\Omega}\left(\mathbf{N}_u^{std}\right)^T\cdot\rho\mathbf{g}d\Omega \tag{5.109}$$

$$\mathbf{F}_a^{ext}=\int_{\Gamma_t}\left(\mathbf{N}_u^{enr}\mathbf{L}\right)^T\cdot\bar{\mathbf{t}}\,d\Gamma+\int_{\Omega}\left(\mathbf{N}_u^{enr}\mathbf{L}\right)^T\cdot\rho\mathbf{g}d\Omega \tag{5.110}$$

$$\mathbf{F}_a^{int}=\int_{\Gamma_d}\left(\bar{\mathbf{N}}_u\mathbf{L}\right)^T\cdot\left(\beta_2 s_{i_d}+1\right)\left(p_w\mathbf{I}\right)_d\mathbf{n}_{\Gamma_d}d\Gamma \tag{5.111}$$

$$\mathbf{F}_u^{intS}=\int_{\Omega}\left(\mathbf{B}_u^{std}\right)^T:\boldsymbol{\sigma}^*d\Omega \tag{5.112}$$

$$\mathbf{F}_a^{\text{intS}} = \int_{\Omega} \left(\mathbf{B}_u^{enr} \mathbf{L} \right)^T : \boldsymbol{\sigma}^* d\Omega \qquad (5.113)$$

5.3.2.4 Choice of elements

In order to satisfy the Babuska-Brezzi convergence condition (Hughes et al., 1986), different order of interpolation function, usually one order lower for pore pressure compared to displacement, are employed in FEM. Thus, second-order element is employed in this work for the displacement field in the FEM part, while first-order element is used for the pressure field.

Considering the physic of the problem, first-order element is employed for the enriched part of the displacement field. To reach an exact approximation of the modified level-set function in Equation (5.45), first-order elements is used for the pressure and temperature fields.

Displacement   Pressure   Temperature

a) 1D elements

Displacement   Pressure   Temperature

b) 2D elements
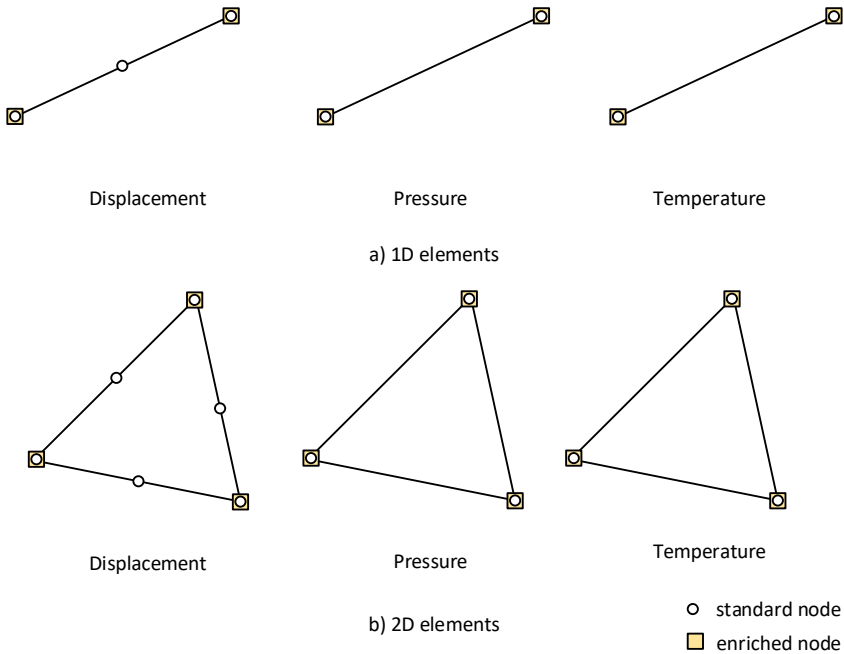
○ standard node
□ enriched node

Figure 17 Elements used for interpolation.

Figure 17 shows the elements employed in this work for approximating different fields of the problem.

5.3.3 Temporal discretization

Since the spatial discretization has been carried out, equations (5.59), (5.60), (5.83), (5.84), (5.103) and (5.104) represent a set of ordinary differential equations in time:

$$
\begin{bmatrix}
0 & 0 & \mathbf{C}_{up} & \mathbf{C}_{ub} & 0 & 0 \\
0 & 0 & \mathbf{C}_{ap} & \mathbf{C}_{ab} & 0 & 0 \\
0 & 0 & \mathbf{Q}_{pp} & \mathbf{Q}_{pb} & \mathbf{C}_{pT} & \mathbf{C}_{pc} \\
0 & 0 & \mathbf{Q}_{bp} & \mathbf{Q}_{bb} & \mathbf{C}_{bT} & \mathbf{C}_{bc} \\
0 & 0 & \mathbf{C}_{Tp} & \mathbf{C}_{Tb} & \mathbf{H}_{TT} & \mathbf{H}_{Tc} \\
0 & 0 & \mathbf{C}_{cp} & \mathbf{C}_{cb} & \mathbf{H}_{cT} & \mathbf{H}_{cc}
\end{bmatrix}
\begin{bmatrix}
\hat{\mathbf{u}} \\ \hat{\mathbf{a}} \\ \hat{\mathbf{p}}_w \\ \hat{\mathbf{b}} \\ \hat{\mathbf{T}} \\ \hat{\mathbf{c}}
\end{bmatrix}
+
\begin{bmatrix}
0 & 0 & 0 & 0 & 0 & 0 \\
0 & 0 & 0 & 0 & 0 & 0 \\
\bar{\mathbf{C}}_{pu} & \bar{\mathbf{C}}_{pa} & 0 & 0 & \bar{\mathbf{C}}_{pT} & \bar{\mathbf{C}}_{pc} \\
\bar{\mathbf{C}}_{bu} & \bar{\mathbf{C}}_{ba} & 0 & 0 & \bar{\mathbf{C}}_{bT} & \bar{\mathbf{C}}_{bc} \\
0 & 0 & 0 & 0 & \bar{\mathbf{H}}_{TT} & \bar{\mathbf{H}}_{Tc} \\
0 & 0 & 0 & 0 & \bar{\mathbf{H}}_{cT} & \bar{\mathbf{H}}_{cc}
\end{bmatrix}
\begin{bmatrix}
\dot{\hat{\mathbf{u}}} \\ \dot{\hat{\mathbf{a}}} \\ \dot{\hat{\mathbf{p}}}_w \\ \dot{\hat{\mathbf{b}}} \\ \dot{\hat{\mathbf{T}}} \\ \dot{\hat{\mathbf{c}}}
\end{bmatrix}
-
$$

$$
\begin{bmatrix}
\mathbf{F}_u^{\text{intS}} \\ \mathbf{F}_a^{\text{intS}} \\ 0 \\ 0 \\ 0 \\ 0
\end{bmatrix}
-
\begin{bmatrix}
0 \\ \mathbf{F}_a^{\text{int}} \\ \mathbf{F}_p^{\text{int}} \\ \mathbf{F}_b^{\text{int}} \\ \mathbf{F}_T^{\text{int}} \\ \mathbf{F}_c^{\text{int}}
\end{bmatrix}
-
\begin{bmatrix}
\mathbf{F}_u^{\text{ext}} \\ \mathbf{F}_a^{\text{ext}} \\ \mathbf{F}_p^{\text{ext}} \\ \mathbf{F}_b^{\text{ext}} \\ \mathbf{F}_T^{\text{ext}} \\ \mathbf{F}_c^{\text{ext}}
\end{bmatrix}
= 0
\tag{5.114}
$$

The time discretization of the equations is performed by the fully implicit first-order accurate finite difference scheme:

$$
\begin{bmatrix}
0 & 0 & \mathbf{C}_{up} & \mathbf{C}_{ub} & 0 & 0 \\
0 & 0 & \mathbf{C}_{ap} & \mathbf{C}_{ab} & 0 & 0 \\
\bar{\mathbf{C}}_{pu} & \bar{\mathbf{C}}_{pa} & \Delta t \mathbf{Q}_{pp} & \Delta t \mathbf{Q}_{pb} & \bar{\mathbf{C}}_{pT} + \Delta t \mathbf{C}_{pT} & \bar{\mathbf{C}}_{pc} + \Delta t \mathbf{C}_{pc} \\
\bar{\mathbf{C}}_{bu} & \bar{\mathbf{C}}_{ba} & \Delta t \mathbf{Q}_{bp} & \Delta t \mathbf{Q}_{bb} & \bar{\mathbf{C}}_{bT} + \Delta t \mathbf{C}_{bT} & \bar{\mathbf{C}}_{bc} + \Delta t \mathbf{C}_{bc} \\
0 & 0 & \Delta t \mathbf{C}_{Tp} & \Delta t \mathbf{C}_{Tb} & \bar{\mathbf{H}}_{TT} + \Delta t \mathbf{H}_{TT} & \bar{\mathbf{H}}_{Tc} + \Delta t \mathbf{H}_{Tc} \\
0 & 0 & \Delta t \mathbf{C}_{cp} & \Delta t \mathbf{C}_{cb} & \bar{\mathbf{H}}_{cT} + \Delta t \mathbf{H}_{cT} & \bar{\mathbf{H}}_{cc} + \Delta t \mathbf{H}_{cc}
\end{bmatrix}_{n+1}
\begin{bmatrix}
\hat{\mathbf{u}} \\ \hat{\mathbf{a}} \\ \hat{\mathbf{p}}_w \\ \hat{\mathbf{b}} \\ \hat{\mathbf{T}} \\ \hat{\mathbf{c}}
\end{bmatrix}_{n+1}
-
$$

$$
\begin{bmatrix}
\mathbf{F}_u^{\text{intS}} \\ \mathbf{F}_a^{\text{intS}} \\ 0 \\ 0 \\ 0 \\ 0
\end{bmatrix}
-
\begin{bmatrix}
0 \\ \mathbf{F}_a^{\text{int}} \\ \Delta t \mathbf{F}_p^{\text{int}} \\ \Delta t \mathbf{F}_b^{\text{int}} \\ \Delta t \mathbf{F}_T^{\text{int}} \\ \Delta t \mathbf{F}_c^{\text{int}}
\end{bmatrix}_{n+1}
-
\begin{bmatrix}
\mathbf{F}_u^{\text{ext}} \\ \mathbf{F}_a^{\text{ext}} \\ \Delta t \mathbf{F}_p^{\text{ext}} \\ \Delta t \mathbf{F}_b^{\text{ext}} \\ \Delta t \mathbf{F}_T^{\text{ext}} \\ \Delta t \mathbf{F}_c^{\text{ext}}
\end{bmatrix}_{n+1}
-
\begin{bmatrix}
0 & 0 & 0 & 0 & 0 & 0 \\
0 & 0 & 0 & 0 & 0 & 0 \\
\bar{\mathbf{C}}_{pu} & \bar{\mathbf{C}}_{pa} & 0 & 0 & \bar{\mathbf{C}}_{pT} & \bar{\mathbf{C}}_{pc} \\
\bar{\mathbf{C}}_{bu} & \bar{\mathbf{C}}_{ba} & 0 & 0 & \bar{\mathbf{C}}_{bT} & \bar{\mathbf{C}}_{bc} \\
0 & 0 & 0 & 0 & \bar{\mathbf{H}}_{TT} & \bar{\mathbf{H}}_{Tc} \\
0 & 0 & 0 & 0 & \bar{\mathbf{H}}_{cT} & \bar{\mathbf{H}}_{cc}
\end{bmatrix}_{n+1}
\begin{bmatrix}
\hat{\mathbf{u}} \\ \hat{\mathbf{a}} \\ \hat{\mathbf{p}}_w \\ \hat{\mathbf{b}} \\ \hat{\mathbf{T}} \\ \hat{\mathbf{c}}
\end{bmatrix}_{n}
= 0
\tag{5.115}
$$

where $\Delta t (= t_{n+1} - t_n)$ is the time step increment.

5.3.4 Linearization

The set of nonlinear Equation (5.115) is solved using Newton-Raphson iterative algorithm to linearize the nonlinear system of equations. By expanding Equation (5.115) with firs-order truncated Taylor series, the following linear approximation will be obtained:

$$
\mathbf{J}_{n+1}^i \cdot \Delta \mathbf{X}_{n+1}^{i+1} = -\mathbf{R}_{n+1}^i
\tag{5.116}
$$

where $\mathbf{J}$ is the Jacobian matrix, $\mathbf{R}$ is the residual vector, and $\Delta \mathbf{X}$ is defined as:

$$\Delta \mathbf{X}_{n+1}^{i+1} = \mathbf{X}_{n+1}^{i+1} - \mathbf{X}_{n+1}^{i} = \begin{bmatrix} \Delta \hat{\mathbf{u}} \\ \Delta \hat{\mathbf{a}} \\ \Delta \hat{\mathbf{p}}_w \\ \Delta \hat{\mathbf{b}} \\ \Delta \hat{\mathbf{T}} \\ \Delta \hat{\mathbf{c}} \end{bmatrix}_{n+1}^{i+1} = \begin{bmatrix} \hat{\mathbf{u}} \\ \hat{\mathbf{a}} \\ \hat{\mathbf{p}}_w \\ \hat{\mathbf{b}} \\ \hat{\mathbf{T}} \\ \hat{\mathbf{c}} \end{bmatrix}_{n+1}^{i+1} - \begin{bmatrix} \hat{\mathbf{u}} \\ \hat{\mathbf{a}} \\ \hat{\mathbf{p}}_w \\ \hat{\mathbf{b}} \\ \hat{\mathbf{T}} \\ \hat{\mathbf{c}} \end{bmatrix}_{n+1}^{i} \tag{5.117}$$

It is worth noting, using a tangential Jacobian matrix in Equation (5.116) might result in ill-posed coefficient matrix. Thus, we propose to use the modified version of Newton method using the elastic stiffness and the saturated permeability as the basis to evaluate the Jacobian matrix. In this way, the Jacobian matrix will be approximated as:

$$\mathbf{J}_{n+1}^{i} = \begin{bmatrix}
\mathbf{K}_{uu} & \mathbf{K}_{ua} & \mathbf{C}_{up} \\[2mm]
\mathbf{K}_{au} & \mathbf{K}_{aa} & \mathbf{C}_{ap} - \dfrac{\partial \mathbf{F}_a^{\text{int}}}{\partial \hat{\mathbf{p}}_w} \\[3mm]
\bar{\mathbf{C}}_{pu} - \Delta t \dfrac{\partial \mathbf{F}_p^{\text{int}}}{\partial \hat{\mathbf{u}}} + \tilde{\mathbf{C}}_{pu} & \bar{\mathbf{C}}_{pa} - \Delta t \dfrac{\partial \mathbf{F}_p^{\text{int}}}{\partial \hat{\mathbf{a}}} + \tilde{\mathbf{C}}_{pa} & \Delta t \left(\mathbf{Q}_{pp} - \dfrac{\partial \mathbf{F}_p^{\text{int}}}{\partial \hat{\mathbf{p}}_w} \right) \\[3mm]
\bar{\mathbf{C}}_{bu} - \Delta t \dfrac{\partial \mathbf{F}_b^{\text{int}}}{\partial \hat{\mathbf{u}}} + \tilde{\mathbf{C}}_{bu} & \bar{\mathbf{C}}_{ba} - \Delta t \dfrac{\partial \mathbf{F}_b^{\text{int}}}{\partial \hat{\mathbf{a}}} + \tilde{\mathbf{C}}_{ba} & \Delta t \left(\mathbf{Q}_{bp} - \dfrac{\partial \mathbf{F}_b^{\text{int}}}{\partial \hat{\mathbf{p}}_w} \right) \\[3mm]
-\Delta t \dfrac{\partial \mathbf{F}_T^{\text{int}}}{\partial \hat{\mathbf{u}}} & -\Delta t \dfrac{\partial \mathbf{F}_T^{\text{int}}}{\partial \hat{\mathbf{a}}} & \Delta t \mathbf{C}_{Tp} \\[3mm]
-\Delta t \dfrac{\partial \mathbf{F}_c^{\text{int}}}{\partial \hat{\mathbf{u}}} & -\Delta t \dfrac{\partial \mathbf{F}_c^{\text{int}}}{\partial \hat{\mathbf{a}}} & \Delta t \mathbf{C}_{cp}
\end{bmatrix}
$$

$$\cdots \begin{bmatrix}
\mathbf{C}_{ub} & \tilde{\mathbf{C}}_{uT} & \tilde{\mathbf{C}}_{uc} \\[2mm]
\mathbf{C}_{ab} - \dfrac{\partial \mathbf{F}_a^{\text{int}}}{\partial \hat{\mathbf{b}}} & \tilde{\mathbf{C}}_{aT} & \tilde{\mathbf{C}}_{ac} \\[3mm]
\Delta t \left(\mathbf{Q}_{pb} - \dfrac{\partial \mathbf{F}_p^{\text{int}}}{\partial \hat{\mathbf{b}}} \right) & \bar{\mathbf{C}}_{pT} + \Delta t \mathbf{C}_{pT} + \tilde{\mathbf{C}}_{pT} & \bar{\mathbf{C}}_{pc} + \Delta t \mathbf{C}_{pc} + \tilde{\mathbf{C}}_{pc} \\[3mm]
\Delta t \left(\mathbf{Q}_{bb} - \dfrac{\partial \mathbf{F}_b^{\text{int}}}{\partial \hat{\mathbf{b}}} \right) & \bar{\mathbf{C}}_{bT} + \Delta t \mathbf{C}_{bT} + \tilde{\mathbf{C}}_{bT} & \bar{\mathbf{C}}_{bc} + \Delta t \mathbf{C}_{bc} + \tilde{\mathbf{C}}_{bc} \\[3mm]
\Delta t \mathbf{C}_{Tb} & \bar{\mathbf{H}}_{TT} + \Delta t \left(\mathbf{H}_{TT} - \dfrac{\partial \mathbf{F}_T^{\text{int}}}{\partial \hat{\mathbf{T}}} \right) + \tilde{\mathbf{C}}_{TT} & \bar{\mathbf{H}}_{Tc} + \Delta t \left(\mathbf{H}_{Tc} - \dfrac{\partial \mathbf{F}_T^{\text{int}}}{\partial \hat{\mathbf{c}}} \right) + \tilde{\mathbf{C}}_{Tc} \\[3mm]
\Delta t \mathbf{C}_{cb} & \bar{\mathbf{H}}_{cT} + \Delta t \left(\mathbf{H}_{cT} - \dfrac{\partial \mathbf{F}_c^{\text{int}}}{\partial \hat{\mathbf{T}}} \right) + \tilde{\mathbf{C}}_{cT} & \bar{\mathbf{H}}_{cc} + \Delta t \left(\mathbf{H}_{cc} - \dfrac{\partial \mathbf{F}_c^{\text{int}}}{\partial \hat{\mathbf{c}}} \right) + \tilde{\mathbf{C}}_{cc}
\end{bmatrix}_{n+1}^{i} \tag{5.118}$$

The detailed calculation of the components of Jacobian matrix are given in appendix A. The residual vector in Equation (5.116) is calculated as:

$$
\mathbf{R}_{n+1}^{i} =
\begin{bmatrix}
0 & 0 & \mathbf{C}_{up} & \mathbf{C}_{ub} & 0 & 0 \\
0 & 0 & \mathbf{C}_{ap} & \mathbf{C}_{ab} & 0 & 0 \\
\bar{\mathbf{C}}_{pu} & \bar{\mathbf{C}}_{pa} & \Delta t\mathbf{Q}_{pp} & \Delta t\mathbf{Q}_{pb} & \bar{\mathbf{C}}_{pT}+\Delta t\mathbf{C}_{pT} & \bar{\mathbf{C}}_{pc}+\Delta t\mathbf{C}_{pc} \\
\bar{\mathbf{C}}_{bu} & \bar{\mathbf{C}}_{ba} & \Delta t\mathbf{Q}_{bp} & \Delta t\mathbf{Q}_{bb} & \bar{\mathbf{C}}_{bT}+\Delta t\mathbf{C}_{bT} & \bar{\mathbf{C}}_{bc}+\Delta t\mathbf{C}_{bc} \\
0 & 0 & \Delta t\mathbf{C}_{Tp} & \Delta t\mathbf{C}_{Tb} & \bar{\mathbf{H}}_{TT}+\Delta t\mathbf{H}_{TT} & \bar{\mathbf{H}}_{Tc}+\Delta t\mathbf{H}_{Tc} \\
0 & 0 & \Delta t\mathbf{C}_{cp} & \Delta t\mathbf{C}_{cb} & \bar{\mathbf{H}}_{cT}+\Delta t\mathbf{H}_{cT} & \bar{\mathbf{H}}_{cc}+\Delta t\mathbf{H}_{cc}
\end{bmatrix}_{n+1}^{i}
\begin{bmatrix}
\hat{\mathbf{u}} \\
\hat{\mathbf{a}} \\
\hat{\mathbf{p}}_{w} \\
\hat{\mathbf{b}} \\
\hat{\mathbf{T}} \\
\hat{\mathbf{c}}
\end{bmatrix}_{n+1}^{i} -
$$

$$
\begin{bmatrix}
\mathbf{F}_{u}^{\mathrm{intS}} \\
\mathbf{F}_{a}^{\mathrm{intS}} \\
0 \\
0 \\
0 \\
0
\end{bmatrix}_{n+1}^{i} -
\begin{bmatrix}
0 \\
\mathbf{F}_{a}^{\mathrm{int}} \\
\Delta t\mathbf{F}_{p}^{\mathrm{int}} \\
\Delta t\mathbf{F}_{b}^{\mathrm{int}} \\
\Delta t\mathbf{F}_{T}^{\mathrm{int}} \\
\Delta t\mathbf{F}_{c}^{\mathrm{int}}
\end{bmatrix}_{n+1}^{i} -
\begin{bmatrix}
\mathbf{F}_{u}^{\mathrm{ext}} \\
\mathbf{F}_{a}^{\mathrm{ext}} \\
\Delta t\mathbf{F}_{p}^{\mathrm{ext}} \\
\Delta t\mathbf{F}_{b}^{\mathrm{ext}} \\
\Delta t\mathbf{F}_{T}^{\mathrm{ext}} \\
\Delta t\mathbf{F}_{c}^{\mathrm{ext}}
\end{bmatrix}_{n+1} -
$$

$$
\begin{bmatrix}
0 & 0 & 0 & 0 & 0 & 0 \\
0 & 0 & 0 & 0 & 0 & 0 \\
\bar{\mathbf{C}}_{pu} & \bar{\mathbf{C}}_{pa} & 0 & 0 & \bar{\mathbf{C}}_{pT} & \bar{\mathbf{C}}_{pc} \\
\bar{\mathbf{C}}_{bu} & \bar{\mathbf{C}}_{ba} & 0 & 0 & \bar{\mathbf{C}}_{bT} & \bar{\mathbf{C}}_{bc} \\
0 & 0 & 0 & 0 & \bar{\mathbf{H}}_{TT} & \bar{\mathbf{H}}_{Tc} \\
0 & 0 & 0 & 0 & \bar{\mathbf{H}}_{cT} & \bar{\mathbf{H}}_{cc}
\end{bmatrix}_{n+1}^{i}
\begin{bmatrix}
\hat{\mathbf{u}} \\
\hat{\mathbf{a}} \\
\hat{\mathbf{p}}_{w} \\
\hat{\mathbf{b}} \\
\hat{\mathbf{T}} \\
\hat{\mathbf{c}}
\end{bmatrix}_{n}
\tag{5.119}
$$

Note that the index $(i, n+1)$ indicates that the Jacobian matrix $\mathbf{J}$ as well as the residual vector $\mathbf{R}$ is updated at each iteration. As a result, a sequence of linearized system of equations is solved to yield a solution satisfying the residual equation within each time step. This iterative process lasts by an appropriate convergence criterion.

Chapter 6 Comparison of calculated results and test results

6.1 Introduction

In this chapter, three labscale one-dimensional freezing test with different boundary and initial conditions are simulated using the proposed model, and the simulated results are compared with the test results These three tests were carried out on Devon silt, which were reported by Konrad and Morgenstern (Konrad, 1980). This material was chosen for its high frost susceptibility, availability and its similarity to silty materials found in northern regions.

The samples were prepared as a slurry at a moisture content of about 50% to 60%. Consolidation of the slurry to 210 kPa is performed in three stages. The water content after consolidation averaged between 27% and 30% and was relatively uniform throughout the specimen.

The material parameters selected for input are summarized in Table 1. The soil freezing characteristic curve is given in Figure 18.

Table 1 Material parameters for Devon silt.

| Parameter	Value
Heat capacity of soil grains, $C_s : J / kgK$	900
Heat capacity of ice, $C_i : J / kgK$	2095
Heat capacity of water, $C_w : J / kgK$	4190
Thermal conductivity of soil particles, $\lambda_s : W / mK$	3
Thermal conductivity of liquid water, $\lambda_w : W / mK$	0.6
Thermal conductivity of ice, $\lambda_i : W / mK$	2.2
Latent heat of fusion, $l : J / kg$	334000
Mass density of soil particles, $\rho_s : kg / m^3$	2600
Mass density of water, $\rho_w : kg / m^3$	1000
Mass density of ice, $\rho_i : kg / m^3$	900
Initial porosity, n	0.38
Bulk freezing temperature, $T_0 : K$	273.16
Temperature for fully frozen condition, $T_{ff} : K$	269.16
Temperature from which unfrozen water saturation in ice lense starts changing, $T_i : K$	273
Tensile strength at zero overburden, $a_0 : kPa$	8
Hydraulic conductivity of unfrozen soil, $k : cm / s$	1×10^{-7}
Residual unfrozen water saturation at temperatures below T_i, $S_{w_{res}}$	0.02
β_1	2.1
β_2	20

κ	3×10^{-4}
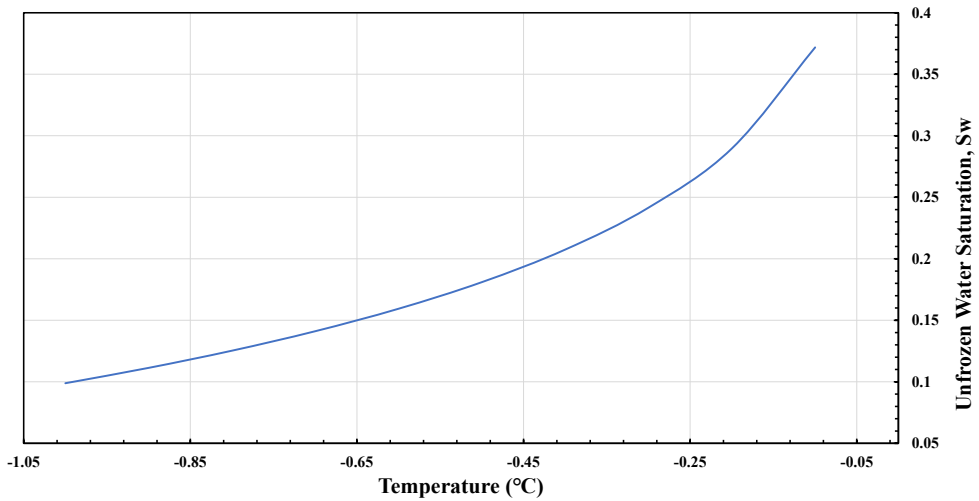
Figure 18 Soil freezing characteristic curve for Devon silt(Konrad & Duquennoi, 1993).

6.2 Numerical solution
6.2.1 Simulating case without overburden pressure

In test 1, a soil sample, with the length of 78 mm and diameter of 100 mm, was initially unfrozen without overburden pressure and a temperature of $+3°C$ throughout. The top surface temperature was then reduced to $-5.5°C$ to trigger the freezing process, and the temperature at the base was kept at $+3°C$ during the test. The duration of test is 42 hours. Water was freely available at the base, at zero pressure.

The pore water pressure and temperature profiles from simulated results are shown in Figure 19. Oscillations are observed in the pore water pressure filed in the frozen area, which are due to the fact that the pore water pressure develops between the ice lenses to cancel the temperature-gradient-induced water flow. The developed pore water pressure would also balance the overburden load, which is zero in this case. The phenomenon of pore water pressure developing is satisfactorily captured by the model.

Below the freezing front, a suction of around 13 kPa has been predicted by the model, while 18 kPa was measured by Konrad and Morgenstern (Konrad, 1980). The difference is most likely from the uncertainties in the estimation of the relative permeability parameters. Figure 20 shows the displacement field with the jumps indicating the ice lens formation and length. As shown in the figure, the final ice lens is predicted to be at 21 mm from the base. Figure 21 compares the calculated and measured heave in time, and reasonable agreement is achieved.
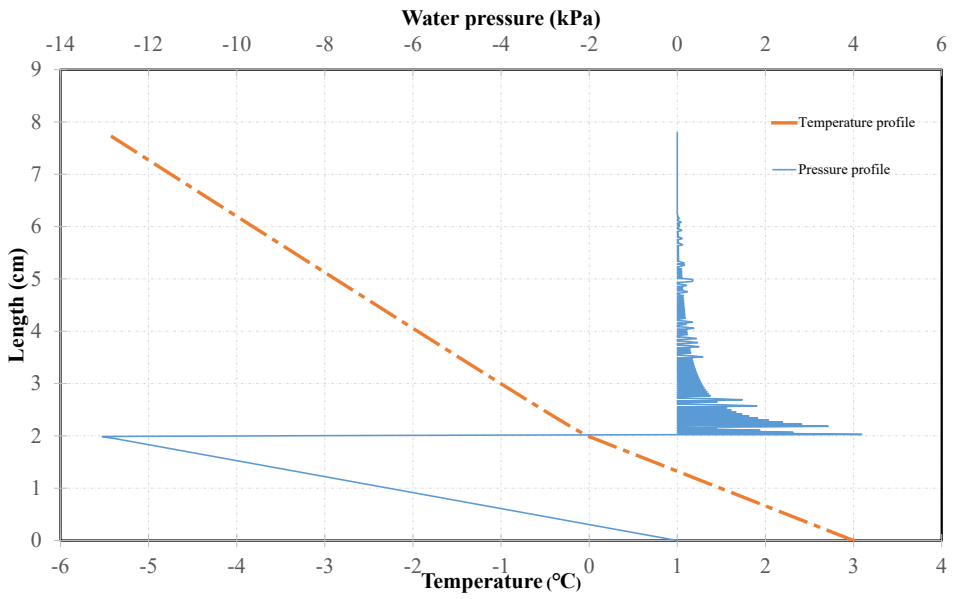
Figure 19 Temperature and pore pressure profile after 42 hours, from model (test 1, without overburden pressure).
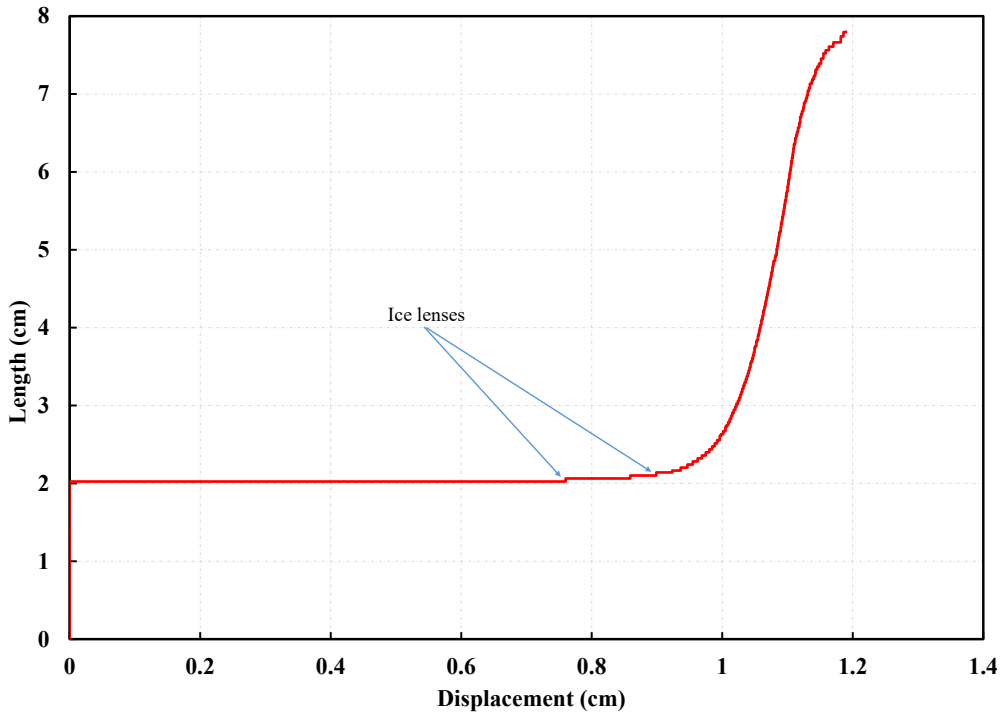
Figure 20 Displacement profile (test 1) after 42 hours from, model (test 1, without overburden pressure).
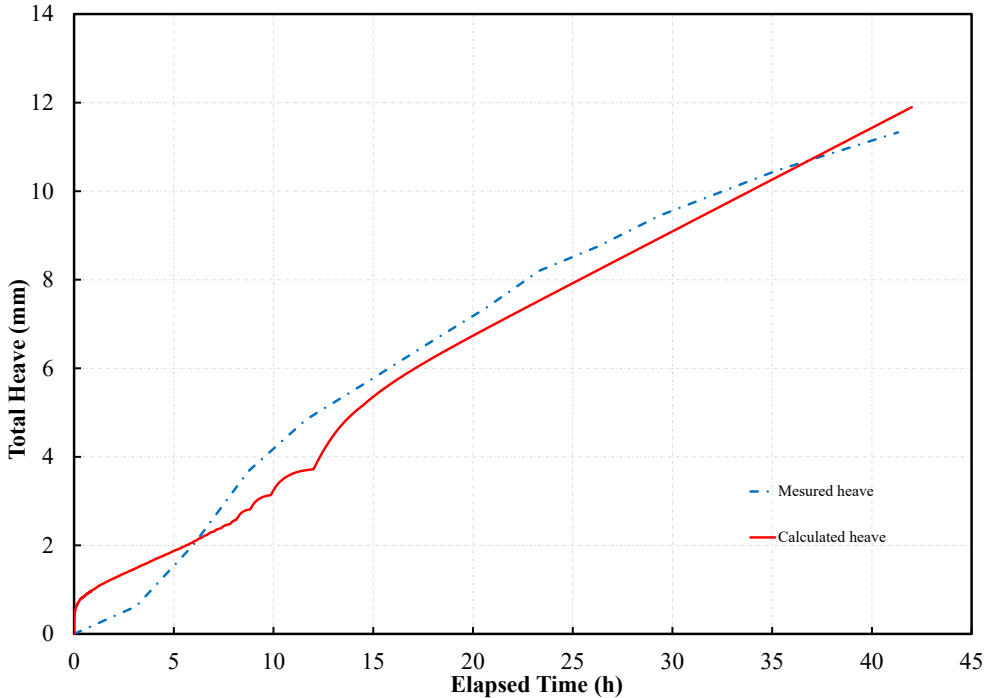
Figure 21 Comparison between the measured (test 1) and predicted frost heave, from model (test 1, without overburden pressure).

6.2.2 Simulating case with overburden pressure of 100 kPa

In test 2, a soil sample, with the length of 100 mm and diameter of 100 mm, was initially unfrozen with overburden pressure of 100 kPa and a temperature of $+1.8°C$ throughout. The top surface temperature was then reduced to $-4.7°C$ to trigger the freezing process, and the temperature at the base was kept at $+3°C$ during the test. The duration of test is 141 hours. Water was freely available at the base, at zero pressure.

The pore water pressure and temperature profiles from simulated results are shown in Figure 22. Figure 23 shows the displacement field. As shown in the figure, the final ice lens is predicted to be at 20 mm from the base. Figure 24 compares the calculated and measured heave in time, and reasonable agreement is achieved.
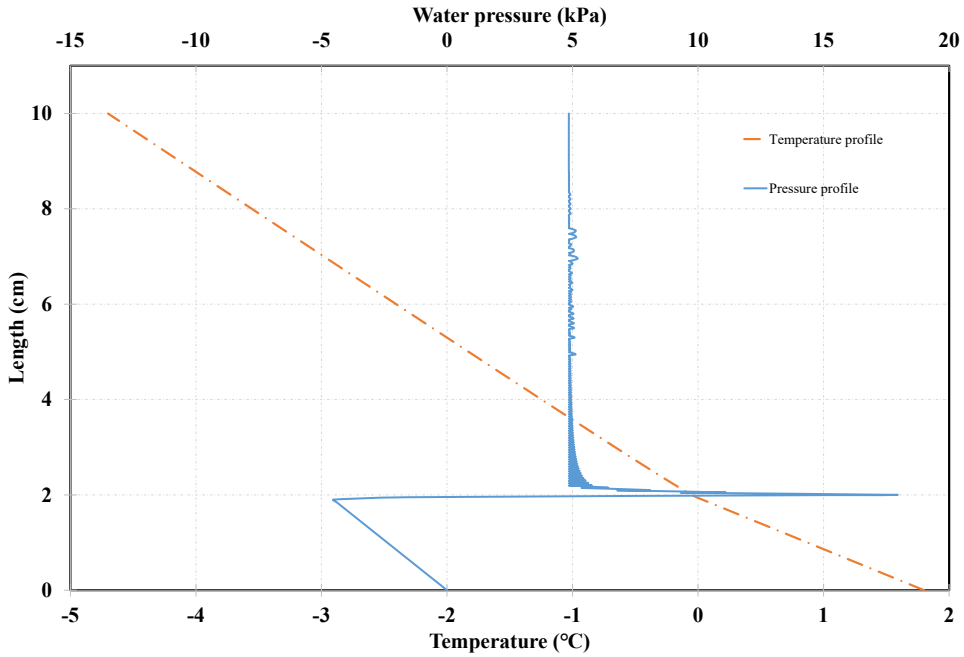
Figure 22 Temperature and pore pressure profile after 141 hours, from model (test 2, with overburden pressure of 100 kPa).
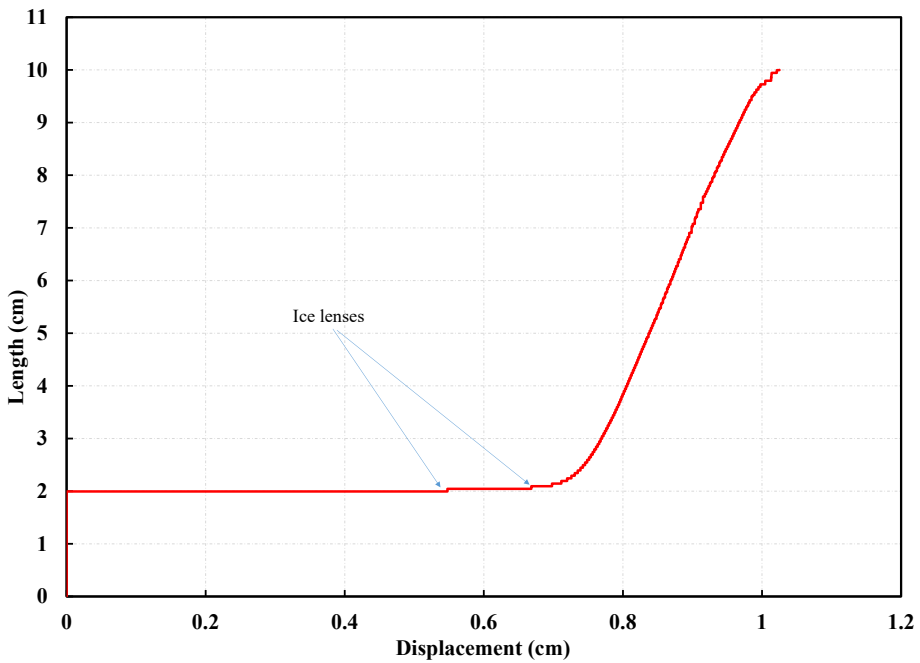
Figure 23 Displacement profile (test 2) after 141 hours, from model (with overburden pressure of 100 kPa).

Figure 24 Comparison between the measured (test 2) and predicted frost heave, , from model (with overburden pressure of 100 kPa).

6.2.3 Simulating case with overburden pressure of 45 kPa

In test 3, a soil sample, with the length of 77 mm and diameter of 100 mm, was initially unfrozen with overburden pressure of 45 kPa and a temperature of $+1°C$ throughout. The top surface temperature was then reduced to $–3.7°C$ to trigger the freezing process, and the temperature at the base was kept at $+1°C$ during the test. The duration of test is 42 hours. Water was freely available at the base, at zero pressure.

The pore water pressure and temperature profiles from simulated results are shown in Figure 25. Figure 26 shows the displacement field. As shown in the figure, the final ice lens is predicted to be at 12 mm from the base. Figure 27compares the calculated and measured heave in time, and reasonable agreement is achieved.

The results of ice lenses formation for each test, which is calculated using the proposed model, are showed in Figure 28.

Figure 25 Temperature and pore pressure profile after 42 hours, from model (test 3, with overburden pressure of 45 kPa).

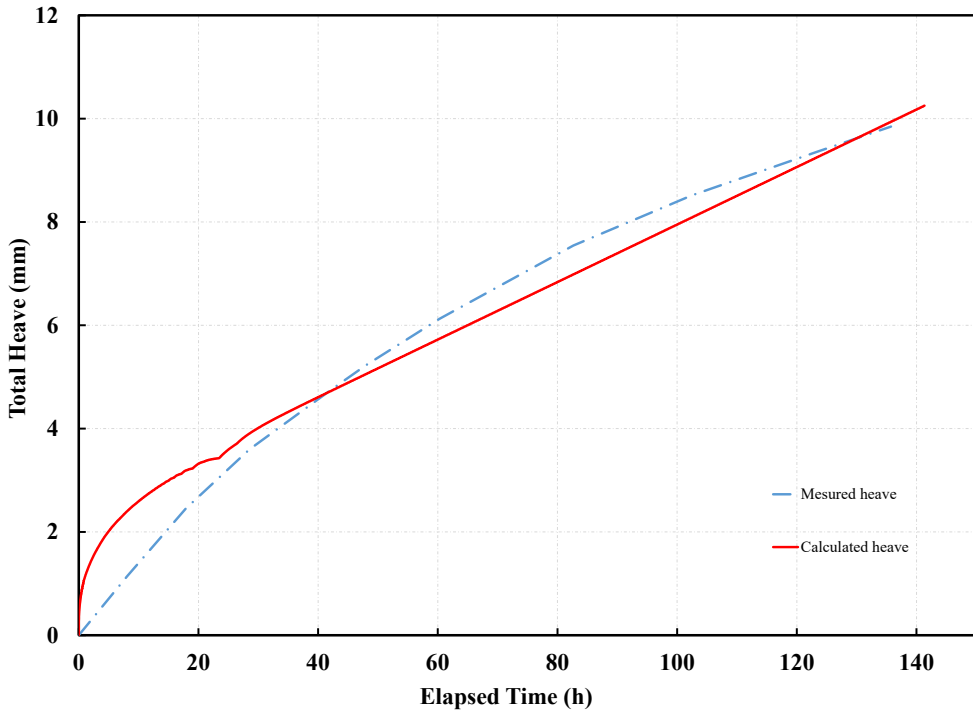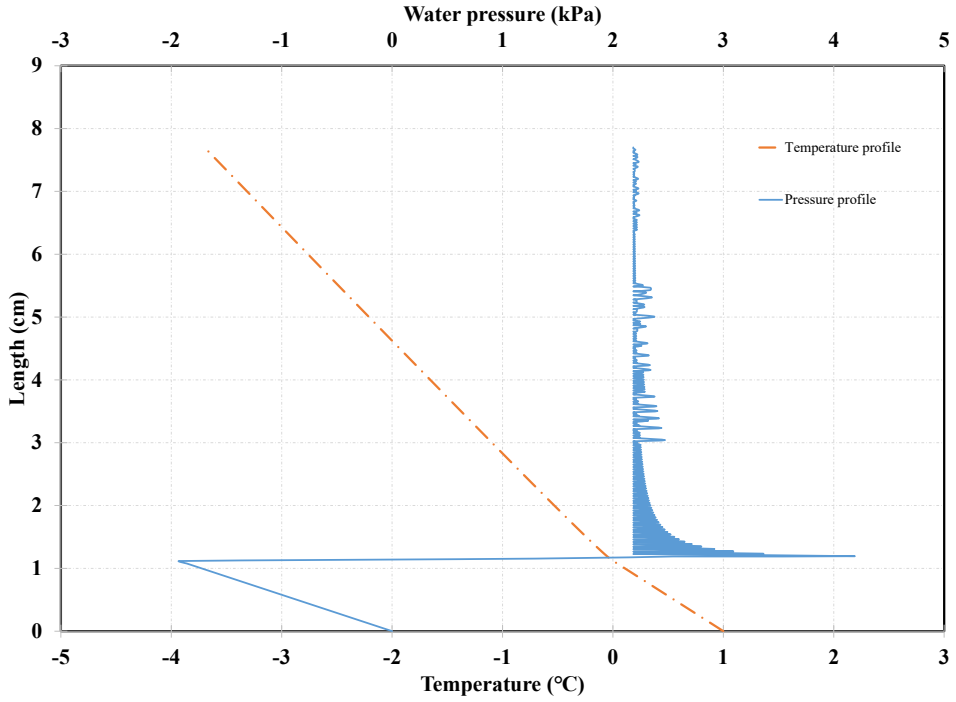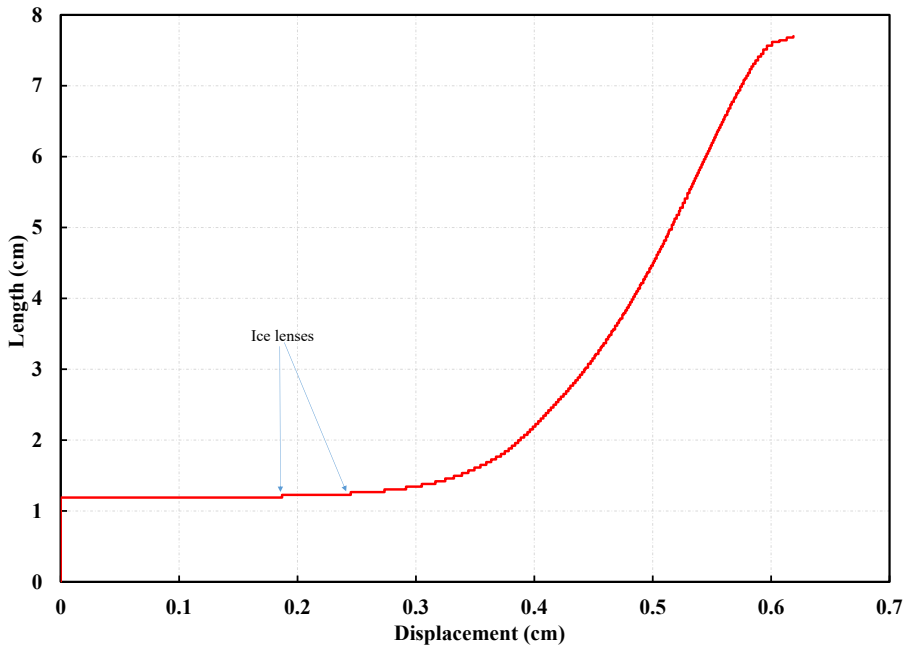*Figure 26 Displacement profile (test 3) after 42 hours, from model (with overburden pressure of 45 kPa).*
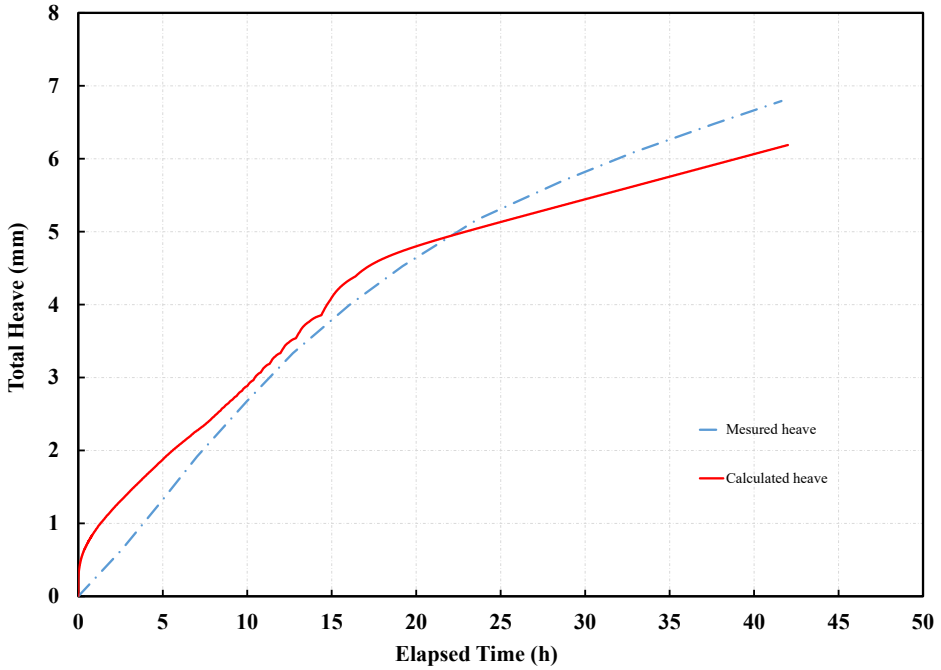
Figure 27 Comparison between the measured (test 3) and predicted frost heave, from model (with overburden pressure of 45 kPa).
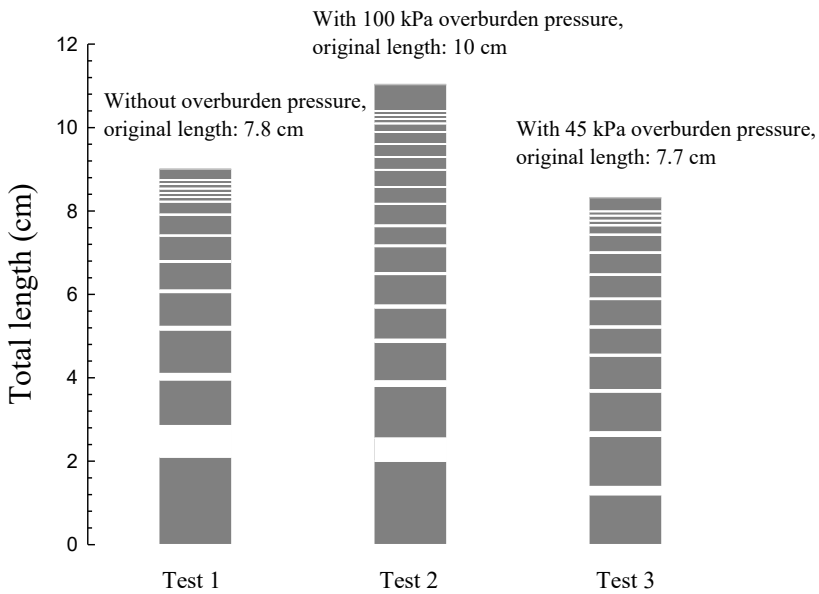
Figure 28 Simulated ice lenses formation.

6.2.4 Shut-off pressure prediction

The shut-off pressure for the soil samples used above has also been calculated by the proposed model. The overburden pressure has been increased to find the shut-off pressure, based on the condition of each test, where the heave is almost zero and the pressure gradient in the unfrozen part is almost zero as Figure 29 shows. It is worth noting that both ρ_i and ρ_w has been set to 1000 kg/m3 to ignore deformation or water flow because of density difference during phase change.
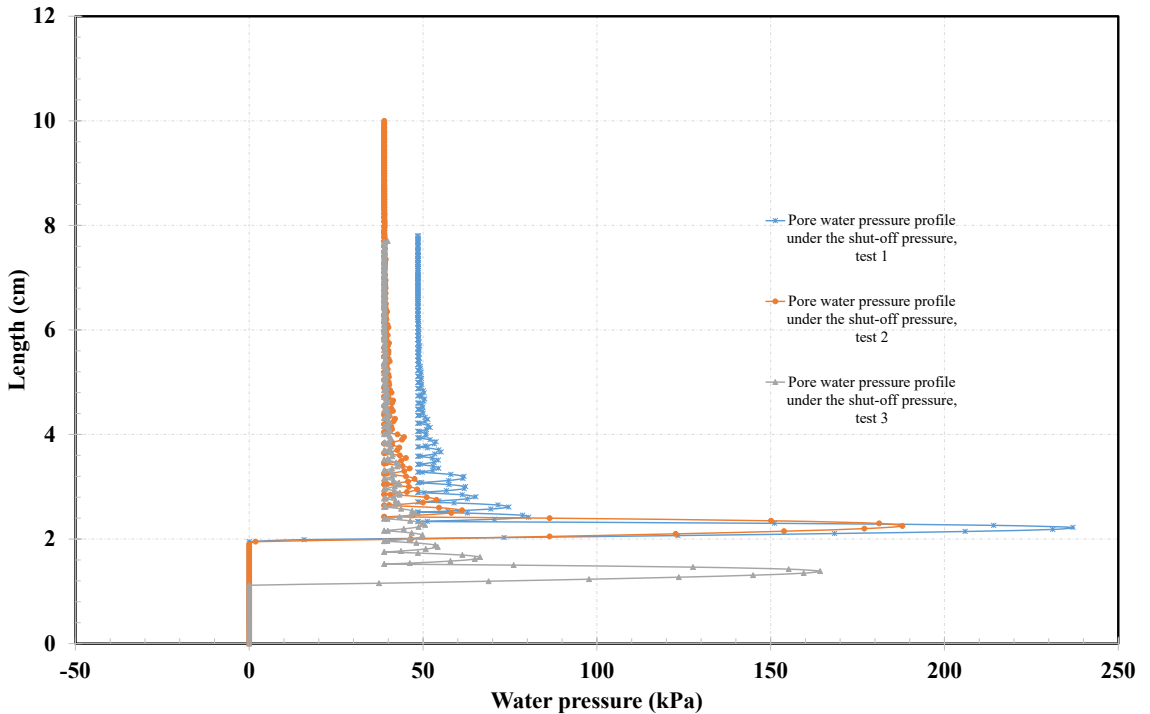
Figure 29 The pressure profile in the unfrozen part for the three tests under shut-off overburden pressure.

For the soil sample under conditions of test 1, the shut-off pressure is around 1000 kPa. While for the soil samples under conditions of tests 2 and 3, the shut-off pressure is around 800 kPa. The estimation of shut-off pressure from Konrad(Konrad & Morgenstern, 1981) which was reported to be around 1000 kPa to 1200 kPa is close to our results, while the estimation from Wayne et al.(Arvidson & Morgenstern, 1977), with 69 and 215 kPa for Devon silt and modified Devon silt, is too low.

The temperature gradient in frozen fringe is obtained after the simulation, it is $-107.3^{\circ}C/m$, $-66.7^{\circ}C/m$ and $-64.1^{\circ}C/m$. A conclusion can be achieved that the shut-off pressure is positively correlated with temperature gradient in frozen fringe as expected from the coupled transport equations.

Chapter 7   Summary and conclusions

7.1 Summary

To predict the influence of soil freezing process to the ground, this study was conducted to develop a THM model for predicting frost heave with multiple ice lenses using discrete method. This Ph.D. project focus on deriving coupled governing equations for the dynamic freezing process of the soil-water-ice system, solving equations with X-FEM and implementation, as well as providing a better understanding of the physical processes behind the frost heave phenomenon.

In this study, non-equilibrium thermodynamic theory is employed to describe the transport of water and heat flow. Water intends to transport towards the colder part, and a counter pressure behind the freezing front will build according to the coupled equations derived from the theory of Kjelstrup et al.(Kjelstrup & Bedeaux, 2008). As a result, a crack might appear owing to decrease of effective stress, which results in the initiation and growth of ice lens.

Based on the conceptual model for frost heave, together with the mass, momentum and energy balance equations, appropriate stress measure and crack criterion are also introduced to describe the dynamic of the system. In deriving the equations, an essential assumption is made that the ice phase has a similar motion of the solid skeleton. Therefore, the Lagrangian form is used for the ice phase and the solid skeleton, while the Eulerian form of the balance equations with respect to the motion of the solid skeleton are used for the unfrozen water phase.

To discretize the governing equations with the existence of discontinuities, X-FEM is employed, which avoids conforming the discretization (mesh) to the line or surface of discontinuity and regenerating the mesh at each step. The primary variables, i.e., displacement, water pressure and temperature are approximated according to the properties of discontinuities. To fulfill the mechanical coupling requirement emanating from water pressure and ice-soil contact stress exerted on the crack surface and the mass and heat transfer coupling requirement originating from the flux of mass and heat flowing through the crack borders, some specific boundary conditions are defined. After a system of ordinary differential equations in time is obtained, the time discretization of the equations is performed by the fully implicit first-order accurate finite difference scheme. Linearization of the system is performed using the Newton-Raphson algorithm.

Three lab scale one-dimensional freezing tests available data on Devon silt, which was chosen for its high frost susceptibility, availability and its similarity to silty materials found in northern regions, are simulated using the proposed model, after the equations have been implemented. The simulated tests include one freezing test without overburden pressure and two freezing tests with different overburden pressure of 100 kPa and 45 kPa. The calculated and measured total frost heave in time are compared, and reasonable agreement is achieved. In addition, the shut-off pressure is estimated based on the three tests' condition, by increasing the overburden pressure to make heave almost zero and the pressure gradient in the unfrozen part

almost zero. The shut-off pressure is around 1000 kPa for the soil sample under conditions of test 1, while it is 800 kPa for the soil samples under conditions of tests 2 and 3.

7.2 Conclusions

Mass and heat transport can be affected by both temperature and pressure gradients simultaneously. In the process of frost heave, the temperature gradient is the main driving force. The soil grains can be separated by increasing pore water pressure, which increases to cancel the water flow induced by temperature gradient. Frost heave happens when three conditions coincide: the temperature is below the normal freezing point of bulk water, the sub-cooled water is connected to a water reservoir, and the mechanical condition of the soil allows the ice lens to grow.

The new model for predicting frost heave presented in this work has also described the initiation and growth of multiple ice lenses in soil freezing. The governing equations with discontinuities are solved using the X-FEM by considering ice lenses as cracks inside the corresponding elements.

The calculated results from the proposed model has been compared with the results from three freezing tests conducted by Konrad(Konrad, 1980), and reasonable agreement is achieved. Furthermore, the model can be applied to estimate the shut-off pressure of soil under freezing. By calculating the shut-off pressure of the soil samples used in Konrad's test(Konrad, 1980), the conclusion can be achieved that the shut-off pressure is positively correlated with temperature gradient in frozen fringe as expected from the coupled transport equations.

Chapter 8   Recommendation for future work

With regards to the work presented in this dissertation, suggestions are provided for further research:

- During this study, all the tests simulated for validating are in one-dimensional model. As future work, investigating the performance of two-dimensional model with multiple ice lenses can expand the understanding further, and it can also improve the accuracy of the results to some extent.

- Based on the existing hazard related to frost heave, the bearing capacity of soil can be substantially reduced after freeze-thaw cycles. During this project, the main effort has been concentrated on freezing phenomena, without considering thaw weakening. To predict the damages of infrastructure by seasonal changes in temperature and soil moisture, the process of thaw weakening can be considered into the THM model to finalize the entire freezing and thawing process of seasonal frozen soil.

- The soil experiencing freezing (and thawing) may have dramatically different properties, depending on its thermal state and overburden pressure. The freezing process could significantly affect the quantitative content of the soil mixture components and alter the mixture microstructure. In addition, soil strength will increase as the soil freezes. During this work, the ideal elastic model has been used for the soil. For further development of the numerical model, some more advanced constitutive models for freezing soil can be employed to describe the elasto-plastic behaviour of freezing soil.

References

Abdelaziz, Y., & Hamouine, A. (2008). A survey of the extended finite element. *Computers & Structures*, *86*(11-12), 1141-1151.

Abed, A. A., & Sołowski, W. T. (2017). A study on how to couple thermo-hydro-mechanical behaviour of unsaturated soils: Physical equations, numerical implementation and examples. *Computers and geotechnics*, *92*, 132-155.

Amiri, S. G., Taheri, E., & Lavasan, A. (2021). A hybrid finite element model for non-isothermal two-phase flow in deformable porous media. *Computers and geotechnics*, *135*, 104199.

Argyris, J. H., & Kelsey, S. (1960). *Energy theorems and structural analysis* (Vol. 60). Springer.

Arvidson, W. D., & Morgenstern, N. R. (1977). Water flow induced by soil freezing. *Canadian Geotechnical Journal*, *14*(2), 237-245. https://doi.org/10.1139/t77-024

Belytschko, T., & Black, T. (1999). Elastic crack growth in finite elements with minimal remeshing. *International Journal for Numerical Methods in Engineering*, *45*(5), 601-620.

Beskow, G. (1930). Erdfliessen und Strukturböden der Hochgebirge im Licht der Frosthebung: Preliminäro Mitteilung. *Geologiska Föreningen i Stockholm Förhandlingar*, *52*(4), 622-638.

Bettess, P. (1977). Infinite elements. *International Journal for Numerical Methods in Engineering*, *11*(1), 53-64.

Biermans, M., Dijkema, K., & De Vries, D. (1978). Water movement in porous media towards an ice front. *Journal of Hydrology*, *37*(1-2), 137-148.

Bronfenbrener, L., & Korin, E. (1997). Kinetic model for crystallization in porous media. *International journal of heat and mass transfer*, *40*(5), 1053-1059.

Brown, J., Ferrians Jr, O., Heginbottom, J. A., & Melnikov, E. (1997). *Circum-Arctic map of permafrost and ground-ice conditions*. US Geological Survey Reston, VA.

Cahn, J., Dash, J., & Fu, H. (1992). Theory of ice premelting in monosized powders. *Journal of crystal growth*, *123*(1-2), 101-108.

Campanella, R. G., & Mitchell, J. K. (1968). Influence of temperature variations on soil behavior. *Journal of the Soil Mechanics and Foundations Division*, *94*(3), 709-734.

Chen, P., Luo, H., & Liu, E. (2020). Moisture Transfer and Formation of Separate Ice in the Freezing Process of Saturated Soils. *Water*, *12*(4), 1044.

Cheng, Y. M. (1996). The use of infinite element. *Computers and geotechnics*, *18*(1), 65-70.

Clough, R. W. (1960). The finite element method in plane stress analysis. Proceedings of 2nd ASCE Conference on Electronic Computation, Pittsburgh Pa., Sept. 8 and 9, 1960,

Committee, P. T. (2010). Snow And Ice Data Yearbook 2010. *B5 Winter Service*.

Dash, J. (1989). Thermomolecular pressure in surface melting: motivation for frost heave. *Science*, *246*(4937), 1591-1593.

Daux, C., Moës, N., Dolbow, J., Sukumar, N., & Belytschko, T. (2000). Arbitrary branched and intersecting cracks with the extended finite element method. *International Journal for Numerical Methods in Engineering*, *48*(12), 1741-1760.

Defay, R., Prigogine, I., & Bellemans, A. (1966). *Surface tension and adsorption*. Wiley.

Derjaguin, B., & Churaev, N. (1978). The theory of frost heaving. *Journal of Colloid and Interface Science*, *67*(3), 391-396.

Derjaguin, B., & Churaev, N. (1986). Flow of nonfreezing water interlayers and frost heaving. *Cold Regions Science and Technology*, *12*(1), 57-66.

Derjaguin, B., & Churaev, N. (1993). Flow of nonfreezing water interlayers and frost heaving. *Progress in Surface Science*, *43*(1-4), 232-240.

Derjaguin, B., Churaev, N., Sobolev, V., & Barer, S. (1981). Thermocrystallization flow of nonfreezing water films on the surface of capillaries. *Journal of Colloid and Interface Science*, *84*(1), 182-190.

Derjaguin, B., Churaev, N., Sobolev, V., & Barer, S. (1993). Thermocrystallization flow of nonfreezing water films on the surface of capillaries. *Progress in Surface Science*, *43*(1-4), 223-231.

DiMillio, A. F. (1999). *A quarter century of geotechnical research*.

Dolbow, J., Moës, N., & Belytschko, T. (2001). An extended finite element method for modeling crack growth with frictional contact. *Computer methods in applied mechanics and engineering*, *190*(51-52), 6825-6846.

Everett, D. (1961). The thermodynamics of frost damage to porous solids. *Transactions of the Faraday society*, *57*, 1541-1551.

Førland, T., & Ratkje, S. K. (1982). Irreversible thermodynamic treatment of frost heave. In *Developments in Geotechnical Engineering* (Vol. 28, pp. 225-229). Elsevier.

Fowler, A. (1989). Secondary frost heave in freezing soils. *SIAM Journal on Applied Mathematics*, *49*(4), 991-1008.

Fremond, M., Ghidouche, H., & Point, N. (1985). Freezing of a porous medium with water supply coupled Stefan problem. *Journal of mathematical analysis and applications*, *108*(2), 371-402.

Gaskin, P. N., & Sutherland, H. B. (1973). Pore water and heaving pressures developed in partially frozen soils. Permafrost: North American Contribution [to The] Second International Conference,

Ghoreishian Amiri, S., Grimstad, G., Kadivar, M., & Nordal, S. (2016). Constitutive model for rate-independent behavior of saturated frozen soils. *Canadian Geotechnical Journal*, *53*(10), 1646-1657.

Gilpin, R. (1980). Theoretical studies of particle engulfment. *Journal of Colloid and Interface Science*, *74*(1), 44-63.

Gilpin, R. R. (1980). A model for the prediction of ice lensing and frost heave in soils. *Water Resources Research*, *16*(5), 918-930.

Gold, L. W. (1957). A possible force mechanism associated with the freezing of water in porous materials. *High. Res. Board Bull*, *168*, 65-72.

Harlan, R. (1973). Analysis of coupled heat–fluid transport in partially frozen soil. *Water Resources Research*, *9*(5), 1314-1323.

Holten, J. G. (2017). *Measuring Negative Pore Pressures in Partially Frozen Saturated Soils* NTNU].

Hopke, S. (1980). A model for frost heave including overburden. *Cold Regions Science and Technology*, *3*(2-3), 111-127.

Horiguchi, K. (1987). An osmotic model for soil freezing. *Cold Regions Science and Technology*, *14*(1), 13-22.

Hromadka II, T., Guymon, G., & Berg, R. (1981). Some approaches to modeling phase change in freezing solis. *Cold Regions Science and Technology*, *4*(2), 137-145.

Huang, C. (2021). Modeling Hydraulic Fracturing Initiation and Propagation in Porous Rock Formationsl.

Hughes, T., Mallet, M., & Mizukami, A. (1986). A new finite element formulation for computational fluid dynamics: II. Beyond SUPG. *Applied Mechanics and Engineering*, *54*, 341-355.

Ibrahimbegovic, A. (2009). *Nonlinear solid mechanics: theoretical formulations and finite element solution methods* (Vol. 160). Springer Science & Business Media.

Jackson, K., & Chalmers, B. (1958). Freezing of liquids in porous media with special reference to frost heave in soils. *Journal of Applied Physics*, *29*(8), 1178-1181.

Jackson, K., Uhlmann, D. R., & Chalmers, B. (1966). Frost heave in soils. *Journal of Applied Physics*, *37*(2), 848-852.

Jeekel, H. (2012). Adaptation to Climate Change.

Jing, L., & Hudson, J. (2002). Numerical methods in rock mechanics. *International Journal of Rock Mechanics and Mining Sciences*, *39*(4), 409-427.

Jing, L., Ma, Y., & Fang, Z. (2001). Modeling of fluid flow and solid deformation for fractured rocks with discontinuous deformation analysis (DDA) method. *International Journal of Rock Mechanics and Mining Sciences*, *38*(3), 343-355.

Karihaloo, B. L., & Xiao, Q. (2003). Modelling of stationary and growing cracks in FE framework without remeshing: a state-of-the-art review. *Computers & Structures*, *81*(3), 119-129.

Khoei, A. R. (2015). Extended finite element method : theory and applications. http://site.ebrary.com/id/11022758

Kjelstrup, S., Amiri, S. G., Loranger, B., Gao, H., & Grimstad, G. (2021). Transport coefficients and pressure conditions for growth of ice lens in frozen soil. *Acta Geotechnica*, 1-9.

Kjelstrup, S., & Bedeaux, D. (2008). *Non-equilibrium thermodynamics of heterogeneous systems*. World Scientific.

Konrad, J.-M. (1980). Frost heave mechanics.

Konrad, J.-M. (1989). Influence of cooling rate on the temperature of ice lens formation in clayey silts. *Cold Regions Science and Technology*, *16*(1), 25-36.

Konrad, J.-M., & Morgenstern, N. (1982). Prediction of frost heave in the laboratory during transient freezing. *Canadian Geotechnical Journal*, *19*(3), 250-259.

Konrad, J.-M., & Morgenstern, N. R. (1980). A mechanistic theory of ice lens formation in fine-grained soils. *Canadian Geotechnical Journal*, *17*(4), 473-486.

Konrad, J.-M., & Morgenstern, N. R. (1981). The segregation potential of a freezing soil. *Canadian Geotechnical Journal*, *18*(4), 482-491.

Konrad, J. M., & Duquennoi, C. (1993). A model for water transport and ice lensing in freezing soils. *Water Resources Research*, *29*(9), 3109-3124.

Kurylyk, B. L., & Watanabe, K. (2013). The mathematical representation of freezing and thawing processes in variably-saturated, non-deformable soils. *Advances in water resources*, *60*, 160-177.

Lai, Y., Pei, W., Zhang, M., & Zhou, J. (2014). Study on theory model of hydro-thermal–mechanical interaction process in saturated freezing silty soil. *International Journal of Heat & Mass Transfer*, *78*(nov.), 805-819.

Li, N., Chen, B., Chen, F., & Xu, X. (2000). The coupled heat-moisture-mechanic model of the frozen soil. *Cold Regions Science and Technology*, *31*, 199-205.

Li, N., Chen, F., Su, B., & Cheng, G. (2002). Theoretical frame of the saturated freezing soil. *Cold Regions Science and Technology*, *35*(2), 73-80.

Liu, E., Lai, Y., Wong, H., & Feng, J. (2018). An elastoplastic model for saturated freezing soils based on thermo-poromechanics. *International Journal of Plasticity*, *107*, 246-285.

Loch, J., & Kay, B. (1978). Water redistribution in partially frozen, saturated silt under several temperature gradients and overburden loads. *Soil Science Society of America Journal*, *42*(3), 400-406.

Loch, J., & Miller, R. (1975). Tests of the concept of secondary frost heaving. *Soil Science Society of America Journal*, *39*(6), 1036-1041.

Lu, J., Tan, Y.-P., & Wang, J.-H. (2011). A phase field model for the freezing saturated porous medium. *International Journal of Engineering Science*, *49*, 768-780.

Michalowski, R. L. (1993). A constitutive model of saturated soils for frost heave simulations. *Cold Regions Science and Technology*, *22*(1), 47-63.

Michalowski, R. L., & Zhu, M. (2006). Frost heave modelling using porosity rate function. *International Journal for Numerical and Analytical Methods in Geomechanics*, *30*(8), 703-722. https://doi.org/https://doi.org/10.1002/nag.497

Miller, R. (1972). Freezing and heaving of saturated and unsaturated soils. *Highway Research Record*, *393*(1), 1-11.

Miller, R. (1977). Lens initiation in secondary heaving. Proceedings of the International Symposium on Frost Action in Soils,

Miller, R., Loch, J., & Bresler, E. (1975). Transport of water and heat in a frozen permeameter. *Soil Science Society of America Journal*, *39*(6), 1029-1036.

Miller, R., & RD, M. (1978). Frost heaving in non-colloidal soils.

Moës, N., Cloirec, M., Cartraud, P., & Remacle, J.-F. (2003). A computational approach to handle complex microstructure geometries. *Computer methods in applied mechanics and engineering*, *192*(28-30), 3163-3177.

Moës, N., Dolbow, J., & Belytschko, T. (1999). A finite element method for crack growth without remeshing. *International Journal for Numerical Methods in Engineering*, *46*(1), 131-150.

Mohammadi, S. (2008). *Extended finite element method: for fracture analysis of structures*. John Wiley & Sons.

Mohammadnejad, T., & Khoei, A. (2013a). An extended finite element method for hydraulic fracture propagation in deformable porous media with the cohesive crack model. *Finite Elements in Analysis and Design*, *73*, 77-95.

Mohammadnejad, T., & Khoei, A. (2013b). Hydro-mechanical modeling of cohesive crack propagation in multiphase porous media using the extended finite element method. *International Journal for Numerical and Analytical Methods in Geomechanics*, *37*(10), 1247-1279.

Monitoring, A. (2017). Snow, Water, Ice and Permafrost in the Arctic (SWIPA); Summary for Policy-makers.

Nakano, Y. (1990). Quasi-steady problems in freezing soils: I. Analysis on the steady growth of an ice layer. *Cold Regions Science and Technology*, *17*(3), 207-226.

Nansen, F. (1914). *Gjennem Sibirien*. Dybwad.

Nikolić, M., Roje-Bonacci, T., & Ibrahimbegović, A. (2016). OVERVIEW OF THE NUMERICAL METHODS FOR THE MODELLING OF ROCK MECHANICS PROBLEMS. *Tehnicki vjesnik/Technical Gazette*, *23*(2).

Nishimura, S., Gens, A., Olivella, S., & Jardine, R. (2009). THM-coupled finite element analysis of frozen soil: formulation and application. *Géotechnique*, *59*(3), 159-171.

Nixon, J. (1991). Discrete ice lens theory for frost heave in soils. *Canadian Geotechnical Journal*, *28*(6), 843-859.

Norway. (2018). *Norway's Seventh National Communication*. N. M. o. C. a. Environment. https://www.regjeringen.no/contentassets/52d65a62e2474bafa21f4476380cffda/t-1563e.pdf

O'Neill, K., & Miller, R. D. (1985). Exploration of a rigid ice model of frost heave. *Water Resources Research*, *21*(3), 281-296.

Onsager, L. (1931). Reciprocal relations in irreversible processes. I. *Physical review*, *37*(4), 405.

Ozawa, H., & Kinosita, S. (1989). Segregated ice growth on a microporous filter. *Journal of Colloid and Interface Science*, *132*(1), 113-124.

Penner, E. (1959). The mechanism of frost heaving in soils. *Highway Research Board Bulletin*(225).

Penner, E. (1967). Heaving pressure in soils during unidirectional freezing. *Canadian Geotechnical Journal*, *4*(4), 398-408.

Penner, E. (1986). Aspects of ice lens growth in soils. *Cold Regions Science and Technology*, *13*(1), 91-100.

Peppin, S. S., & Style, R. W. (2013). The physics of frost heave and ice-lens growth. *Vadose Zone Journal*, *12*(1).

Potts, D. M., Cui, W., & Zdravković, L. (2021). A coupled THM finite element formulation for unsaturated soils and a strategy for its nonlinear solution. *Computers and geotechnics*, *136*, 104221.

Prigogine, I., & Defay, R. (1954). *Treatise on Thermodynamics: Chemical Thermodynamics* (Vol. 1). Longmans, Green.

Radd, F., & Oertle, D. (1973). Experimental pressure studies of frost heave mechanism and the growth-fusion behavior of ice. Proceeding of the Second International Conference on Permafrost. North American Contribution, publication National Academy of Science, Washington DC Yakutsk, USSR,

Ratkje, S., Yamamoto, H., Takashi, T., Ohrai, T., & Okamoto, J. (1982). The hydraulic conductivity of soils during frost heave. In CRREL Proc. of the 3d Intern. Symp. on Ground Freezing,

Remmers, J. J., de Borst, R., & Needleman, A. (2008). The simulation of dynamic crack propagation using the cohesive segments method. *Journal of the Mechanics and Physics of Solids*, *56*(1), 70-92.

Rempel, A. (2007). Formation of ice lenses and frost heave. *Journal of Geophysical Research: Earth Surface*, *112*(F2).

Rempel, A., Wettlaufer, J., & Worster, M. (2001). Interfacial premelting and the thermomolecular force: thermodynamic buoyancy. *Physical review letters*, *87*(8), 088501.

Rempel, A. W., Wettlaufer, J., & Worster, M. G. (2004). Premelting dynamics in a continuum model of frost heave. *Journal of fluid mechanics*, *498*, 227-244.

Réthoré, J., Borst, R. d., & Abellan, M. A. (2007). A two‐scale approach for fluid flow in fractured porous media. *International Journal for Numerical Methods in Engineering*, *71*(7), 780-800.

Shahzamanian, M., Kainat, M., Ghodsi, N. Y., & Adeeb, S. (2021). Systematic Literature Review of the Application of Extended Finite Element Method in Failure Prediction of Pipelines. *Journal of Pipeline Science and Engineering*.

Sheshukov, A., & Egorov, A. (2002). Frozen barrier evolution in saturated porous media. *Advances in water resources*, *25*(6), 591-599.

Spohr, K., Hamilton, D. S., & Moyer, J. C. (2021). *The Arctic and World Order*. Brookings Institution Press.

Stolarska, M., & Chopp, D. (2003). Modeling thermal fatigue cracking in integrated circuits by level sets and the extended finite element method. *International Journal of Engineering Science*, *41*(20), 2381-2410.

Sukumar, N., Chopp, D. L., Moës, N., & Belytschko, T. (2001). Modeling holes and inclusions by level sets in the extended finite-element method. *Computer methods in applied mechanics and engineering*, *190*(46-47), 6183-6200.

Taber, S. (1916). The growth of crystals under external pressure. *American Journal of Science*, *4*(246), 532-556.

Taber, S. (1929). Frost heaving. *The Journal of Geology*, *37*(5), 428-461.

Taber, S. (1930). The mechanics of frost heaving. *The Journal of Geology*, *38*(4), 303-317.

Takagi, S. (1980). The adsorption force theory of frost heaving. *Cold Regions Science and Technology*, *3*(1), 57-81.

Talamucci, F. (2003). Freezing processes in porous media: formation of ice lenses, swelling of the soil. *Mathematical and computer modelling*, *37*(5-6), 595-602.

Thomas, H., Cleall, P., Li, Y.-C., Harris, C., & Kern-Luetschg, M. (2009). Modelling of cryogenic processes in permafrost and seasonally frozen soils. *Geotechnique*, *59*, 173-184.

Ulam, S., Kuhn, H. W., Tucker, A. W., & Shannon, C. E. (2013). *John von Neumann, 1903-1957*. Harvard University Press.

van Genuchten, M. T. (1980). A Closed-form Equation for Predicting the Hydraulic Conductivity of Unsaturated Soils. *Soil Science Society of America Journal*, *44*(5), 892-898. https://doi.org/https://doi.org/10.2136/sssaj1980.03615995004400050002x

Van Staden, R., Guan, H., & Loo, Y.-C. (2006). Application of the finite element method in dental implant research. *Computer methods in biomechanics and biomedical engineering*, *9*(4), 257-270.

Walder, J., & Hallet, B. (1985). A theoretical model of the fracture of rock during freezing. *Geological Society of America Bulletin*, *96*(3), 336-346.

Watanabe, K., & Osada, Y. (2016). Comparison of Hydraulic Conductivity in Frozen Saturated and Unfrozen Unsaturated Soils. *Vadose Zone Journal*, *15*(5), vzj2015.2011.0154. https://doi.org/https://doi.org/10.2136/vzj2015.11.0154

Wettlaufer, J., & Worster, M. (1995). Dynamics of premelted films: frost heave in a capillary. *Physical Review E*, *51*(5), 4679.

Wettlaufer, J., & Worster, M. G. (2006). Premelting dynamics. *Annu. Rev. Fluid Mech.*, *38*, 427-452.

Wettlaufer, J. S., & Worster, M. G. (2006). Premelting dynamics. *Annual Review of Fluid Mechanics*, *38*(1), 427-452. https://doi.org/doi:10.1146/annurev.fluid.37.061903.175758

Wilen, L., & Dash, J. (1995). Frost heave dynamics at a single crystal interface. *Physical review letters*, *74*(25), 5076.

Williams, P., Riseborough, D., & Smith, M. (1993). The France-Canada joint study of deformation of an experimental pipe line by differential frost heave. *International Journal of Offshore and Polar Engineering*, *3*(01).

Wilson, E. L., & Nickell, R. E. (1966). Application of the finite element method to heat conduction analysis. *Nuclear engineering and design*, *4*(3), 276-286.

Wriggers, P. (2008). *Nonlinear finite element methods*. Springer Science & Business Media.

Xu, L., Davies, S., Schofield, A. B., & Weitz, D. A. (2008). Dynamics of drying in 3D porous media. *Physical review letters*, *101*(9), 094502.

You, J., Wang, Z., & Worster, M. G. (2021). Thermal regelation of single particles and particle clusters in ice. *Soft Matter*, *17*(7), 1779-1787.

Zhang, T., Barry, R. G., Knowles, K., Heginbottom, J., & Brown, J. (1999). Statistics and characteristics of permafrost and ground‐ice distribution in the Northern Hemisphere. *Polar Geography*, *23*(2), 132-154.

Zhang, Y., & Michalowski, R. L. (2015). Thermal-hydro-mechanical analysis of frost heave and thaw settlement. *Journal of geotechnical and geoenvironmental engineering*, *141*(7), 04015027.

Zhao, H. X., Zhong, J., & Wang, Z. J. (2014). Experimental study on the influence of different cooling rate to frost heave of silty clay. Advanced Materials Research,

Zhou, J., & Li, D. (2012). Numerical analysis of coupled water, heat and stress in saturated freezing soil. *Cold Regions Science & Technology*, *72*(none), 43-49.

Zhou, M. (2014). *Computaional simulation of freezing: Multiphase modeling and strength upscaling* Ph. D Dissertation, Ruhr University Bochum].

Zienkiewicz, O., Emson, C., & Bettess, P. (1983). A novel boundary infinite element. *International Journal for Numerical Methods in Engineering*, *19*(3), 393-404.

Appendix-A

The detailed calculation of the components of Jacobian matrix.

$$\mathbf{K}_{uu} = -\frac{\partial \mathbf{F}_u^{\text{intS}}}{\partial \hat{u}} = \int_\Omega \left(\mathbf{B}_u^{std}\right)^T \cdot \mathbf{D}^e \cdot \mathbf{B}_u^{std} \, d\Omega \tag{1.1}$$

$$\mathbf{K}_{ua} = -\frac{\partial \mathbf{F}_u^{\text{intS}}}{\partial \hat{a}} = \int_\Omega \left(\mathbf{B}_u^{std}\right)^T \cdot \mathbf{D}^e \cdot \mathbf{B}_u^{enr} \mathbf{L} \, d\Omega \tag{1.2}$$

$$\tilde{\mathbf{C}}_{uT} = \frac{\partial \mathbf{C}_{up}}{\partial \hat{\mathbf{T}}} \hat{\mathbf{p}}_w + \frac{\partial \mathbf{C}_{ub}}{\partial \hat{\mathbf{T}}} \hat{\mathbf{b}} - \frac{\partial \mathbf{F}_u^{\text{intS}}}{\partial \hat{T}} = -\int_\Omega \frac{\partial s_w}{\partial T} \left(\mathbf{B}_u^{std}\right)^T \mathbf{N}_T^{std} \cdot p_w \mathbf{I} d\Omega$$
$$-\int_\Omega \left(\mathbf{B}_u^{std}\right)^T \cdot (\Delta \boldsymbol{\varepsilon} - \Delta \boldsymbol{\varepsilon}_T) \cdot \frac{\partial \mathbf{D}^e}{\partial s_w} \cdot \frac{\partial s_w}{\partial T} \mathbf{N}_T^{std} d\Omega - \int_\Omega \left(\mathbf{B}_u^{std}\right)^T \cdot \mathbf{D}^e \cdot \frac{\mathbf{m}}{3} \beta_s \mathbf{N}_T^{std} d\Omega \tag{1.3}$$

$$\tilde{\mathbf{C}}_{uc} = \frac{\partial \mathbf{C}_{up}}{\partial \hat{\mathbf{c}}} \hat{\mathbf{p}}_w + \frac{\partial \mathbf{C}_{ub}}{\partial \hat{\mathbf{c}}} \hat{\mathbf{b}} - \frac{\partial \mathbf{F}_u^{\text{intS}}}{\partial \hat{\mathbf{c}}} = -\int_\Omega \frac{\partial s_w}{\partial T} \left(\mathbf{B}_u^{std}\right)^T \mathbf{N}_T^{enr} \cdot p_w \mathbf{I} d\Omega$$
$$-\int_\Omega \left(\mathbf{B}_u^{std}\right)^T \cdot (\Delta \boldsymbol{\varepsilon} - \Delta \boldsymbol{\varepsilon}_T) \cdot \frac{\partial \mathbf{D}^e}{\partial s_w} \cdot \frac{\partial s_w}{\partial T} \mathbf{N}_T^{enr} d\Omega - \int_\Omega \left(\mathbf{B}_u^{std}\right)^T \cdot \mathbf{D}^e \cdot \frac{\mathbf{m}}{3} \beta_s \mathbf{N}_T^{enr} d\Omega \tag{1.4}$$

$$\mathbf{K}_{au} = -\frac{\partial \mathbf{F}_a^{\text{intS}}}{\partial \hat{u}} = \int_\Omega \left(\mathbf{B}_u^{enr} \mathbf{L}\right)^T \cdot \mathbf{D}^e \cdot \mathbf{B}_u^{std} \, d\Omega \tag{1.5}$$

$$\mathbf{K}_{aa} = -\frac{\partial \mathbf{F}_a^{\text{intS}}}{\partial \hat{a}} = \int_\Omega \left(\mathbf{B}_u^{enr} \mathbf{L}\right)^T \cdot \mathbf{D}^e \cdot \mathbf{B}_u^{enr} \mathbf{L} \, d\Omega \tag{1.6}$$

$$\frac{\partial \mathbf{F}_a^{\text{int}}}{\partial \hat{\mathbf{p}}_w} = \int_{\Gamma_d} \left(\bar{\mathbf{N}}_u \mathbf{L}\right)^T \left(\beta_2 s_{i_d} + 1\right) \left(\mathbf{N}_p^{std} \mathbf{I}\right) \mathbf{n}_{\Gamma_d} \, d\Gamma \tag{1.7}$$

$$\frac{\partial \mathbf{F}_a^{\text{int}}}{\partial \hat{\mathbf{b}}} = \int_{\Gamma_d} \left(\bar{\mathbf{N}}_u \mathbf{L}\right)^T \cdot \left(\beta_2 s_{i_d} + 1\right) \left(\mathbf{N}_p^{enr} \mathbf{I}\right) \mathbf{n}_{\Gamma_d} \, d\Gamma \tag{1.8}$$

$$\tilde{\mathbf{C}}_{aT} = \frac{\partial \mathbf{C}_{ap}}{\partial \hat{\mathbf{T}}} \hat{\mathbf{p}}_w + \frac{\partial \mathbf{C}_{ab}}{\partial \hat{\mathbf{T}}} \hat{\mathbf{b}} - \frac{\partial \mathbf{F}_a^{\text{intS}}}{\partial \hat{T}} = -\int_\Omega \frac{\partial s_w}{\partial T} \left(\mathbf{B}_u^{enr} \mathbf{L}\right)^T \mathbf{N}_T^{std} \cdot p_w \mathbf{I} d\Omega -$$
$$\int_\Omega \left(\mathbf{B}_u^{enr}\right)^T \cdot (\Delta \boldsymbol{\varepsilon} - \Delta \boldsymbol{\varepsilon}_T) \cdot \frac{\partial \mathbf{D}^e}{\partial s_w} \cdot \frac{\partial s_w}{\partial T} \mathbf{N}_T^{std} d\Omega - \int_\Omega \left(\mathbf{B}_u^{enr}\right)^T \cdot \mathbf{D}^e \cdot \frac{\mathbf{m}}{3} \beta_s \mathbf{N}_T^{std} d\Omega \tag{1.9}$$

$$\tilde{\mathbf{C}}_{ac} = \frac{\partial \mathbf{C}_{ap}}{\partial \hat{\mathbf{c}}} \hat{\mathbf{p}}_w + \frac{\partial \mathbf{C}_{ab}}{\partial \hat{\mathbf{c}}} \hat{\mathbf{b}} - \frac{\partial \mathbf{F}_a^{\text{intS}}}{\partial \hat{\mathbf{c}}} = -\int_\Omega \frac{\partial s_w}{\partial T} \left(\mathbf{B}_u^{enr} \mathbf{L} \right)^T \mathbf{N}_T^{enr} p_w \mathbf{I} d\Omega$$
$$-\int_\Omega \left(\mathbf{B}_u^{enr} \right)^T \cdot (\Delta \boldsymbol{\varepsilon} - \Delta \boldsymbol{\varepsilon}_T) \cdot \frac{\partial \mathbf{D}^e}{\partial s_w} \cdot \frac{\partial s_w}{\partial T} \mathbf{N}_T^{enr} d\Omega - \int_\Omega \left(\mathbf{B}_u^{enr} \right)^T \cdot \mathbf{D}^e \cdot \frac{\mathbf{m}}{3} \beta_s \mathbf{N}_T^{enr} d\Omega$$

(1.10)

$$\frac{\partial \boldsymbol{F}_p^{\text{int}}}{\partial \hat{\mathbf{u}}} = -\frac{1}{\Delta t} \int_{\Gamma_d} \left(\boldsymbol{N}_p^{std} \right)^T (s_{w_d} \rho_w + s_{i_d} \rho_i) [\![u_{y'}]\!] (\boldsymbol{n}_{x'}^T \cdot \boldsymbol{B}_u^{std} \boldsymbol{n}_{x'}) d\Gamma$$

(1.11)

$$\tilde{\mathbf{C}}_{pu} = \frac{\partial \overline{\mathbf{C}}_{pT}}{\partial \hat{\mathbf{u}}} \hat{\mathbf{T}} + \frac{\partial \overline{\mathbf{C}}_{pc}}{\partial \hat{\mathbf{u}}} \hat{\mathbf{c}} = \int_\Omega \left(\boldsymbol{N}_p^{std} \right)^T \left\{ \left[(1-n)(\rho_w - \rho_i) \frac{\partial s_w}{\partial T} \right] \mathbf{m}^T \mathbf{B}_u^{std} - \chi_{\hat{\mathbf{u}}}' \right\} T d\Omega$$

(1.12)

$$\frac{\partial \boldsymbol{F}_p^{\text{int}}}{\partial \hat{\boldsymbol{a}}} = -\int_{\Gamma_d} \left(\boldsymbol{N}_p^{std} \right)^T \cdot \bar{\boldsymbol{N}}_u \cdot [(\rho_w - \rho_i) \dot{s}_{w_d}] d\Gamma + \int_{\Gamma_d} \left(\left(\frac{\partial \boldsymbol{N}_p^{std}}{\partial x'} \right)^T \cdot q_{w_{x'}} \right) \cdot \rho_w \bar{\boldsymbol{N}}_u d\Gamma -$$
$$\frac{1}{\Delta t} \int_{\Gamma_d} \left(\boldsymbol{N}_p^{std} \right)^T (s_{w_d} \rho_w + s_{i_d} \rho_i) [\![u_{y'}]\!] (\boldsymbol{n}_{x'}^T \cdot \boldsymbol{B}_u^{enr} \boldsymbol{L} \boldsymbol{n}_{x'}) d\Gamma + \int_{\Gamma_d} \left(\boldsymbol{N}_p^{std} \right)^T (s_{w_d} \rho_w + s_{i_d} \rho_i) \bar{\boldsymbol{N}}_u \dot{\varepsilon}_{x'x'} d\Gamma -$$
$$\frac{1}{\Delta t} \int_{\Gamma_d} \left(\boldsymbol{N}_p^{std} \right)^T (s_{w_d} \rho_w + s_{i_d} \rho_i) \bar{\boldsymbol{N}}_u d\Gamma$$

(1.13)

$$\tilde{\mathbf{C}}_{pa} = \frac{\partial \overline{\mathbf{C}}_{pT}}{\partial \hat{\mathbf{a}}} \hat{\mathbf{T}} + \frac{\partial \overline{\mathbf{C}}_{pc}}{\partial \hat{\mathbf{a}}} \hat{\mathbf{c}} = \int_\Omega \left(\boldsymbol{N}_p^{std} \right)^T \left\{ \left[(1-n)(\rho_w - \rho_i) \frac{\partial s_w}{\partial T} \right] \mathbf{m}^T \mathbf{B}_u^{enr} - \chi_{\hat{\mathbf{u}}}' \right\} T d\Omega$$

(1.14)

$$\frac{\partial \boldsymbol{F}_p^{\text{int}}}{\partial \hat{\boldsymbol{p}}_w} = \int_{\Gamma_d} \left(\left(\frac{\partial \boldsymbol{N}_p^{std}}{\partial x'} \right)^T \cdot (-k_d \boldsymbol{B}_p^{std} \boldsymbol{n}_{x'}) \right) \cdot \rho_w [\![u_{y'}]\!] d\Gamma$$

(1.15)

$$\frac{\partial \boldsymbol{F}_p^{\text{int}}}{\partial \hat{\boldsymbol{b}}} = \int_{\Gamma_d} \left(\left(\frac{\partial \boldsymbol{N}_p^{std}}{\partial x'} \right)^T \cdot (-k_d \boldsymbol{B}_p^{enr} \boldsymbol{n}_{x'}) \right) \cdot \rho_w [\![u_{y'}]\!] d\Gamma$$

(1.16)

$$\tilde{\mathbf{C}}_{pT} = \frac{\partial \overline{\mathbf{C}}_{pu}}{\partial \hat{\mathbf{T}}} \hat{\mathbf{u}} + \frac{\partial \overline{\mathbf{C}}_{pa}}{\partial \hat{\mathbf{T}}} \hat{\mathbf{a}} + \Delta t \frac{\partial \mathbf{Q}_{pp}}{\partial \hat{\mathbf{T}}} \hat{\mathbf{p}}_w + \Delta t \frac{\partial \mathbf{Q}_{pb}}{\partial \hat{\mathbf{T}}} \hat{\mathbf{b}} + \Delta t \frac{\partial \mathbf{C}_{pT}}{\partial \hat{\mathbf{T}}} \hat{\mathbf{T}} + \Delta t \frac{\partial \mathbf{C}_{pc}}{\partial \hat{\mathbf{T}}} \hat{\mathbf{c}} =$$
$$-\int_\Omega \left(\mathbf{N}_p^{std} \right)^T \left[\left(\frac{\partial s_w}{\partial T} \rho_w + \frac{\partial s_i}{\partial T} \rho_i \right) + (s_w \rho_{wT}' + s_i \rho_{iT}') \right] \mathbf{N}_T^{std} \varepsilon_v d\Omega +$$
$$\Delta t \int_\Omega \left(\mathbf{B}_p^{std} \right)^T \cdot \left(\frac{\partial k_r}{\partial T} \frac{K}{\mu_w} \rho_w + \frac{k_r K}{\mu_w} \rho_{wT}' \right) \cdot \mathbf{N}_T^{std} \cdot \nabla p_w d\Omega +$$
$$\Delta t \int_\Omega \left(\mathbf{B}_p^{std} \right)^T \cdot \alpha \left(\frac{\partial k_r}{\partial T} - \frac{k_r}{T} + k_r \rho_{iT}' + k_r \rho_{wT}' \right) \frac{K}{\mu_w} \frac{\rho_i l}{T} \rho_w \cdot \mathbf{N}_T^{std} \cdot \nabla T d\Omega$$

(1.17)

75

$$\tilde{\mathbf{C}}_{pc} = \frac{\partial \overline{\mathbf{C}}_{pu}}{\partial \hat{\mathbf{c}}} \hat{\mathbf{u}} + \frac{\partial \overline{\mathbf{C}}_{pa}}{\partial \hat{\mathbf{c}}} \hat{\mathbf{a}} + \Delta t \frac{\partial \mathbf{Q}_{pp}}{\partial \hat{\mathbf{c}}} \hat{\mathbf{p}}_w + \Delta t \frac{\partial \mathbf{Q}_{pb}}{\partial \hat{\mathbf{c}}} \hat{\mathbf{b}} + \Delta t \frac{\partial \mathbf{C}_{pT}}{\partial \hat{\mathbf{c}}} \hat{\mathbf{T}} + \Delta t \frac{\partial \mathbf{C}_{pc}}{\partial \hat{\mathbf{c}}} \hat{\mathbf{c}} =$$

$$-\int_{\Omega} \left(\mathbf{N}_p^{std}\right)^T \left[\left(\frac{\partial s_w}{\partial T}\rho_w + \frac{\partial s_i}{\partial T}\rho_i\right) + (s_w \rho'_{wT} + s_i \rho'_{iT})\right] \mathbf{N}_T^{enr} \varepsilon_v d\Omega +$$

$$\Delta t \int_{\Omega} \left(\mathbf{B}_p^{std}\right)^T \cdot \left(\frac{\partial k_r}{\partial T}\frac{K}{\mu_w}\rho_w + \frac{k_r K}{\mu_w}\rho'_{wT}\right) \cdot \mathbf{N}_T^{enr} \cdot \nabla p_w d\Omega +$$

$$\Delta t \int_{\Omega} \left(\mathbf{B}_p^{std}\right)^T \cdot \alpha \left(\frac{\partial k_r}{\partial T} - \frac{k_r}{T} + k_r \rho'_{iT} + k_r \rho'_{wT}\right) \frac{K}{\mu_w}\frac{\rho_i l}{T}\rho_w \cdot \mathbf{N}_T^{enr} \cdot \nabla T d\Omega \tag{1.18}$$

$$\frac{\partial \boldsymbol{F}_b^{\text{int}}}{\partial \hat{\mathbf{u}}} = -\frac{1}{\Delta t}\int_{\Gamma_d} \left(\boldsymbol{N}_p^{enr}\right)^T (s_{w_d}\rho_w + s_{i_d}\rho_i)[\![u_{y'}]\!](\boldsymbol{n}_{x'}^T \boldsymbol{B}_u^{std}\boldsymbol{n}_{x'})d\Gamma \tag{1.19}$$

$$\tilde{\mathbf{C}}_{bu} = \frac{\partial \overline{\mathbf{C}}_{bT}}{\partial \hat{\mathbf{u}}} \hat{\mathbf{T}} + \frac{\partial \overline{\mathbf{C}}_{bc}}{\partial \hat{\mathbf{u}}} \hat{\mathbf{c}} = \int_{\Omega} \left(\boldsymbol{N}_p^{enr}\right)^T \left\{\left[(1-n)(\rho_w - \rho_i)\frac{\partial s_w}{\partial T}\right]\mathbf{m}^T \mathbf{B}_u^{std} - \chi'_{\hat{\mathbf{u}}}\right\} T d\Omega \tag{1.20}$$

$$\frac{\partial \boldsymbol{F}_b^{\text{int}}}{\partial \hat{\boldsymbol{a}}} = -\int_{\Gamma_d} \left(\boldsymbol{N}_p^{enr}\right)^T \cdot \bar{\boldsymbol{N}}_u \cdot [(\rho_w - \rho_i)\dot{s}_{w_d}]d\Gamma + \int_{\Gamma_d} \left(\left(\frac{\partial \boldsymbol{N}_p^{enr}}{\partial x'}\right)^T \cdot q_{w_{x'}}\right) \cdot \rho_w \bar{\boldsymbol{N}}_u d\Gamma -$$

$$\frac{1}{\Delta t}\int_{\Gamma_d} \left(\boldsymbol{N}_p^{enr}\right)^T (s_{w_d}\rho_w + s_{i_d}\rho_i)[\![u_{y'}]\!](\boldsymbol{n}_{x'}^T \boldsymbol{B}_u^{enr}\boldsymbol{L}\boldsymbol{n}_{x'})d\Gamma + \int_{\Gamma_d} \left(\boldsymbol{N}_p^{enr}\right)^T (s_{w_d}\rho_w + s_{i_d}\rho_i)\bar{\boldsymbol{N}}_u \dot{\varepsilon}_{x'x'}d\Gamma -$$

$$\frac{1}{\Delta t}\int_{\Gamma_d} \left(\boldsymbol{N}_p^{enr}\right)^T (s_{w_d}\rho_w + s_{i_d}\rho_i)\bar{\boldsymbol{N}}_u d\Gamma \tag{1.21}$$

$$\tilde{\mathbf{C}}_{ba} = \frac{\partial \overline{\mathbf{C}}_{bT}}{\partial \hat{\mathbf{a}}} \hat{\mathbf{T}} + \frac{\partial \overline{\mathbf{C}}_{bc}}{\partial \hat{\mathbf{a}}} \hat{\mathbf{c}} = \int_{\Omega} \left(\boldsymbol{N}_p^{enr}\right)^T \left\{\left[(1-n)(\rho_w - \rho_i)\frac{\partial s_w}{\partial T}\right]\mathbf{m}^T \mathbf{B}_u^{enr} - \chi'_{\hat{\mathbf{u}}}\right\} T d\Omega \tag{1.22}$$

$$\frac{\partial \boldsymbol{F}_b^{\text{int}}}{\partial \hat{\boldsymbol{p}}_w} = \int_{\Gamma_d} \left(\left(\frac{\partial \boldsymbol{N}_p^{enr}}{\partial x'}\right)^T \cdot (-k_d \boldsymbol{B}_p^{std}\boldsymbol{n}_{x'})\right) \cdot \rho_w [\![u_{y'}]\!]d\Gamma \tag{1.23}$$

$$\frac{\partial \boldsymbol{F}_b^{\text{int}}}{\partial \hat{\boldsymbol{b}}} = \int_{\Gamma_d} \left(\left(\frac{\partial \boldsymbol{N}_p^{enr}}{\partial x'}\right)^T \cdot (-k_d \boldsymbol{B}_p^{enr}\boldsymbol{n}_{x'})\right) \cdot \rho_w [\![u_{y'}]\!]d\Gamma \tag{1.24}$$

$$\tilde{\mathbf{C}}_{bT} = \frac{\partial \overline{\mathbf{C}}_{bu}}{\partial \hat{\mathbf{T}}} \hat{\mathbf{u}} + \frac{\partial \overline{\mathbf{C}}_{ba}}{\partial \hat{\mathbf{T}}} \hat{\mathbf{a}} + \Delta t \frac{\partial \mathbf{Q}_{bp}}{\partial \hat{\mathbf{T}}} \hat{\mathbf{p}}_w + \Delta t \frac{\partial \mathbf{Q}_{bb}}{\partial \hat{\mathbf{T}}} \hat{\mathbf{b}} + \Delta t \frac{\partial \mathbf{C}_{bT}}{\partial \hat{\mathbf{T}}} \hat{\mathbf{T}} + \Delta t \frac{\partial \mathbf{C}_{bc}}{\partial \hat{\mathbf{T}}} \hat{\mathbf{c}} =$$

$$-\int_\Omega \left(\mathbf{N}_p^{enr}\right)^T \left[\left(\frac{\partial s_w}{\partial T} \rho_w + \frac{\partial s_i}{\partial T} \rho_i \right) + (s_w \rho'_{wT} + s_i \rho'_{iT}) \right] \mathbf{N}_T^{std} \varepsilon_v d\Omega$$

$$+\Delta t \int_\Omega \left(\mathbf{B}_p^{enr}\right)^T \cdot (\frac{\partial k_r}{\partial T} \frac{K}{\mu_w} \rho_w + \frac{k_r K}{\mu_w} \rho'_{wT}) \cdot \mathbf{N}_T^{std} \cdot \nabla p_w d\Omega +$$

$$\Delta t \int_\Omega \left(\mathbf{B}_p^{enr}\right)^T \cdot \alpha \left(\frac{\partial k_r}{\partial T} - \frac{k_r}{T} + k_r \rho'_{iT} + k_r \rho'_{wT} \right) \frac{K}{\mu_w} \frac{\rho_i l}{T} \rho_w \cdot \mathbf{N}_T^{std} \cdot \nabla T d\Omega \qquad (1.25)$$

$$\tilde{\mathbf{C}}_{bc} = \frac{\partial \overline{\mathbf{C}}_{bu}}{\partial \hat{\mathbf{c}}} \hat{\mathbf{u}} + \frac{\partial \overline{\mathbf{C}}_{ba}}{\partial \hat{\mathbf{c}}} \hat{\mathbf{a}} + \Delta t \frac{\partial \mathbf{Q}_{bp}}{\partial \hat{\mathbf{c}}} \hat{\mathbf{p}}_w + \Delta t \frac{\partial \mathbf{Q}_{bb}}{\partial \hat{\mathbf{c}}} \hat{\mathbf{b}} + \Delta t \frac{\partial \mathbf{C}_{bT}}{\partial \hat{\mathbf{c}}} \hat{\mathbf{T}} + \Delta t \frac{\partial \mathbf{C}_{bc}}{\partial \hat{\mathbf{c}}} \hat{\mathbf{c}} =$$

$$-\int_\Omega \left(\mathbf{N}_p^{enr}\right)^T \left[\left(\frac{\partial s_w}{\partial T} \rho_w + \frac{\partial s_i}{\partial T} \rho_i \right) + (s_w \rho'_{wT} + s_i \rho'_{iT}) \right] \mathbf{N}_T^{enr} \varepsilon_v d\Omega$$

$$+\Delta t \int_\Omega \left(\mathbf{B}_p^{enr}\right)^T \cdot (\frac{\partial k_r}{\partial T} \frac{K}{\mu_w} \rho_w + \frac{k_r K}{\mu_w} \rho'_{wT}) \cdot \mathbf{N}_T^{enr} \cdot \nabla p_w d\Omega +$$

$$\Delta t \int_\Omega \left(\mathbf{B}_p^{enr}\right)^T \cdot \alpha \left(\frac{\partial k_r}{\partial T} - \frac{k_r}{T} + k_r \rho'_{iT} + k_r \rho'_{wT} \right) \frac{K}{\mu_w} \frac{\rho_i l}{T} \rho_w \cdot \mathbf{N}_T^{enr} \cdot \nabla T d\Omega \qquad (1.26)$$

$$\frac{\partial \boldsymbol{F}_T^{\text{int}}}{\partial \hat{\boldsymbol{u}}} = \frac{1}{\Delta t} \int_\Omega \left(\boldsymbol{N}_T^{std}\right)^T \cdot l \cdot s_i \cdot \rho_i \cdot \boldsymbol{m}^T \boldsymbol{B}_u^{std} \cdot d\Omega - \int_\Omega \left(\boldsymbol{N}_T^{std}\right)^T \cdot l \cdot \dot{s}_w \cdot \rho_i \cdot (1-n) \boldsymbol{m}^T \boldsymbol{B}_u^{std} \cdot d\Omega$$

$$- \int_\Omega \left(\boldsymbol{N}_T^{std}\right)^T \cdot l \cdot s_i \cdot \rho_i \beta_s \cdot \boldsymbol{m}^T \boldsymbol{B}_u^{std} \cdot \dot{T} d\Omega - \int_\Omega \left(\boldsymbol{N}_T^{std}\right)^T \cdot l \cdot s_i \cdot \rho'_{iT} \cdot \boldsymbol{m}^T \boldsymbol{B}_u^{std} \cdot \dot{T} d\Omega +$$

$$\frac{1}{\Delta t} \int_{\Gamma_d} \left(\boldsymbol{N}_T^{std}\right)^T \cdot l \cdot s_{i_d} \rho_i \cdot [\![u_{y'}]\!] (\boldsymbol{n}_x^T \boldsymbol{B}_u^{std} \boldsymbol{n}_{x'}) d\Gamma \qquad (1.27)$$

$$\frac{\partial \boldsymbol{F}_T^{\text{int}}}{\partial \hat{\boldsymbol{a}}} = \frac{1}{\Delta t} \int_\Omega \left(\boldsymbol{N}_T^{std}\right)^T \cdot l \cdot s_i \cdot \rho_i \cdot \boldsymbol{m}^T \boldsymbol{B}_u^{enr} \boldsymbol{L} \ .d\Omega - \int_\Omega \left(\boldsymbol{N}_T^{std}\right)^T \cdot l \cdot \dot{s}_w \cdot \rho_i \cdot (1-n) \boldsymbol{m}^T \boldsymbol{B}_u^{enr} \cdot d\Omega -$$

$$\int_{\Gamma_d} \left(\boldsymbol{N}_T^{std}\right)^T \cdot \bar{\boldsymbol{N}}_u \cdot (\rho C)_{\text{eff}_d} \dot{T} d\Gamma - \int_{\Gamma_d} \left(\boldsymbol{N}_T^{std}\right)^T \cdot l \cdot \rho_i \cdot \bar{\boldsymbol{N}}_u \dot{s}_{w_d} d\Gamma$$

$$- \int_\Omega \left(\boldsymbol{N}_T^{std}\right)^T \cdot l \cdot s_i \cdot \rho_i \beta_s \cdot \boldsymbol{m}^T \boldsymbol{B}_u^{enr} \cdot \dot{T} d\Omega - \int_\Omega \left(\boldsymbol{N}_T^{std}\right)^T \cdot l \cdot s_i \cdot \rho'_{iT} \cdot \boldsymbol{m}^T \boldsymbol{B}_u^{enr} \cdot \dot{T} d\Omega$$

$$\frac{1}{\Delta t} \int_{\Gamma_d} \left(\boldsymbol{N}_T^{std}\right)^T \cdot l \cdot s_{i_d} \rho_i \cdot [\![u_{y'}]\!] (\boldsymbol{n}_x^T \boldsymbol{B}_u^{enr} \boldsymbol{L} \boldsymbol{n}_{x'}) d\Gamma - \int_{\Gamma_d} \left(\boldsymbol{N}_T^{std}\right)^T \cdot l \cdot s_{i_d} \rho_i \cdot \bar{\boldsymbol{N}}_u \dot{\varepsilon}_{x'x'} d\Gamma$$

$$+\frac{1}{\Delta t} \int_{\Gamma_d} \left(\boldsymbol{N}_T^{std}\right)^T \cdot l \cdot s_{i_d} \rho_i \cdot \bar{\boldsymbol{N}}_u d\Gamma \qquad (1.28)$$

$$\frac{\partial \boldsymbol{F}_T^{\text{int}}}{\partial \hat{\boldsymbol{T}}} = -\frac{1}{\Delta t} \int_\Omega \left(\boldsymbol{N}_T^{std}\right)^T \cdot l \cdot n(\rho_i \frac{\partial s_w}{\partial T} + \rho'_{iT} s_w) \boldsymbol{N}_T^{std} d\Omega$$

$$- \int_\Omega \left(\boldsymbol{N}_T^{std}\right)^T \cdot l \cdot (\rho_i \frac{\partial s_i}{\partial T} \dot{\varepsilon}_v + \rho'_{iT} s_i) \boldsymbol{N}_T^{std} d\Omega$$

$$+\frac{1}{\Delta t} \int_\Omega \left(\boldsymbol{N}_T^{std}\right)^T \cdot l \cdot (n-1)\beta_s \cdot (\rho'_{iT} T s_i + \rho_i s_i + \rho_i T \frac{\partial s_i}{\partial T}) \boldsymbol{N}_T^{std} d\Omega +$$

$$\frac{1}{\Delta t}\int_{\Omega}\left(\boldsymbol{N}_T^{std}\right)^T \cdot l \cdot n(s_i\rho_{iT}' + \frac{\partial s_i}{\partial T}\rho_i)\cdot \boldsymbol{N}_T^{std}d\Omega$$

$$-\frac{1}{\Delta t}\int_{\Gamma_d}\left(\boldsymbol{N}_T^{std}\right)^T\cdot l\cdot[\![u_{y'}]\!]\cdot(\rho_i\cdot\frac{\partial s_{w_d}}{\partial T} + \rho_{iT}'\cdot s_{w_d})\boldsymbol{N}_T^{std}d\Gamma -$$

$$\frac{1}{\Delta t}\int_{\Gamma_d}\left(\boldsymbol{N}_T^{std}\right)^T\cdot[\![u_{y'}]\!]\cdot\left[(\rho C)_{\text{eff}_d}+\frac{\partial(\rho C)_{\text{eff}_d}}{\partial T}T\right]\boldsymbol{N}_T^{std}d\Gamma$$

$$+\int_{\Gamma_d}\left(\boldsymbol{N}_T^{std}\right)^T\cdot l\cdot(\frac{\partial s_{i_d}}{\partial T}\rho_i + s_{i_d}\rho_{iT}')\cdot[\![\dot{u}_{y'}]\!]\boldsymbol{N}_T^{std}d\Gamma - \frac{1}{\Delta t}\int_{\Gamma_d}\left(\boldsymbol{N}_T^{std}\right)^T\cdot l\cdot(\frac{\partial s_{i_d}}{\partial T}\rho_i + s_{i_d}\rho_{iT}')\cdot$$

$$[\![u_{y'}]\!]\varepsilon_{x'x'}\boldsymbol{N}_T^{std}d\Gamma \tag{1.29}$$

$$\tilde{\mathbf{C}}_{TT} = \frac{\partial \mathbf{C}_{Tp}}{\partial\hat{\mathbf{T}}}\hat{\mathbf{p}}_w + \frac{\partial\mathbf{C}_{Tb}}{\partial\hat{\mathbf{T}}}\hat{\mathbf{b}} = \int_{\Omega}\left(\mathbf{B}_T^{std}\right)^T\cdot\alpha(\frac{\partial k_r}{\partial T}\rho_i + k_r\rho_{iT}')\frac{K}{\mu_w}l\,\boldsymbol{N}_T^{std}\cdot\nabla p_w d\Omega \tag{1.30}$$

$$\frac{\partial \boldsymbol{F}_T^{\text{int}}}{\partial\hat{\mathbf{c}}} = -\frac{1}{\Delta t}\int_{\Omega}\left(\boldsymbol{N}_T^{std}\right)^T\cdot l\cdot n(\rho_i\frac{\partial s_w}{\partial T} + \rho_{iT}'s_w)\frac{\partial s_w}{\partial T}\boldsymbol{N}_T^{enr}\ \ d\Omega -$$

$$\int_{\Omega}\left(\boldsymbol{N}_T^{std}\right)^T\cdot l\cdot(\rho_i\frac{\partial s_i}{\partial T}\dot{\varepsilon}_v + \rho_{iT}'s_i)\boldsymbol{N}_T^{enr}\ \ d\Omega$$

$$+\frac{1}{\Delta t}\int_{\Omega}\left(\boldsymbol{N}_T^{std}\right)^T\cdot l\cdot(n-1)\beta_s\cdot(\rho_{iT}'Ts_i + \rho_i s_i + \rho_i T\frac{\partial s_i}{\partial T})\,\boldsymbol{N}_T^{enr}d\Omega +$$

$$\frac{1}{\Delta t}\int_{\Omega}\left(\boldsymbol{N}_T^{std}\right)^T\cdot l\cdot n(s_i\rho_{iT}' + \frac{\partial s_i}{\partial T}\rho_i)\cdot\boldsymbol{N}_T^{enr}d\Omega$$

$$-\frac{1}{\Delta t}\int_{\Gamma_d}\left(\boldsymbol{N}_T^{std}\right)^T\cdot l\cdot[\![u_{y'}]\!]\cdot(\rho_i\cdot\frac{\partial s_{w_d}}{\partial T} + \rho_{iT}'\cdot s_{w_d})\boldsymbol{N}_T^{enr}d\Gamma -$$

$$\frac{1}{\Delta t}\int_{\Gamma_d}\left(\boldsymbol{N}_T^{std}\right)^T\cdot[\![u_{y'}]\!]\cdot\left[(\rho C)_{\text{eff}_d}+\frac{\partial(\rho C)_{\text{eff}_d}}{\partial T}T\right]\boldsymbol{N}_T^{enr}d\Gamma +$$

$$\int_{\Gamma_d}\left(\boldsymbol{N}_T^{std}\right)^T\cdot l\cdot(\frac{\partial s_{i_d}}{\partial T}\rho_i + s_{i_d}\rho_{iT}')\cdot[\![\dot{u}_{y'}]\!]\boldsymbol{N}_T^{enr}d\Gamma - \frac{1}{\Delta t}\int_{\Gamma_d}\left(\boldsymbol{N}_T^{std}\right)^T\cdot l\cdot(\frac{\partial s_{i_d}}{\partial T}\rho_i + s_{i_d}\rho_{iT}')\cdot$$

$$[\![u_{y'}]\!]\varepsilon_{x'x'}\boldsymbol{N}_T^{enr}d\Gamma \tag{1.31}$$

$$\tilde{\mathbf{C}}_{Tc} = \frac{\partial\mathbf{C}_{Tp}}{\partial\hat{\mathbf{c}}}\hat{\mathbf{p}}_w + \frac{\partial\mathbf{C}_{Tb}}{\partial\hat{\mathbf{c}}}\hat{\mathbf{b}} = \int_{\Omega}\left(\mathbf{B}_T^{std}\right)^T\cdot\alpha(\frac{\partial k_r}{\partial T}\rho_i + k_r\rho_{iT}')\frac{K}{\mu_w}\rho_i l\,\boldsymbol{N}_T^{enr}\cdot\nabla p_w d\Omega \tag{1.32}$$

$$\frac{\partial\boldsymbol{F}_c^{\text{int}}}{\partial\hat{\boldsymbol{u}}} = \frac{1}{\Delta t}\int_{\Omega}(\boldsymbol{N}_T^{enr})^T\cdot l\cdot s_i\cdot\rho_i\cdot\boldsymbol{m}^T\boldsymbol{B}_u^{std}\cdot d\Omega - \int_{\Omega}(\boldsymbol{N}_T^{enr})^T\cdot l\cdot\dot{s}_w\cdot\rho_i\cdot(1-n)\boldsymbol{m}^T\boldsymbol{B}_u^{std}.d\Omega$$

$$-\int_{\Omega}(\boldsymbol{N}_T^{enr})^T\cdot l\cdot s_i\cdot\rho_i\beta_s\cdot\boldsymbol{m}^T\boldsymbol{B}_u^{std}\cdot\dot{T}d\Omega - \int_{\Omega}(\boldsymbol{N}_T^{enr})^T\cdot l\cdot s_i\cdot\rho_{iT}'\cdot\boldsymbol{m}^T\boldsymbol{B}_u^{std}\cdot\dot{T}d\Omega +$$

$$\frac{1}{\Delta t}\int_{\Gamma_d}(\boldsymbol{N}_T^{enr})^T\cdot l\cdot s_{i_d}\rho_i\cdot[\![u_{y'}]\!](\boldsymbol{n}_x^T\boldsymbol{B}_u^{std}\boldsymbol{n}_{x'})d\Gamma \tag{1.33}$$

$$\frac{\partial \boldsymbol{F}_c^{\text{int}}}{\partial \widehat{\boldsymbol{a}}} = \frac{1}{\Delta t}\int_{\Omega}(\boldsymbol{N}_T^{enr})^T \cdot l \cdot s_i \cdot \rho_i \cdot \boldsymbol{m}^T \boldsymbol{B}_u^{enr}\boldsymbol{L} \ \ .d\Omega - \int_{\Omega}(\boldsymbol{N}_T^{enr})^T \cdot l \cdot \dot{s}_w \cdot \rho_i \cdot (1-n)\boldsymbol{m}^T \boldsymbol{B}_u^{enr}.d\Omega -$$

$$\int_{\Gamma_d}(\boldsymbol{N}_T^{enr})^T \cdot \bar{\boldsymbol{N}}_u \cdot (\rho C)_{\text{eff}_d}\dot{T}d\Gamma - \int_{\Gamma_d}(\boldsymbol{N}_T^{enr})^T \cdot l \cdot \rho_i \cdot \bar{\boldsymbol{N}}_u \dot{s}_{w_d}d\Gamma +$$

$$-\int_{\Omega}(\boldsymbol{N}_T^{enr})^T \cdot l \cdot s_i \cdot \rho_i \beta_s \cdot \boldsymbol{m}^T \boldsymbol{B}_u^{enr} \cdot \dot{T}d\Omega - \int_{\Omega}(\boldsymbol{N}_T^{enr})^T \cdot l \cdot s_i \cdot \rho'_{iT} \cdot \boldsymbol{m}^T \boldsymbol{B}_u^{enr} \cdot \dot{T}d\Omega$$

$$\frac{1}{\Delta t}\int_{\Gamma_d}(\boldsymbol{N}_T^{enr})^T \cdot l \cdot s_{i_d}\rho_i \cdot [\![u_{y'}]\!](\boldsymbol{n}_{x'}^T \boldsymbol{B}_u^{enr}\boldsymbol{L}\boldsymbol{n}_{x'})d\Gamma - \int_{\Gamma_d}(\boldsymbol{N}_T^{enr})^T \cdot l \cdot s_{i_d}\rho_i \cdot \bar{\boldsymbol{N}}_u \dot{\varepsilon}_{x'x'}d\Gamma +$$

$$\frac{1}{\Delta t}\int_{\Gamma_d}(\boldsymbol{N}_T^{enr})^T \cdot l \cdot s_{i_d}\rho_i \cdot \bar{\boldsymbol{N}}_u d\Gamma \tag{1.34}$$

$$\frac{\partial \boldsymbol{F}_c^{\text{int}}}{\partial \widehat{\boldsymbol{T}}} = \frac{1}{\Delta t}\int_{\Omega}(\boldsymbol{N}_T^{enr})^T \cdot l \cdot n(\rho_i \frac{\partial s_w}{\partial T} + \rho'_{iT}s_w)\frac{\partial s_w}{\partial T}\boldsymbol{N}_T^{std} \ \ d\Omega -$$

$$\int_{\Omega}(\boldsymbol{N}_T^{enr})^T \cdot l \cdot (\rho_i \frac{\partial s_i}{\partial T}\dot{\varepsilon}_v + \rho'_{iT}s_i)\boldsymbol{N}_T^{std} \ \ d\Omega$$

$$+\frac{1}{\Delta t}\int_{\Omega}(\boldsymbol{N}_T^{enr})^T \cdot l \cdot (n-1)\beta_s \cdot (\rho'_{iT}Ts_i + \rho_i s_i + \rho_i T\frac{\partial s_i}{\partial T})\boldsymbol{N}_T^{std}d\Omega +$$

$$\frac{1}{\Delta t}\int_{\Omega}(\boldsymbol{N}_T^{enr})^T \cdot l \cdot n(s_i\rho'_{iT} + \frac{\partial s_i}{\partial T}\rho_i) \cdot \boldsymbol{N}_T^{std}d\Omega$$

$$-\frac{1}{\Delta t}\int_{\Gamma_d}(\boldsymbol{N}_T^{enr})^T \cdot l \cdot [\![u_{y'}]\!] \cdot (\rho_i \cdot \frac{\partial s_{w_d}}{\partial T} + \rho'_{iT} \cdot s_{w_d})\boldsymbol{N}_T^{std}d\Gamma -$$

$$\frac{1}{\Delta t}\int_{\Gamma_d}(\boldsymbol{N}_T^{enr})^T \cdot [\![u_{y'}]\!] \cdot \left[(\rho C)_{\text{eff}_d} + \frac{\partial(\rho C)_{\text{eff}_d}}{\partial T}T\right]\boldsymbol{N}_T^{std}d\Gamma +$$

$$\int_{\Gamma_d}(\boldsymbol{N}_T^{enr})^T \cdot l \cdot (\frac{\partial s_{i_d}}{\partial T}\rho_i + s_{i_d}\rho'_{iT}) \cdot [\![\dot{u}_{y'}]\!]\boldsymbol{N}_T^{std}d\Gamma - \frac{1}{\Delta t}\int_{\Gamma_d}(\boldsymbol{N}_T^{enr})^T \cdot l \cdot (\frac{\partial s_{i_d}}{\partial T}\rho_i + s_{i_d}\rho'_{iT}) \cdot$$

$$[\![u_{y'}]\!]\varepsilon_{x'x'}\boldsymbol{N}_T^{std}d\Gamma \tag{1.35}$$

$$\widetilde{\boldsymbol{C}}_{cT} = \frac{\partial \boldsymbol{C}_{cp}}{\partial \widehat{\boldsymbol{T}}}\widehat{\boldsymbol{p}}_w + \frac{\partial \boldsymbol{C}_{cb}}{\partial \widehat{\boldsymbol{T}}}\widehat{\boldsymbol{b}} = \int_{\Omega}\left(\boldsymbol{B}_T^{enr}\right)^T \cdot \alpha(\frac{\partial k_r}{\partial T}\rho_i + k_r\rho'_i)\frac{K}{\mu_w}l\,\boldsymbol{N}_T^{std} \cdot \nabla p_w d\Omega \tag{1.36}$$

$$\frac{\partial \boldsymbol{F}_c^{\text{int}}}{\partial \widehat{\boldsymbol{c}}} = -\frac{1}{\Delta t}\int_{\Omega}(\boldsymbol{N}_T^{enr})^T \cdot l \cdot n(\rho_i \frac{\partial s_w}{\partial T} + \rho'_{iT}s_w)\frac{\partial s_w}{\partial T}\boldsymbol{N}_T^{enr} \ \ d\Omega -$$

$$\int_{\Omega}(\boldsymbol{N}_T^{enr})^T \cdot l \cdot (\rho_i \frac{\partial s_i}{\partial T}\dot{\varepsilon}_v + \rho'_{iT}s_i)\boldsymbol{N}_T^{enr} \ \ d\Omega$$

$$+\frac{1}{\Delta t}\int_{\Omega}(\boldsymbol{N}_T^{enr})^T \cdot l \cdot (n-1)\beta_s \cdot (\rho'_{iT}Ts_i + \rho_i s_i + \rho_i T\frac{\partial s_i}{\partial T})\boldsymbol{N}_T^{enr}d\Omega +$$

$$\frac{1}{\Delta t}\int_{\Omega}(\boldsymbol{N}_T^{enr})^T \cdot l \cdot n(s_i\rho'_{iT} + \frac{\partial s_i}{\partial T}\rho_i) \cdot \boldsymbol{N}_T^{enr}d\Omega$$

$$-\frac{1}{\Delta t}\int_{\Gamma_d}(\boldsymbol{N}_T^{enr})^T \cdot l \cdot [\![u_{y'}]\!] \cdot (\rho_i \cdot \frac{\partial s_{w_d}}{\partial T} + \rho'_{iT} \cdot s_{w_d})\boldsymbol{N}_T^{enr}d\Gamma -$$

$$\frac{1}{\Delta t}\int_{\Gamma_d}(\boldsymbol{N}_T^{enr})^T \cdot [\![u_{y'}]\!] \cdot \left[(\rho C)_{\text{eff}_d} + \frac{\partial(\rho C)_{\text{eff}_d}}{\partial T}T\right]\boldsymbol{N}_T^{enr}d\Gamma +$$

$$\int_{\Gamma_d} (\boldsymbol{N}_T^{enr})^T \cdot l \cdot (\frac{\partial s_{i_d}}{\partial T} \rho_i + s_{i_d} \rho'_{iT}) \cdot [\![\dot{u}_{y'}]\!] \boldsymbol{N}_T^{enr} d\Gamma - \frac{1}{\Delta t} \int_{\Gamma_d} (\boldsymbol{N}_T^{enr})^T \cdot l \cdot (\frac{\partial s_{i_d}}{\partial T} \rho_i + s_{i_d} \rho'_{iT}) \cdot$$
$$[\![u_{y'}]\!] \varepsilon_{x'x'} \boldsymbol{N}_T^{enr} d\Gamma \tag{1.37}$$

$$\tilde{\mathbf{C}}_{cc} = \frac{\partial \mathbf{C}_{cp}}{\partial \hat{\mathbf{c}}} \hat{\mathbf{p}}_w + \frac{\partial \mathbf{C}_{cb}}{\partial \hat{\mathbf{c}}} \hat{\mathbf{b}} = \int_{\Omega} \left(\mathbf{B}_T^{enr} \right)^T \cdot \alpha (\frac{\partial k_r}{\partial T} \rho_i + k_r \rho'_{iT}) \frac{K}{\mu_w} l \, \mathbf{N}_T^{enr} \cdot \nabla p_w d\Omega \tag{1.38}$$